Lateral torsional buckling of thin-walled rectangular and I-section laminated composite beams with arbitrary layups

by

Abdul Halim Halim

B.S., Kabul University, Afghanistan, 2007
M.S., Kansas State University, 2010

AN ABSTRACT OF A DISSERTATION

submitted in partial fulfillment of the requirements for the degree

DOCTOR OF PHILOSOPHY

Department of Civil Engineering
Carl R. Ice College of Engineering

KANSAS STATE UNIVERSITY
Manhattan, Kansas

2020

Abstract

Structural elements made of fibrous composites are increasingly used in aerospace, automotive, civil and marine structures due to their high stiffness/strength-to-weight ratio and corrosion resistance properties. Most of the composite structural elements are thin-walled and their design is often controlled by stability considerations mainly due to slenderness effects. Hence, for thin-walled slender composite beams, lateral torsional buckling (LTB) is the dominant failure mode regardless of the fiber orientations.

In this study, closed form analytical solutions for generally anisotropic (arbitrary layup) thin-walled rectangular-section cantilever and I-shape beams under pure bending are presented. Corresponding differential equations are formulated using the kinematics, constitutive and equilibrium equations for the beams and solved using infinite series approach. Restrained warping is also considered in the formulation for I-section beam. A parametric study is performed to investigate the effects of beam length to depth ratio (l/h) and flange and web thickness effects on the critical buckling load. Good agreement between analytical solution and finite element results was obtained for both section types. The solution is also validated against Timoshenko's classical buckling solution for isotropic beam for both rectangular and I-sections and a perfect match was observed. Analytical solutions could be adapted for rectangular or I-section beams subjected to various loading and boundary conditions. The solution is equally applicable for hybrid thin-walled laminated beams for the given sections. Some experiments on basic orthotropic beams are also conducted.

Lateral torsional buckling of thin-walled rectangular and I-section laminated composite beams with arbitrary layups

by

Abdul Halim Halim

B.S., Kabul University, Afghanistan, 2007
M.S., Kansas State University, 2010

A DISSERTATION

submitted in partial fulfillment of the requirements for the degree

DOCTOR OF PHILOSOPHY

Department of Civil Engineering
Carl R. Ice College of Engineering

KANSAS STATE UNIVERSITY
Manhattan, Kansas

2020

Approved by:

Major Professor
Dr. Hayder A. Rasheed

Copyright

Abstract

Structural elements made of fibrous composites are increasingly used in aerospace, automotive, civil and marine structures due to their high stiffness/strength-to-weight ratio and corrosion resistance properties. Most of the composite structural elements are thin-walled and their design is often controlled by stability considerations mainly due to slenderness effects. Hence, for thin-walled slender composite beams, lateral torsional buckling (LTB) is the dominant failure mode regardless of the fiber orientations.

In this study, closed form analytical solutions for generally anisotropic (arbitrary layup) thin-walled rectangular section cantilever and I-shape beams under pure bending are presented. Corresponding differential equations are formulated using the kinematics, constitutive and equilibrium equations for the beams and solved using infinite series approach. Restrained warping is also considered in the formulation for I-section beam. A parametric study is performed to investigate the effects of beam length to depth ratio (l/h) and flange and web thickness effects on the critical buckling load. Good agreement between analytical solution and finite element results was obtained for both section types. The solution is also validated against Timoshenko's classical buckling solution for isotropic beam for both rectangular and I-sections and a perfect match was observed. Analytical solutions could be adapted for rectangular or I-section beams subjected to various loading and boundary conditions. The solution is equally applicable for hybrid thin-walled laminated beams for the given sections. Some experiments on basic orthotropic beams are also conducted.

Table of Contents

List of Figures

List of Tables

Acknowledgements

I would like to express my deepest gratitude for the continuous support and guidance of my major advisor, Dr. Hayder A. Rasheed, whose insight and knowledge into the subject matter steered me through this research.

I would also like to thank Dr. Christopher Jones, Dr. Bacim Alali, Dr. Jack Xin, and Dr. James Laverty for their willingness to serve on my supervisory committee and for providing invaluable comments and suggestions during my preliminary and final exam.

Finally, I would like to specially thank my parents Mohammad Wazir and Bibi Mariam, my esteemed sisters Shafiqa, Maymona, Karima and younger brother Shafi Mayar, my wife Leeda Sana and our lovely daughter Asmaa Halim, for their love and care, sacrifices, commitment to my education, and continuous prayers. You are and will always be a source of strength for me.

Dedication

To my parents, my wife, and my professors and colleagues at Kabul University/College of Engineering

Chapter 1 - Introduction

1.1 Overview

Structural materials can be classified into four basic groups: composites, polymers, ceramic, and metals. Composites are made of two or more materials combined in a macroscopic structural unit. This implies that metal alloys are not considered composites as the structural unit is formed at the microscopic level. Composites are very useful in the sense that required properties could be achieved by combining the properties of each constituent material separately.

Composite fibers are well known and widely used in a variety of applications. However, it is unclear when and where exactly humans have first used fibrous composite. Evidence of using straw-reinforced bricks in Mesopotamia in Iraq 5,500 years ago indicates that fibrous composites have long been used by humans for structural applications [1]. Likewise, native residents of Central and South America seemingly used plant fibers in their pottery possibly to protect clay against cracking [2].

Surprisingly most materials are stronger when in fiber form than in bulk form. In the early twentieth century, Griffith [3] measured the tensile strength of glass rods and glass fibers. He observed that the tensile strength of the rod was inversely proportional to the rod diameter. In other words, thinner rods had higher tensile strength compared to rods with larger diameter simply because failure inducing surface cracks are less likely to form in thinner rods during fabrication or handling. This is similar to the concept of size effect in solid mechanics, which is known as the effect of the characteristic size on the nominal strength of an element when geometrically identical elements are compared [4].

Fibrous composite is the most common type which consists of reinforcing fibers embedded in resin or matrix. Resin is only responsible to hold fibers together and maintain their alignment.

Fibers serve as the main load carrying element in the layup. Components of different shapes i.e., circular, hollow square or rectangular, and I-section are fabricated using different processes. Fabrication process for composites depends on the type of matrix and of fiber reinforcement used. Common fabrication processes for polymer matrix are: pultrusion, autoclave, filament winding, and thermoplastic molding.

Structural elements made of fibrous composites are now extensively used in aerospace, automotive and marine structures due to their high stiffness/strength-to-weight ratio and corrosion/fatigue resistance properties. Most of the composite structural elements are thin-walled. A significant advantage of using composite materials in thin-walled section beams e.g., I-beams is that the mechanical properties can be optimized for a specific application [5]. For instance, in I-beam section, web shall contain laminates with +/-45 degree to increase shear resistance while flanges are made of unidirectional layups to maximize bending stiffness [6]. In addition, composite construction leads to smooth surfaces compared to metals where typically rivets or bolts are needed at the connections. This has special importance in aerospace applications as it reduces drag force. Boeing 757 and 767 were among the first commercial airliners making extensive use of composites. Approximately 30 percent of Boeing 767 exterior surface is made of composite [2] and nearly half of Boeing 787 are made of Carbon fiber composites [7].

In civil engineering, fiber reinforced composite are mostly used for strengthening applications in the form of sheets attached to the member of interest using epoxy. Typical pultruded structural shapes are used in lightweight industrial buildings due to their lightweight, corrosion resistance, low thermal and electrical conductivity [8]. Similarly, all composite, fiber reinforced polymer honeycomb sandwich panels are becoming increasingly popular to use as full-depth bridge decks [9].

As discussed above, fiber reinforced composites are becoming more prevalent material with the advancement in fabrication process and new applications. However, due to their complex behavior mainly due to coupling terms i.e., extension-shear, extension-twist, bending-shear, bending-twist which depends on the fiber orientation in the layup, design guidelines developed for conventional homogeneous or homogenized isotropic materials such as steel or concrete could not be applied directly [10].

Unlike metallic beams where shear deformations are ignored, the ratio of elastic modulus and shear modulus (E/G) is about four times larger for composite beams meaning that shear deformations shall be considered especially for short span beams [6]. Factors affecting shear deformation depend on the length to height ratio, shape of beam section, and material properties. Unfortunately, introducing shear deformations into the corresponding equations makes the formulation even more complex and non-intuitive. Another complexity arise from the restrained warping effects that hasn't been investigated yet for composite beams with arbitrary layups. To the best of author's knowledge, there is no formulation relating warping effects to shear, bending or twisting moments for composite beams having arbitrary layups.

Design of thin-walled members is often controlled by stability consideration mainly due to slenderness effects. Hence, for thin-walled slender composite beams, lateral torsional buckling is the dominant failure mode regardless of the fiber orientation. Most of the work in the literature corresponds to orthotropic or balanced layups where axial load or bending do not cause twisting. This leads to simplified engineering equations that are relatively easy to solve. However, not every layup used in practice is orthotropic or balanced.

This research is devoted to obtain closed form analytical solutions to the lateral torsional buckling problem of rectangular and I-beams with arbitrary layups and takes into account all possible couplings between in-plane and out-of-plane loads and deformations.

1.2 Objectives

The main objectives of this research are:

- Obtain closed form analytical solutions to the lateral-torsional buckling problem of thin-walled rectangular and I-shape beams with arbitrary layups.
- Validate the solution against experimental and finite element results.
- Investigate warping and out of plane shear effects on the lateral torsional buckling of thin-walled composite section.
- Develop simplified experimental technique(s) to measure twisting rotation of the section as well as vertical and lateral deflection for a load controlled case

1.3 Scope

This dissertation includes six chapters describing the step-by-step derivation of required equations, solutions, constraints, assumptions and finite element modeling using ABAQUS. Chapter two is devoted to the literature review and briefly discusses the contribution by different researchers to the buckling problem of thin walled composite beams in general. Chapter three presents experimental vs. numerical buckling / post buckling response of cantilever orthotropic web beams under tip force. In chapter four, closed form analytical solution for the lateral torsional buckling problem of thin walled rectangular beam with arbitrary layups is presented. The solution is then validated against experimental and numerical results for a cantilever beam. Chapter five deals with lateral torsional buckling of thin-walled I-beams with arbitrary layups under pure bending considering warping and out of plane shear effects. Chapter six concludes research findings and provide recommendations for future work. Furthermore, a step-by-step procedure to model composite beams in ABAQUS is provided in Appendix.

Chapter 2 - Literature Review

Fiber Reinforced Polymer (FRP) composites are widely used in many engineering applications especially aerospace industry due to high-strength, lightweight, thermally and electrically non-conductive (Glass only, Carbon is conductive), and corrosion resistance properties. For example, in fighter aircrafts, vertical and horizontal stabilizers, wing skins, and flaps are made of advanced composites causing weight saving of as much as 20 percent [2]. In civil engineering, fiber reinforced composite are mostly used for strengthening applications in the form of sheets attached to a member of interest using epoxy. Typical pultruded structural shapes are also used in lightweight industrial buildings [8]. Similarly, all composite, fiber reinforced polymer honeycomb sandwich panels are becoming increasingly popular to use as full-depth bridge decks [9]. Composites are also commonly used in sport equipment such as tennis rackets, golf clubs, commercial boats, etc. because of high stiffness and lightweight.

In the construction industry, application of carbon and glass FRP elements for strengthening and replacing some typical steel and aluminum elements are becoming increasingly popular. Plates, bars and different thin-walled open and closed section structural shapes made of carbon or glass FRP are produced by various manufacturers.

Design of thin-walled open or closed isotropic or anisotropic section is often controlled by stability considerations due to slenderness effects. Thin-walled open section beam elements tend to experience flexural-torsional buckling prior to material failure when loaded about strong axis. Timoshenko's solution for lateral torsional buckling of isotropic beam and beam-column serves as a basis for most of the available solutions in the literature. Vlasov [11] presented the theory of open or closed section thin-walled isotropic beams. Based on kinematic assumptions consistent with Timoshenko beam theory Barbero et al. [12] presented an approach to study structural response of orthotropic composite beams subjected to bending and axial load. Turvey [13] studied the effect of load position on the lateral buckling response of pultruded Glass Reinforced Polymer (GRP) cantilever beams. It was concluded that the effect of pre-buckling deformations and any geometric nonlinearity should be considered for appropriate correlation between analytical and experimental results.

He and Gao [14] studied the effects of fiber content on the flexural properties of unidirectional laminated composite beams. It was observed that fiber volume fraction of 70% leads to the largest fracture force while any fiber volume fraction higher than or equal to 80% yield poor flexural properties.

J. N. Reddy [15] presented a generalized non-linear theory for plates using consistent strain, and third order displacement field. Murthy [16] presented an improved shear deformation theory for anisotropic plates under bending without need for arbitrary shear correction factor.

J. N. Reddy [17] presented a higher-order shear deformation theory that accounts for parabolic distribution of transverse shear strain through the thickness of plate. It is more accurate than the first-order shear deformation theory in terms of predicting deflection and stress in composite plates.

Most beam design theories are based on the assumption that plane sections remain plane before and after deformation. However, this assumption may not always hold true particularly for generally anisotropic composite sections. Kollar and Pluzsik [18] presented a theory where corresponding properties can be determined from accurate beam equations using limit transitions considering in-plane and torsional warping shear deformations.

Unlike isotropic materials, carbon FRP composites are linearly elastic until failure along fiber direction, which makes the calculations simpler. However, the existence of extension-shear, bending-twist, extension-twist and bending-shear couplings make the calculations a lot more complicated. To avoid complexities in calculations, most often researchers and designers consider layups to be orthotropic, symmetric, balanced or a combination of them. Orthotropic means that normal forces and bending moments applied along the two mutually perpendicular directions in the plane of the laminate do not cause shear or twist. In a symmetric layup, there is no in-plane-out-of-plane coupling which means that in-plane forces do not cause out-of-plane deformations (curvatures) and moments do not cause in-plane deformations. For a balanced laminate, there is no extension-shear coupling.

2.1 Buckling of Thin-Walled Rectangular Beams

Ahmadi and Rasheed [19] presented a semi-analytical approach to determine critical load for a simply supported thin-walled composite beam with lateral torsional buckling as dominant failure mode. Good agreement between the proposed solution and finite element results is reported by the authors. Symmetric and anti-symmetric balanced angle-ply laminate of 20 degree seems to have the highest buckling load in its category. Vo and Lee [20] developed a model to analyze flexural, torsional and flexural torsional buckling of thin-walled composite box beams under axial load. Their model is based on classical laminated plate theory which takes into account flexural torsional coupling for any arbitrary layup and different boundary conditions.

2.2 Buckling of Thin-Walled I-Beams

Davalos and Qiao [10] studied flexural-torsional and lateral-distortional buckling response of wide flange balanced-symmetric pultruded beams. Using the principles of energy, an equation was derived for the total potential energy for flexural torsional buckling using nonlinear elastic theory. Lee and Kim [21] presented a generalized analytical model which is applicable to flexural, torsional or flexural-torsional buckling of composite I-sections with arbitrary layups under axial load. Kabir and Sherbourne [22] have studied the interactive buckling of fibrous composite I-section beams. It was concluded that when local buckling and overall lateral buckling are viewed as separate entities, they result in stable post critical behavior respectively. However, when combined, leads to more degradative effect on the failure load capacity of thin-walled beams.

Cardoso and Vieira [23] presented explicit equations to estimate local buckling critical stress of thin walled composite beam under compression or pure bending. In addition to considering interaction between flange and web and different orthotropy ratios, the procedure allows for a range of flange and web thicknesses and flange to web ratios.

Zeinali, Nazari, and Showkati [24] performed experimental-numerical study on lateral torsional buckling of pultruded FRP I-section beams having different span to height ratios under pure bending. Using Eurocode 3 provisions, reasonable agreement between experimental and numerical results has been reported.

Pandey, Kabir, and Sherbourne [25] have studied the optimal fiber orientation to enhance lateral buckling strength of thin-walled open section composite beams. They concluded that for I-section beams with unidirectional flange layups, the web fiber angle has significant influence on lateral buckling of long span beams. Additionally, for length to height ratio (l/h) of 12 or higher, optimal fiber orientation for the flanges and web are 0° and +/-45° respectively. Barbero and Raftoyiannis [26] studied the elastic buckling modes of pultruded I-beams for different loading conditions. It was concluded that coupling of local and lateral buckling modes always occurs due to lower material stiffness in the transverse direction. Moreover, lateral buckling was found to be the dominant failure mode for I-beams with high depth to width ratios while coupled local and distortional buckling for lower depth to width ratios contributed to the reduction in the critical load compared to pure local or pure lateral buckling loads.

2.3 Buckling of Beams with Generalized Sections

Mottram [27] found that the classical one-dimensional isotropic theories for lateral torsional buckling of beam could be adapted for orthotropic composite beams with proper substitution of moduli parameters. Kollar and Pluzsik [28] derived stiffness matrix for thin-walled composite open and closed section beams with arbitrary layup ignoring the effects of shear deformations and restrained warping. Pluzsik and Kollar [29] developed simple expressions to determine the effect of shear deformations for thin-walled beams having symmetrical, unsymmetrical, orthotropic or anisotropic layups. They demonstrated that warping stiffness derived for orthotropic beams could be equally applied to open section anisotropic beams with balanced layups. Likewise, Pluzsik and Kollar [30] presented a theory for torsion of closed section thin-walled orthotropic beams considering shear deformation due to restrained warping induced torque.

Shan and Qiao [31] performed a combined analytical and experimental study to determine flexural torsional buckling of pultruded C-shape beam taking into account shear effects and bending-twist coupling. Comparison between experimental and finite element loads show that the latter gives higher buckling loads for nearly all of the cases considered.

Massa and Barbero [32] presented a simple approach for analysis of thin-walled composite beams subjected to torque, bending, axial, and shear forces. Instead of geometric properties of the cross section used in the classical beam theory i.e., area, first moment of area, center of gravity, they used equivalent mechanical properties such as axial stiffness, mechanical first moment of area, and mechanical center of gravity in their formulation.

Kollar [33] studied the stability of open section thin-walled orthotropic axially loaded columns using modified Vlasov's theory in which the transverse shear and restrained warping induced shear deformations were considered. The solution clearly gives the effect of shear deformation on the buckling load.

Chapter 3 - Experimental vs. Numerical Buckling/Post-Buckling Response of Cantilever Orthotropic Web Beams Under Tip Force

3.1 Abstract

A combined numerical and experimental study of lateral torsional buckling of orthotropic rectangular section beam is presented. Pre and post-buckling response of beams is studied using ABAQUS Riks analysis and compared with experimental results. Timoshenko's solution with replacement stiffnesses is adopted to calculate the lateral torsional buckling load of six orthotropic beams. Four beams with 0° layups and two beams with 90° layups are prepared in lab. Beams had different length to height (l/h) ratios ranging from 6.67 to 20 to study its effect on the critical load. All beams are assumed cantilever and tested under a concentrated load at the free end. Two laser pointers mounted horizontally at the free end are used to measure twisting rotation of beam section (β) for every load increment. Load vs. β plots are generated and compared with numerical and analytical results. The proposed experimental technique could be adopted to study lateral-torsional buckling response of beams with arbitrary fiber orientations (generally anisotropic) under different load and support conditions. The technique also helps to generate load vs. lateral and vertical deflection simultaneously while measuring the section twisting rotation angle (β).

3.2 Introduction

Fiber Reinforced Polymer (FRP) composites are widely used in many engineering applications especially aerospace industry due to their high-strength, lightweight and corrosion resistance properties. In the construction industry, application of carbon and glass FRP elements for strengthening and replacing some typical steel and aluminum elements is rapidly increasing. Plates, bars and different thin-walled open and closed section structural shapes made of carbon or glass FRP are now produced by various manufacturers. Design of thin-walled open or closed isotropic or anisotropic section is often controlled by stability considerations due to slenderness effects. Specifically, beam elements with thin-walled open section tend to experience flexural-torsional buckling prior to material failure. Timoshenko and Gere [34] theory for lateral torsional buckling behavior of isotropic beam and beam-column elements serves as basis for nearly all solutions available in the literature. Vlasov [11] presented the theory of thin-walled isotropic beams with open and closed section. Based on kinematic assumptions consistent with Timoshenko's beam theory, Barbero et al. [12] presented an approach to study structural response of orthotropic composite beams subjected to bending and axial load. Turvey [13] studied the effect of load position on the lateral buckling response of pultruded Glass Reinforced Polymer (GRP) cantilever beams. It was concluded that the effect of pre-buckling deformations and any geometric nonlinearity should be considered for proper correlation between analytical and experimental results.

Davalos and Qiao [10] studied flexural-torsional and lateral-distortional buckling response of wide flange balanced-symmetric pultruded beams. Energy principles were applied to derive total potential energy equations for flexural torsional buckling using nonlinear elastic theory. Mottram [27] found that the classical one-dimensional isotropic theories for lateral torsional buckling of beam can be adapted for orthotropic composite beams with proper substitution of moduli parameters. Kollar and Pluzsik [28] derived stiffness matrix for thin-walled composite open and closed section beams with arbitrary layup ignoring the effects of shear deformation and restrained warping. Shan and Qiao [31] performed a combined analytical and experimental study to determine flexural torsional buckling of pultruded C-shape beam considering shear effect and bending-twist coupling. Comparison between experimental and finite element loads show that the latter gives higher buckling loads for nearly all cases considered.

Lee and Kim [21] presented a general analytical model applicable to flexural, torsional or flexural-torsional buckling of composite I-beam with arbitrary layups under axial load Ahmadi and Rasheed [17] presented a semi-analytical approach to determine critical load for a simply supported thin-walled composite beam with lateral torsional buckling as dominant failure mode. Good agreement between the semi-analytical solution and finite element prediction is reported by the authors.

Analytical solutions in the literature for buckling analysis of composite beams of different cross sections are often verified against finite element results. In this research, a combined experimental and numerical study is conducted to determine lateral-torsional buckling load for a rectangular section of orthotropic layup. Additionally, Timoshenko's solution for lateral torsional buckling of cantilever beam was adapted by substituting for the lateral bending stiffness and torsional constant terms.

3.3 Composite Beam Fabrication Process

Wet layup/hand layup method was used to prepare six rectangular beam samples. All beams consisted of four laminas of V-Wrap C100 with the properties given in Table 3.1. A two component epoxy resin V-Wrap 770 was mixed and applied to the fabric. Properties of V-Wrap

770 are presented in Table 3.2. Fabric sheets were cut 50 mm longer on each side than the exact dimensions in Table 3.4. A fiber volume fraction (vf) of 0.237 was calculated for all beams. Four beams consisted of 0° layups and two beams of 90° layups. Mechanical properties of cured laminates are listed in Table 3.3. After 7-days of curing in lab under room temperature, beams were cut[1] to the exact dimensions. Properties not given in the manufacturer's technical data sheets were calculated using micro/macro-mechanics approach.

Table 3.1: V-Wrap C100 [11] fiber properties (dry)

Primary fiber direction	0° (unidirectional)
Weight per square yard	300 g/m^2
Tensile strength	4,480 MPa
Tensile modulus	234,400 MPa
Shear modulus	83,722 MPa
Thickness	0.1651 mm
Elongation	1.9%
Poisson's ratio	0.4

Table 3.2: V-Wrap 770 Epoxy adhesive properties

Flexural modulus	2,620 MPa
Shear modulus	1,270 MPa
Poisson's ratio	0.0315

1 Beams were cut 70 mm longer than the exact dimensions for embedment at the fixed end.

Table 3.3: Cured laminate properties

Tensile strength	965 MPa
Young's modulus at fiber direction, E1	57,488 MPa
Young's modulus at transverse direction, E2	4,198 MPa
Poisson's ratio, $\upsilon 12$	0.119
Poisson's ratio, $\upsilon 21$	0.00869
Shear modulus, G12	2,026 MPa
Shear modulus, G13	2,026 MPa
Shear modulus, G23	2,035 MPa

Table 3.4: Exact beam dimensions and weight

Beam Designation	**Width, mm**	**Thickness, mm**	**Length, mm**	**Weight, N**
C100-500x75 $[0]_4$	74.15	2.4	502	1.27
C100-500x50 $[0]_4$	49.05	2.62	502	0.91
C100-500x25 $[0]_4$	23.37	2.79	502	0.45
C100-400x50 $[0]_4$	49.32	2.67	401	0.74
C100-500x25 $[90]_4$	25.11	2.34	505	0.44
C100-400x50 $[90]_4$	48.85	2.37	402	0.69
Steel beam 316	25	0.609	250	0.35

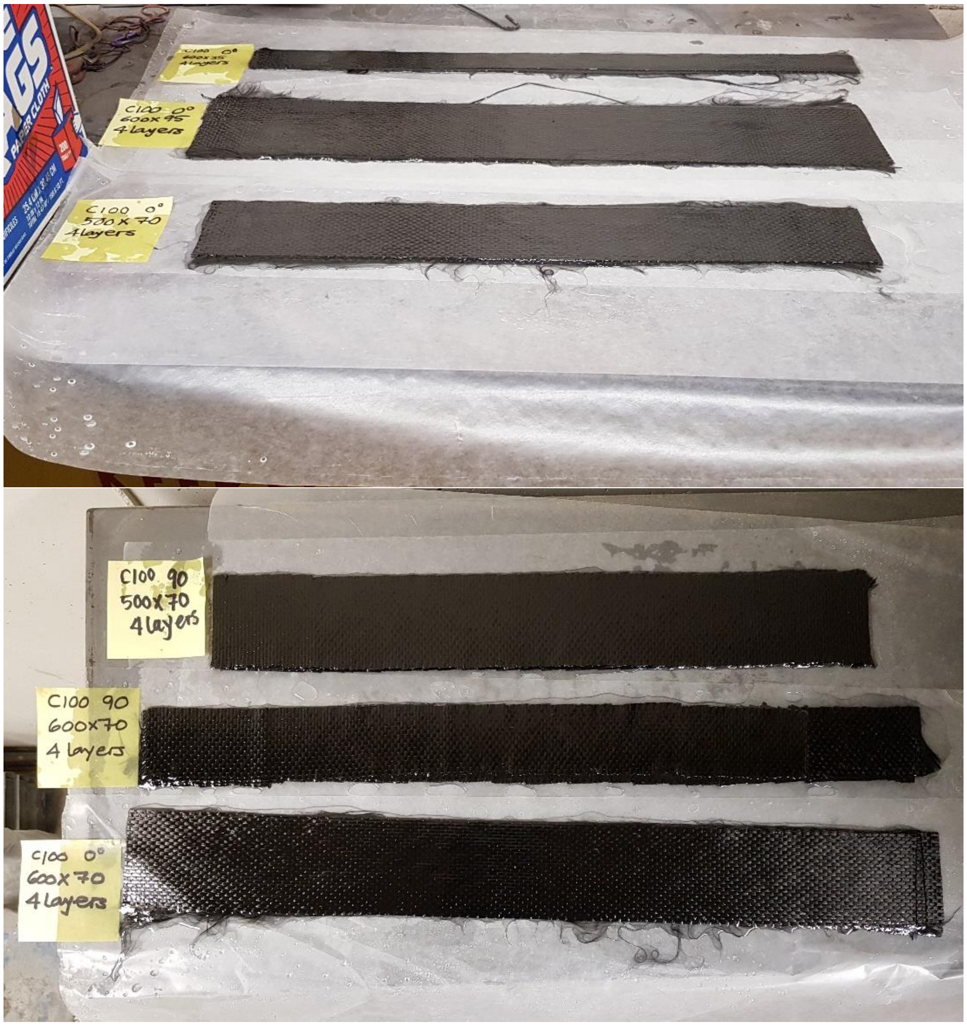

Figure 3.1: Rectangular beams prepared using hand layup method before cutting into exact dimensions

Figure 3.2: Cutting beam into exact dimensions

3.4 Experimental Setup

All six beams were tested in cantilever configuration. The clamped end of the beams was achieved using a vise. A 3 mm diameter hole was drilled along the longitudinal centerline close to the free end of the beam. Beam length was measured from the center of the hole to the clamped end. For loading beams at the free end, an annular steel bush of 4 mm diameter was inserted into the hole to avoid beam damage due to stress concentration and provide a nearly frictionless surface at the contact area of the 550 mm nylon string passing through the hole and connecting the 300 mm steel rod with eye-bolt on two ends. Two mini laser dot diode module head WL red 650 nm, 6mm long, 5V, 5mW were attached horizontally using super glue at the top and bottom along section length direction at the free end of the beam, Figure 3.3. Mini laser heads were connected using MWS 134-AWP wires and powered using 6V Rayovac battery. Bubble level was used to make sure the beam is placed horizontally prior to loading.

Because the numerical load causing lateral torsional buckling in the beam varied from 2.48 N to 51.58 N it was critical to apply load in small increments. Hence, lead shots were used for a controlled loading process. A small size plastic bucket weighing 0.12 N was used for putting lead shots to load beams with lower capacity. A metal bucket weighing 1.97 N measuring 100x135x135 mm was used for beams with higher capacity. A PVC frame 510x760x1300 mm with a plexiglass measuring 400x760 mm attached vertically to the longer side of the frame was used to mark location of the laser dots as it moves during loading. A gridline sheet was attached to the plexiglass as shown in Figure 3.5.

First, location of the two laser dots was marked on the sheet and connected with a straight line to serve as reference line for later readings. This was repeated for each load increment and several lines with varying orientations were obtained, Figure 3.4. The change in orientation gave the corresponding angle of twisting rotation (β) for beam cross-section which was measured using protractor. Thus, load vs β plots were generated for each beam. Using the same sheet, horizontal and vertical displacement of beam tip can be measured accurately.

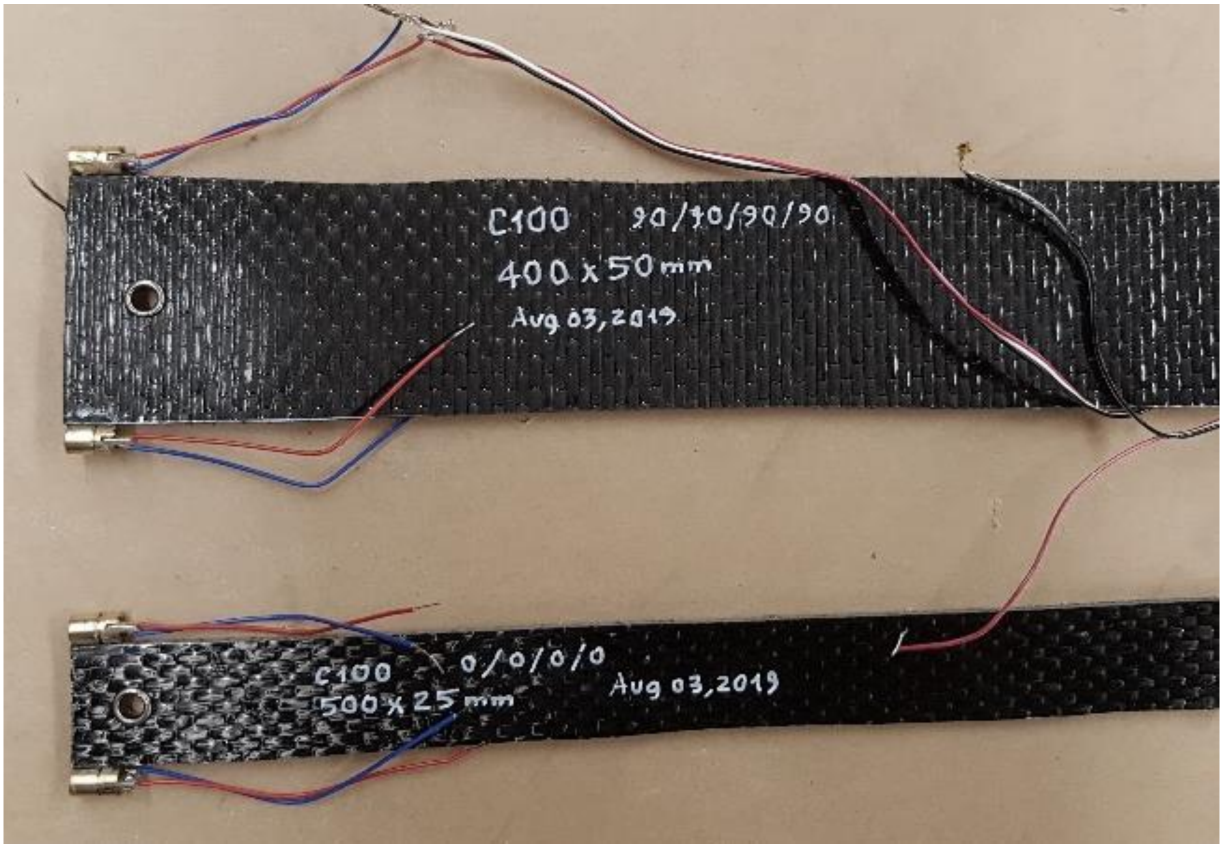

Figure 3.3: Carbon fiber reinforced plastic (CFRP) beams with mini lasers mounted horizontally on the section top and bottom

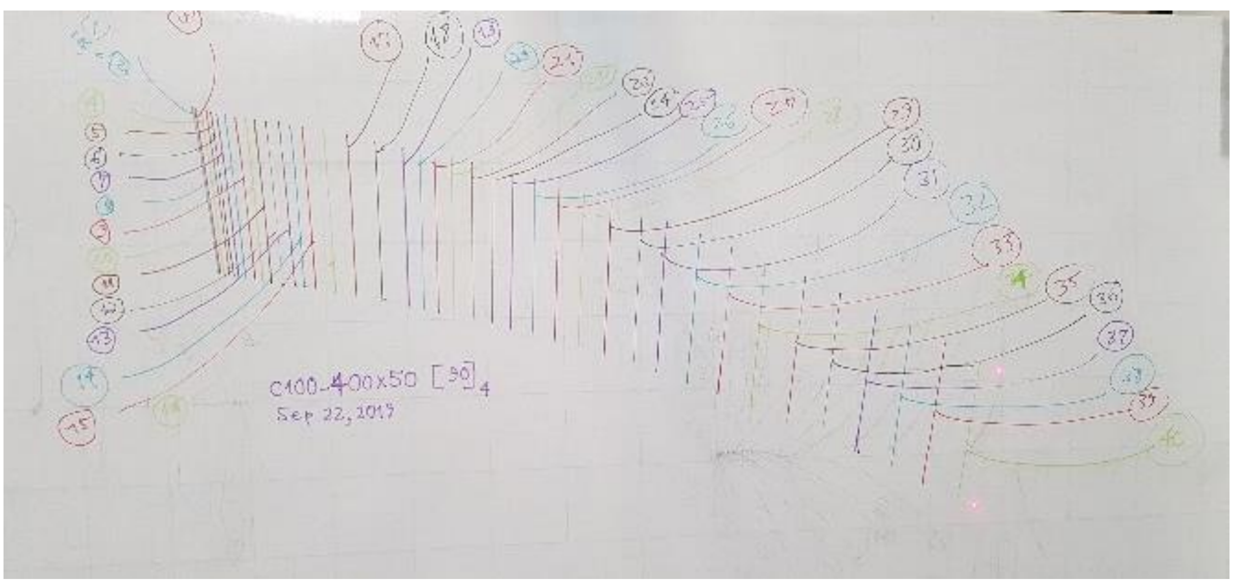

Figure 3.4: Lines showing change in the twisting rotation angle (β) of the beam section at the free end

3.5 Numerical Analysis

Numerical analysis was performed in two steps using ABAQUS. First, find load corresponding to the first Eigen mode. Second, use the same load to execute Riks analysis. In the following, each step is briefly described.

3.5.1 Eigen Value Analysis

Conventional shell with S8R element type and 5 mm element size was used for modeling beams in ABAQUS. Mechanical properties of cured laminates (Table 3.3) were either obtained from technical data sheets [35] or calculated using micro/macro-mechanics approach [8]. The Eigen Value analysis is that performed on Finite Element mesh implemented in the ABAQUS software. A unit load was applied at the shear center of beam at the free end. Since ABAQUS gives the critical load in terms of Eigen Values, buckling load was calculated by multiplying the first Eigen Value by the unit load. Grid Convergence Index analysis according to [36] was performed to investigate the effect of mesh refinement on the critical load (Table 3.5). A reduced mesh size was observed to have no effect on the buckling load; hence, a 5 mm element size was followed throughout this work. To know the response of a similar isotropic beam and verify the experimental setup, a steel beam was cut from 316-steel plate to the given dimensions (Table 3.4) and solved using Timoshenko's equation for cantilever beam.

Table 3.5: C100-500x50 $[0]_4$ Grid Convergence Index (GCI) Analysis

Mesh	Element Size (mm)	Critical Buckling Load, P_{cr}, (N)	f_3-f_2	f_2-f_1	p	f_h=0	GCI_{12}	GCI_{23}	GCI_{23}/r^pGCI_{12}
1	5	29.519	0.26	0.01	5.68	29.52	0.00042	0.02159	1.00
2	10	29.524							
3	20	29.780							

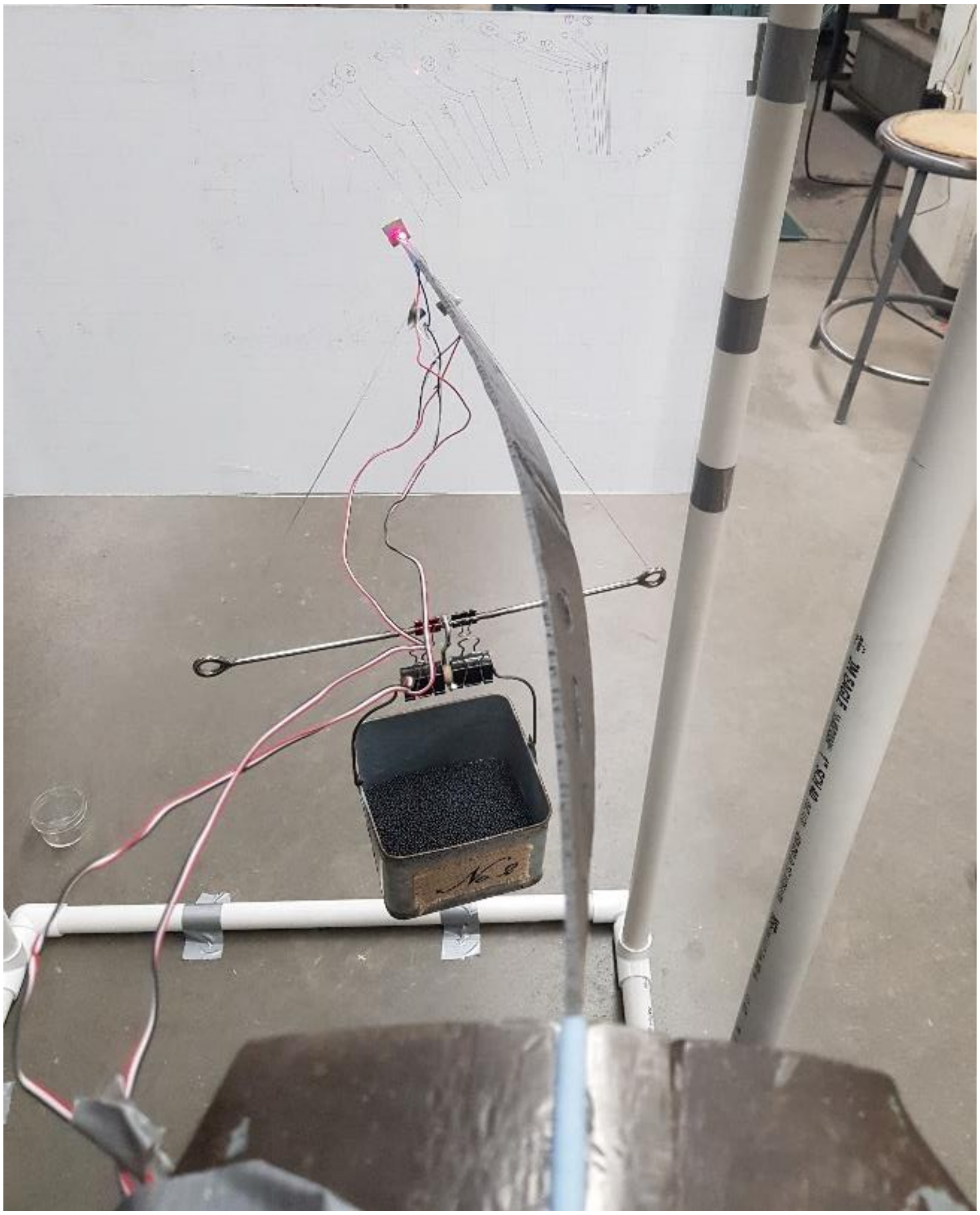

Figure 3.5: CFRP cantilever beam during loading phase

Table 3.6: Comparison of results from Eigen value and replacement stiffness

Beam Designation	Buckling load / Eigen value, N	Buckling load / replacement stiffness, N	(EigVal-repl.stiff)/EigVal*100 (%)
C100-500x75 $[0]_4$	37.71	29.59	21.53
C100-500x50 $[0]_4$	29.51	25.47	13.69
C100-500x25 $[0]_4$	15.13	14.62	3.37
C100-400x50 $[0]_4$	51.53	42.63	17.27
C100-500x25 $[90]_4$	2.48	2.51	-1.21
C100-400x50 $[90]_4$	8.25	7.94	3.75
Steel beam 316	7.85	N/A	N/A

3.5.2 Riks Analysis

Subsequent to step 1, a nonlinear post-buckling analysis was performed using Riks analysis. To account for the imperfections, notion loads were applied at the top and bottom node of the free end of the section as a couple during step 2. Direction of the notion load was based on the first mode shape of the beam and the magnitude varied from 1-2% of the corresponding buckling load. The maximum number of increments was assumed 200 and the initial, minimum and maximum arc length increment were 0.0005, 1e-35, and 1 respectively. Load vs β plots were generated by multiplying load proportionality factor (LPF) by the buckling load (Eigen value) and average twisting rotation of the section at the free end was calculated using lateral displacement of the top, middle and bottom nodes and section height.

3.6 Results and Discussion

In addition to the Eigen value and Riks analysis, the critical load causing lateral torsional buckling is calculated using replacement stiffness approach which adapts Timoshenko's solution with modified stiffness. It is valid for orthotropic beams only.

$$P_{cr} = \frac{4.013}{l^2}\sqrt{EI_\eta C} \qquad \text{Eq. (3.1)}$$

$$EI_\eta = \frac{b}{\delta_{11}} \qquad \text{Eq. (3.2)}$$

$$C = GI_t = 4\left(\frac{b}{\delta_{66}}\right) \qquad \text{Eq. (3.3)}$$

Where b is the height of section in mm, $\boldsymbol{l}$ is beam length in mm, δ_{11} and δ_{66} are elements of the compliance matrix relating curvatures K_x and K_{xy} to bending moment M_x, and torsional moment M_{xy}, respectively [32, 35].

Buckling load from replacement stiffness method (Table 3.6) is in good agreement with first Eigen value for C100-500x25 $[0]_4$, C100-500x25 $[90]_4$ and C100-400x50 $[90]_4$. They tend to be the same for l/h ratio greater than or equal to 20. However, there is a significant difference between the two buckling loads for shorter span beams (smaller l/h ratios) of 0° layups (Figure 3.5, 3.6, 3.7). In general, replacement stiffness method gives conservative results for shorter-span orthotropic beams. One reason might be that such beams are affected by lateral-distortional instability as concluded in [31] which is not taken into account in the replacement stiffness method.

Experimental results match well with Riks analysis for all beams except C100-400x50 $[90]_4$ where post-buckling stiffening happens at a higher rate when β is greater than 6 degrees. This could be due to the smaller load increments resulting in insignificant change in the angle β that is difficult to accurately measure using a regular protractor. Likewise, in Figure 3.6 to Figure 3.9 the angle β is assumed unchanged for the few initial readings as β was measured using regular protractor and small changes in angle were not captured.

A notion load equivalent to 0.5-2% of the first Eigen value was used in the Riks analysis to account for the imperfections and was applied at the top and bottom node of the free end as a couple. However, because C100-500x25 $[90]_4$ had extremely high imperfections, notion load was increased to 20%. Graphs from Riks analysis with 1% and 20% notion loads are presented in Figure 3.10.

Maximum longitudinal stress and shear stress from the nonlinear Riks analysis in the 90° layups at the onset of buckling was checked to see how close they are to the failure as such layups have very low transverse tensile and shear strengths. These were found to be $\sigma_{11,max}$=4.34 MPa, $\sigma_{12,max}$=18.7 MPa for C100-500x25 $[90]_4$ and $\sigma_{11,max}$=4.08 MPa, $\sigma_{12,max}$=12.4 MPa for C100-400x50 $[90]_4$ which are much lower than the strength in transverse tension (41 MPa) and in-plane shear (80 MPa) depicted for typical carbon FRP with 60% fiber volume fraction [8]. These figures are not expected to change drastically when the fiber volume fraction is lower. Also, in-plane shear is known to behave in a nonlinear fashion which affects the deformation more than the stresses. It would be advisable to include nonlinear in-plane shear in future work.

To capture post-buckling response, all beams were loaded beyond their first Eigen value despite significant deformations were observed at the corresponding load. Unlike a simple bifurcation problem, it is difficult to find the exact buckling load from Figure 3.6– Figure 3.11 because of the stiffening effects taking place during post-buckling response as well as imperfections in the beams.

For further investigation, a 316-steel beam 250x25x0.609 mm was tested under the same boundary and loading conditions to compare the first Eigen value and Timoshenko's solution with experimental results, Figure 3.12. Classical solution for lateral torsional buckling of isotropic cantilever beam is given by Timoshenko and Gere [34]. As shown in the figure, experimental curve flattens out when reaching Timoshenko's solution although not capturing the full response due to higher load increment after the last point on the curve causing the beam to yield and snap laterally. Overall, experimental results are consistent with ABAQUS predictions and the setup successfully served its purpose.

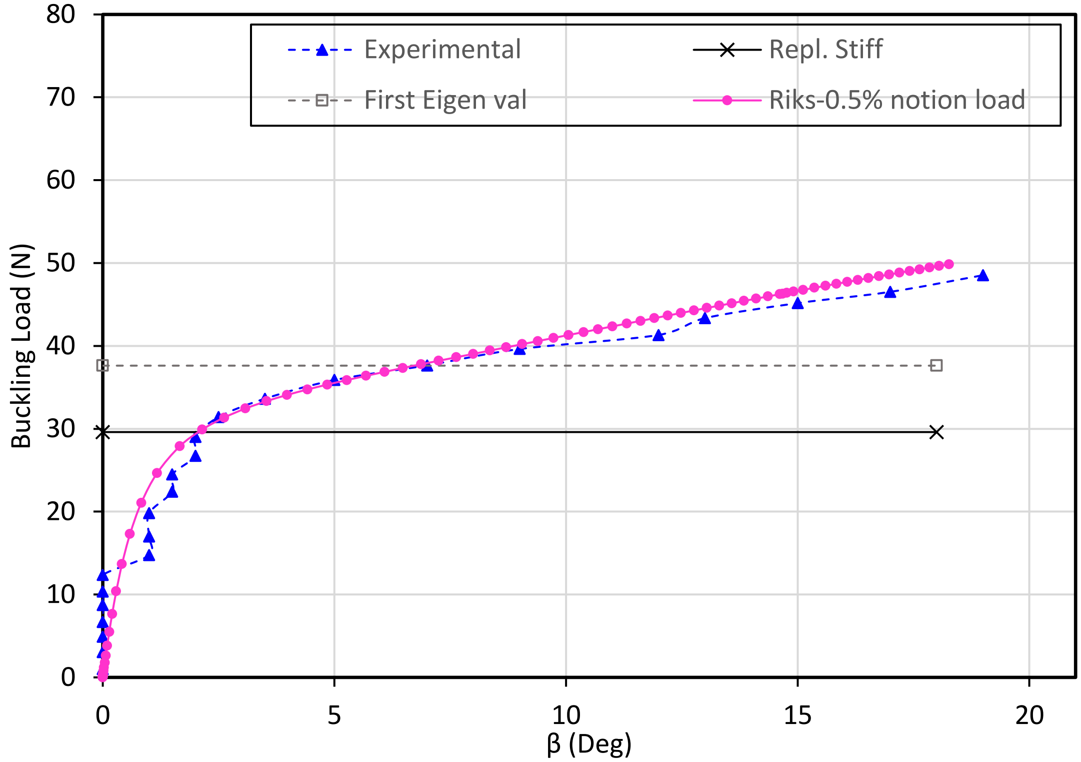

Figure 3.6: Buckling load vs β for C100-500x75 [0]$_4$

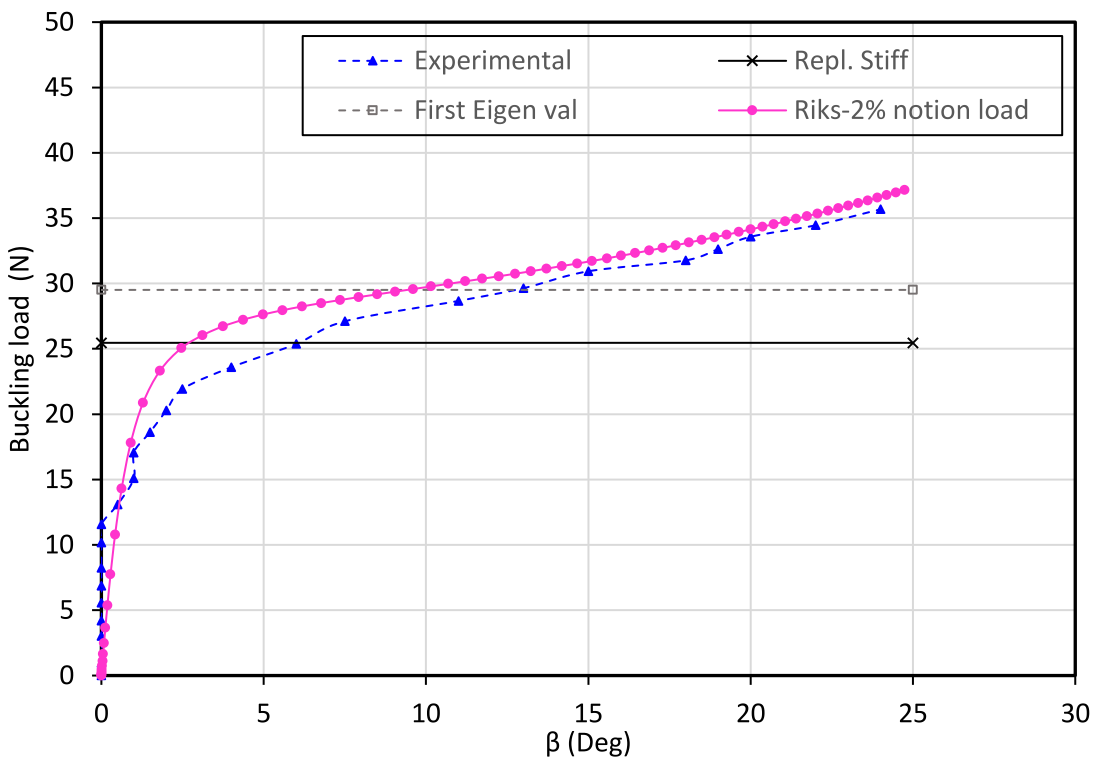

Figure 3.7: Buckling load vs β for C100-500x50 [0]$_4$

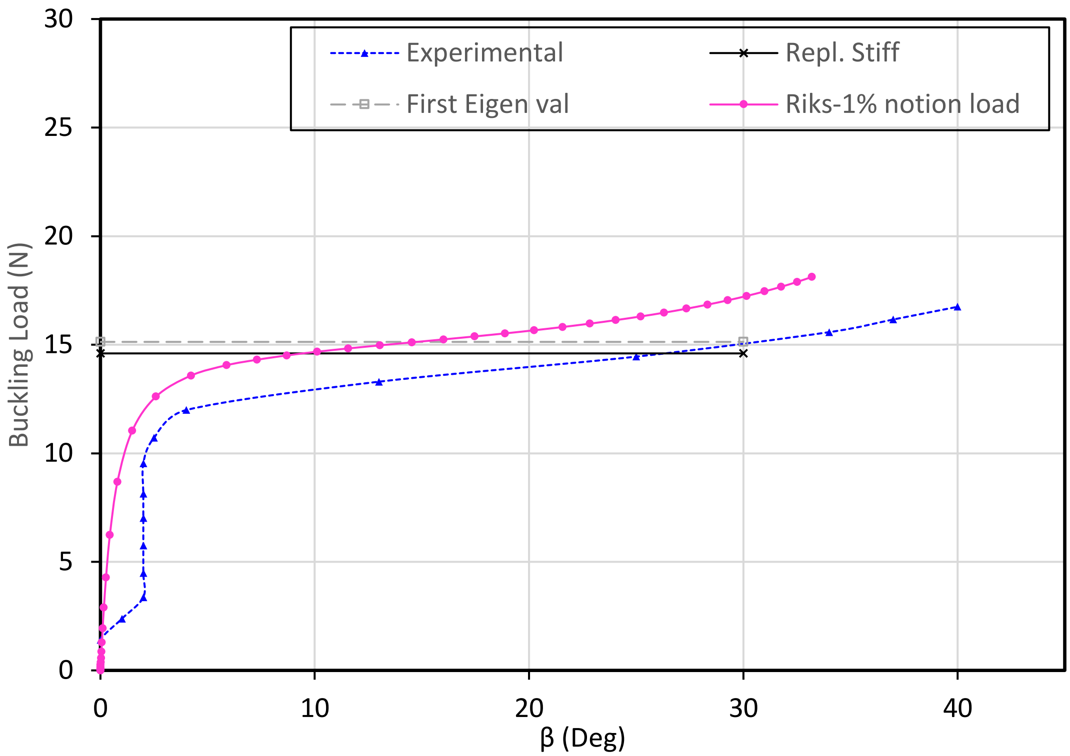

Figure 3.8: Buckling load vs β for C100-500x25 [0]4

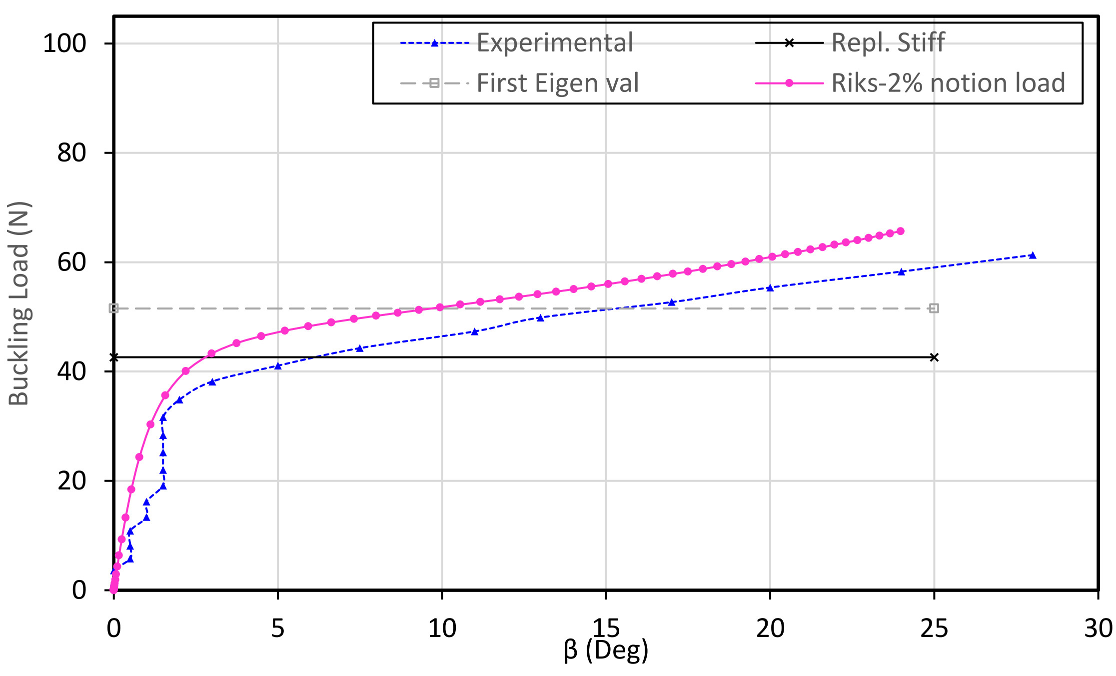

Figure 3.9: Buckling load vs β for C100-400x50 [0]4

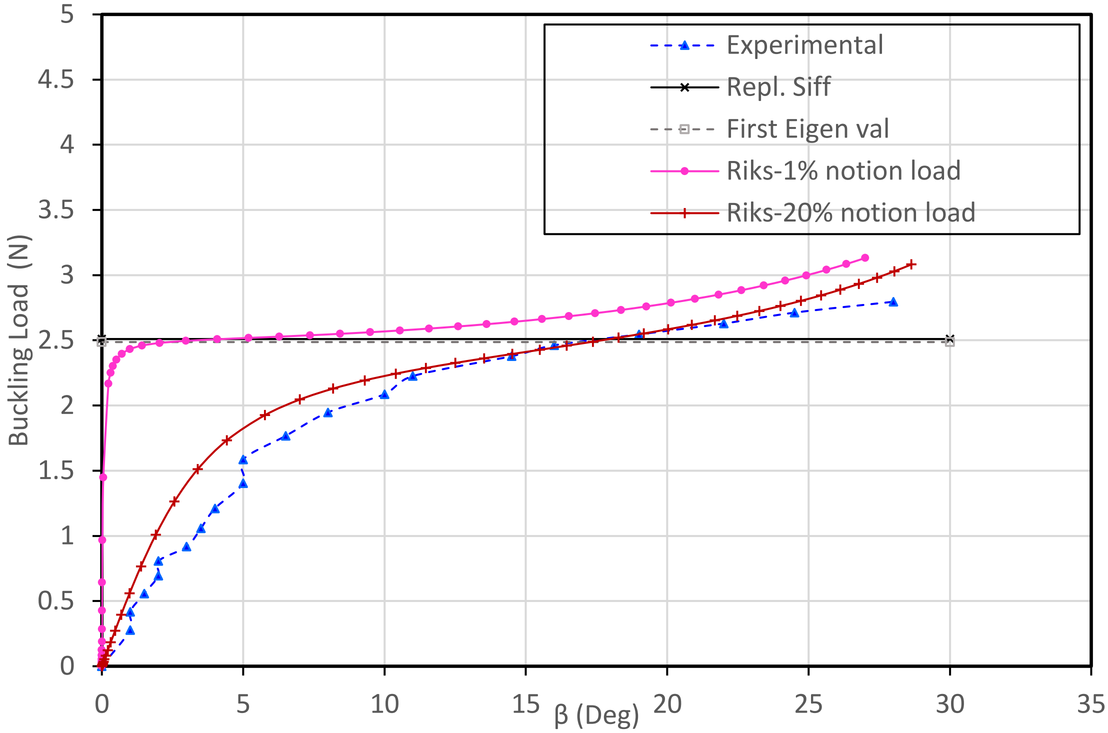

Figure 3.10: Buckling load vs β for C100-500x25 [90]$_4$ with significant imperfection

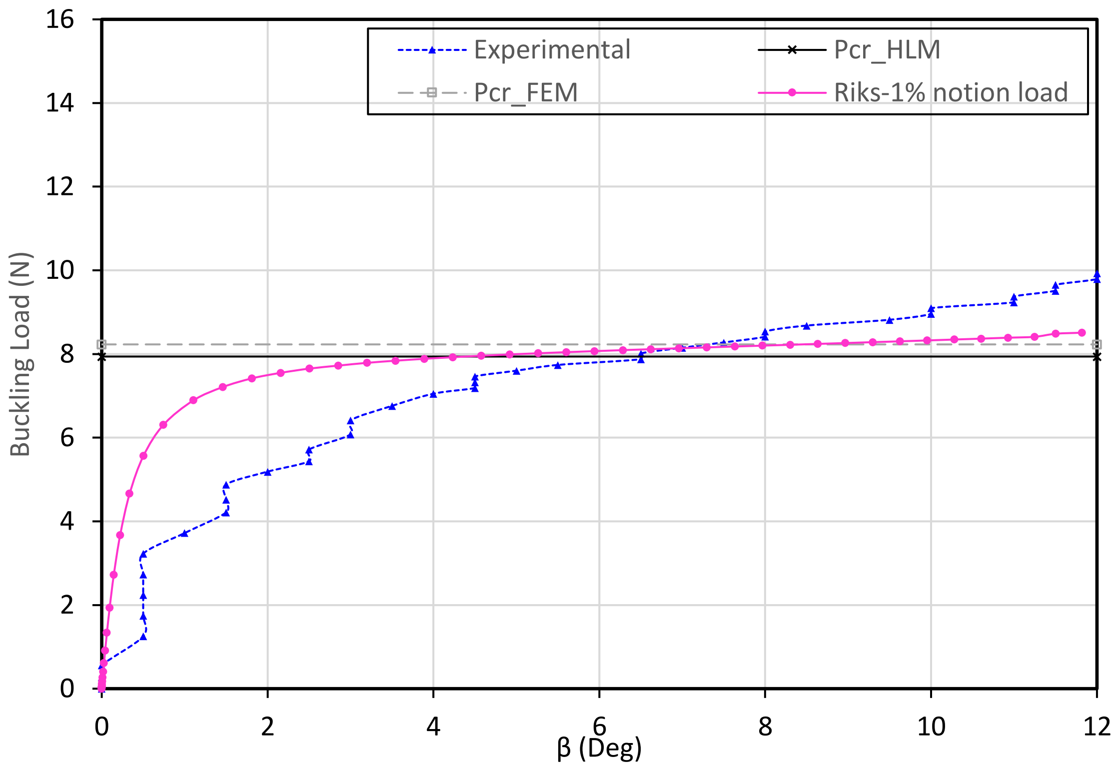

Figure 3.11: Buckling load vs β for C100-400x50 [90]$_4$

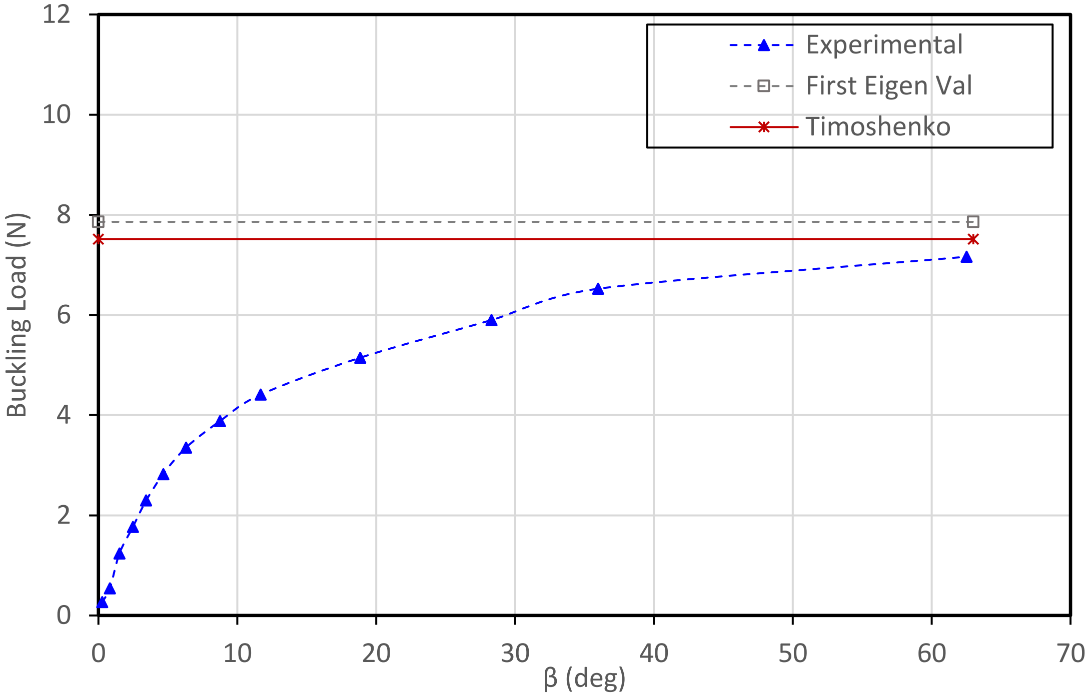

Figure 3.12: Buckling load vs β for rectangular steel beam 250x25x0.609 mm

3.7 Conclusion

There seems to be a fundamental difference in the buckling-post buckling response of 0° and 90° layups. While the 90° layups exercise some plateau curve prior to undergoing post-buckling, the 0° layups seem to switch to post-buckling response quickly without undergoing any plateau. This may be attributed to the fact that 90° beams behave like isotropic materials where the angle of twist mainly remains straight due to the fibers running in the transverse direction. On the other hand, 0° beams are very flexible transversely making them more prone to distortion or curvature change in the angle of twist at a specific section. On the other hand, the classical solution still assumes them to have a constant angle of twist per section.

Chapter 4 - Lateral Torsional Buckling Analysis of Thin-Walled Cantilever Composite Beams with Arbitrary Layups

4.1 Abstract

In this chapter, lateral torsional buckling of a rectangular cantilever beam with arbitrary layups under a single transverse load at the tip is investigated. Analytical solution is derived using classical laminated plate theory and verified both experimentally and numerically using ABAQUS. A differential equation for the lateral torsional buckling with variable coefficients is formulated using the kinematics, constitutive and equilibrium equations. The differential equation is then solved using the infinite series approach yielding closed-form solutions that favorably compares to the numerical and experimental results confirming their accuracy. The analytical solution can be easily adapted for generally anisotropic (arbitrary layup) thin-walled rectangular beams with different load and boundary conditions. As part of the experimental work, four beams with 0-degree layups and two beams with 90-degree layups each having four layers are prepared in the lab. The length to depth ratio (l/h) varied from 6.67 to 20 for the beams. Lateral and vertical displacements as well as the twisting rotation of beam section (β) is measured accurately using laser pointers for every load increment. Load vs. β plots are generated and compared with nonlinear Riks analysis results using ABAQUS. A parametric study is also conducted to investigate the effect of various parameters on the buckling response.

4.2 Introduction

Structural elements made of Fiber Reinforced Polymer (FRP) composites are now extensively used in aerospace, automotive and marine structures due to their high stiffness-to-weight ratio and corrosive resistance properties. In civil engineering structures, FRP composite elements are increasingly used due to their cost and structural efficiency. Most of the composite structural elements are thin-walled and one of the most significant advantage they offer is that mechanical properties can be optimized for specific applications [5]. For instance, in I-beam section, web shall contain laminates with +/-45 degree to increase shear resistance while flanges are made of unidirectional layups to maximize bending stiffness.

In civil engineering structures, fiber reinforced composite are mostly used for strengthening applications in the form of sheets attached to a member using epoxy. Similarly, typical pultruded structural shapes are used in lightweight industrial buildings due to their lightweight, corrosion resistance, low thermal and electrical conductivities [8]. Another application would be the All-Composite Fiber Reinforced Polymer Honeycomb Sandwich Panels which are increasingly used as full-depth bridge decks [9].

As discussed above, fiber reinforced composites are becoming more prevalent material with the advancement in fabrication process and new applications. However, their behavior is more complex because in-plane forces could cause out-of-plane deformations and bending moments could cause in-plane deformations depending on the orientation of fibers in a particular layup. As a result, design guidelines developed for conventional isotropic materials such as steel or concrete could not be applied directly [10]. Another complexity arise because of the prominent shear deformations unlike most metallic beam elements where shear deformations are significantly small. The reason for having such large shear deformations is the ratio of elastic and shear moduli (E/G) which is about four times larger than most metallic elements. Research show that shear deformations shall be considered especially for short span beams [6]. Factors affecting shear deformation depend on the length to height ratio, shape of beam section, and material properties.

As with thin-walled open section metallic elements, shear deformations due to restrained warping is another source of complication in calculations. To the best knowledge of the author, there is no formulation relating warping effects to shear, bending or twisting moments for composite beams with arbitrary layups. A considerable portion of the published work in the literature assume layups to be orthotropic; meaning that normal forces and bending moments applied along the two mutually perpendicular directions in the laminate plane do not cause shear or twisting. This assumption leads to more simplified engineering equations that are easier to solve. Likewise, some of the formulations in the literature assume layups to be either symmetrical or balanced; both leading to simplified equations. For symmetrical layups, there is no in-plane-out-of-plane coupling, which means that in-plane forces do not cause out-of-plane deformations (curvatures) and moments do not cause in-plane deformations. While for balanced laminates, there is no extension shear coupling.

Design of thin-walled composite members either open or closed section is often controlled by stability consideration mainly due to slenderness effects. Hence, for thin-walled slender composite beams, lateral torsional buckling is the dominant failure mode regardless of fiber orientation.

Ahmadi and Rasheed [17] presented a semi-analytical approach to determine critical load for a simply supported thin-walled composite beam with lateral torsional buckling as dominant failure mode. Good agreement between the semi-analytical solution and finite element results is reported by the authors. Symmetric and anti-symmetric balanced angle-ply laminate of 20 degree was found to have the highest buckling load in its category. Vo and Lee [20] Developed a model to analyze flexural, torsional and flexural torsional buckling of thin-walled composite box beams under axial load. Their model is based on classical laminate plate theory which takes into account flexural torsional coupling for any arbitrary layups and different boundary conditions. This research is devoted to determine critical load of thin-walled rectangular beam with arbitrary layups also called generally anisotropic beams. The critical load here refers to the load causing lateral torsional buckling in the beam.

4.3 Problem Statement

Obtain a closed form analytical solution for lateral torsional buckling problem of thin-walled rectangular section cantilever beam with arbitrary layups.

4.4 Formulation

A model similar to H. Ahmadi and H. A. Rasheed [19] is adopted with the distinction that in-plane shear deformations are also taken into account. Out-of-plane shear deformations are ignored due to small thickness to height ratio of the beam. A differential equation for lateral torsional buckling with variable coefficients is formulated using the kinematics, constitutive and equilibrium equations. The equation is then solved using the infinite series approach yielding closed-form solutions that favorably compare to the numerical and experimental results confirming their accuracy. The solution can be easily adapted for generally anisotropic (arbitrary layup) thin-walled rectangular beams with different load and boundary conditions. The following sign convention is followed for forces, bending and twist moments.

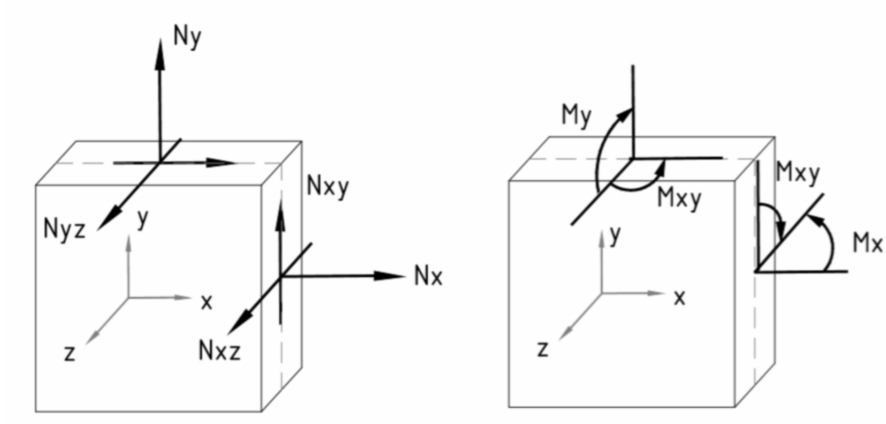

Figure 4.1: Direction of positive moment, shear and axial forces

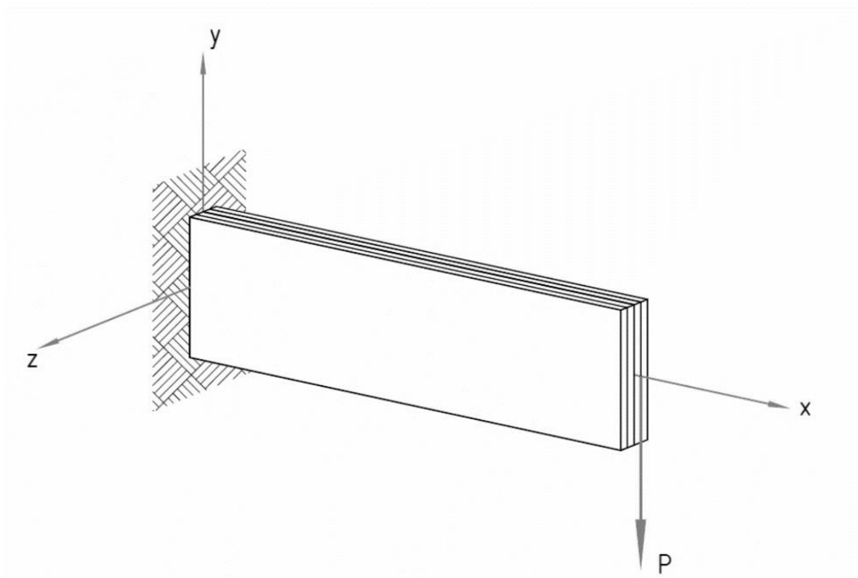

Figure 4.2: Rectangular section cantilever beam with tip force

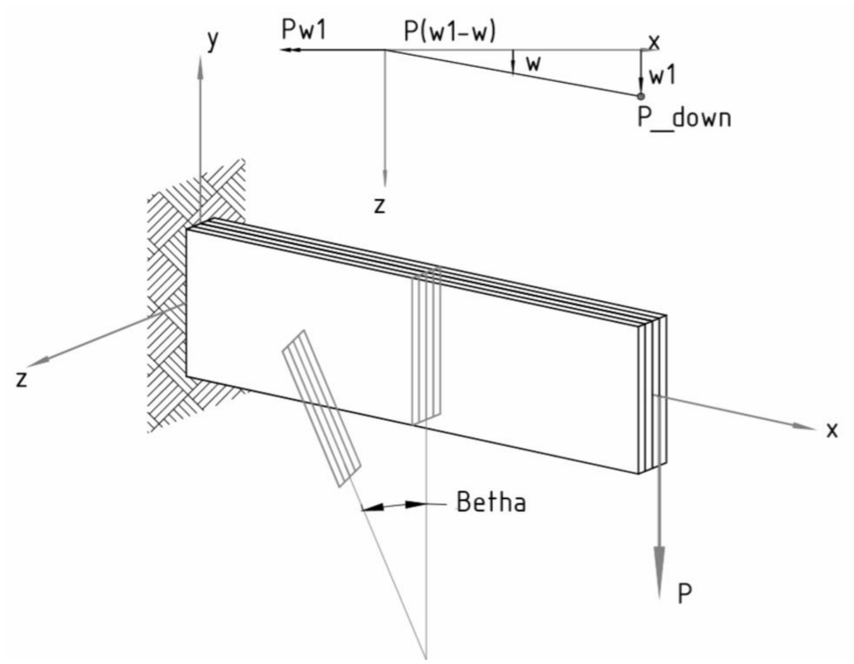

Figure 4.3: Counterclockwise lateral torsional buckling of cantilever beam

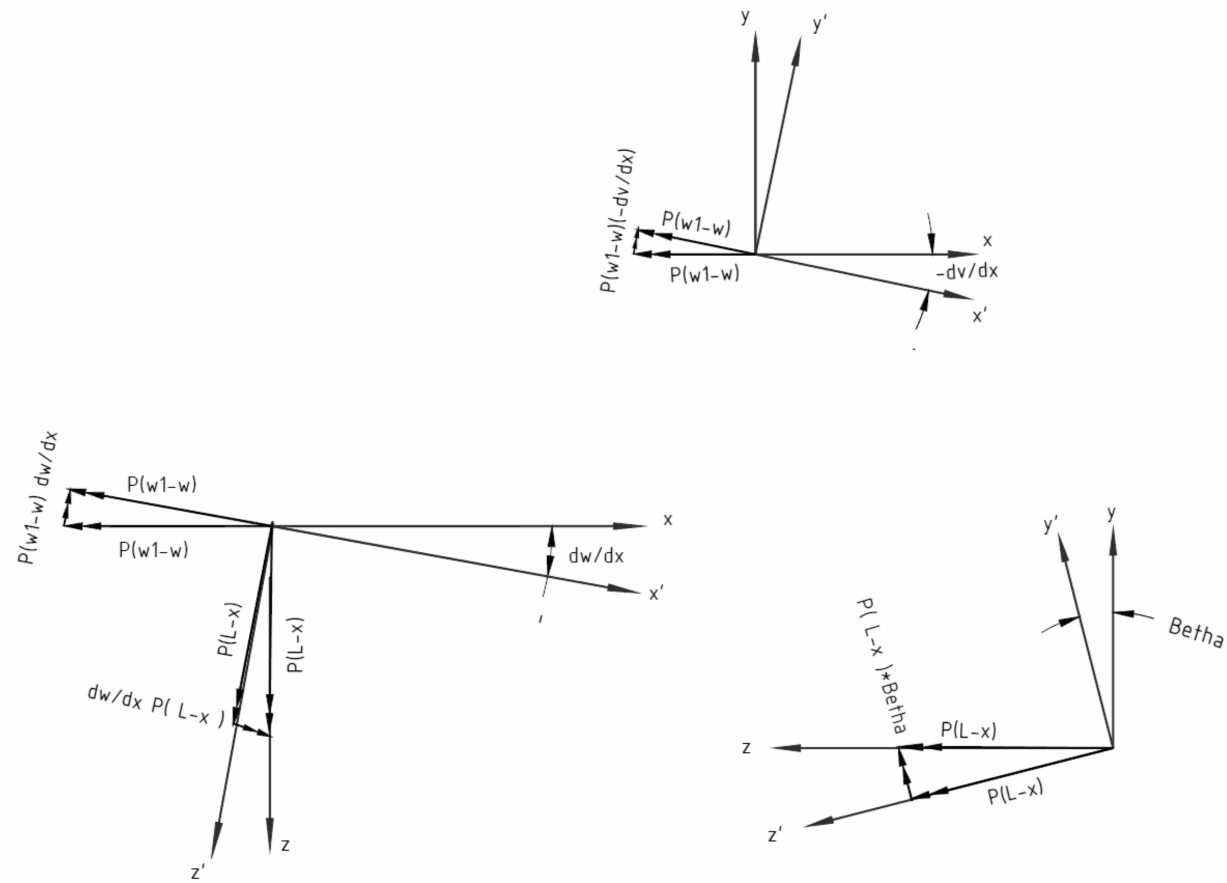

Figure 4.4: Internal moment components about original and deformed axes

Using classical laminate plate theory, the stiffness matrix for a composite laminate is:

$$\begin{Bmatrix} Nx \\ Ny \\ Nxy \\ Mx \\ My \\ Mxy \end{Bmatrix} = \begin{bmatrix} A11 & A12 & A16 & B11 & B12 & B16 \\ A12 & A22 & A26 & B12 & B22 & B26 \\ A16 & A26 & A66 & B16 & B26 & B66 \\ B11 & B12 & B16 & D11 & D12 & D16 \\ B12 & B22 & B26 & D12 & D22 & D26 \\ B16 & B26 & B66 & D16 & D26 & D66 \end{bmatrix} \begin{Bmatrix} \varepsilon x \\ \varepsilon y \\ \gamma xy \\ Kx \\ Ky \\ Kxy \end{Bmatrix} \qquad \text{Eq. (4.1)}$$

The coefficients A_{ij}, B_{ij} and D_{ij} are functions of the thickness, stacking sequence, fiber orientation and materials properties of the layers. A_{ij} relates in-plane strains to in plane forces, B_{ij} relates in-plane strains and curvatures to moments and in-plane forces respectively, and D_{ij} relates curvatures to bending moments. $[B]$ is called bending-extension coupling matrix while $[D]$ is called bending stiffness matrix.

For a cantilever beam with the load applied at the tip the force displacement relationship becomes

$$\begin{Bmatrix} Nx = 0 \\ Ny = 0 \\ Nxy = \dfrac{P}{h} * h \\ Mx * h \\ My = 0 \\ Mxy * h \end{Bmatrix} \qquad \text{Eq. (4.2)}$$

$$= h \begin{bmatrix} A11 & A12 & A16 & B11 & B12 & B16 \\ A12 & A22 & A26 & B12 & B22 & B26 \\ A16 & A26 & A66 & B16 & B26 & B66 \\ B11 & B12 & B16 & D11 & D12 & D16 \\ B12 & B22 & B26 & D12 & D22 & D26 \\ B16 & B26 & B66 & D16 & D26 & D66 \end{bmatrix} \begin{Bmatrix} \varepsilon x \\ \varepsilon y \\ \gamma xy \\ Kx \\ Ky \\ Kxy \end{Bmatrix}$$

Where h is beam depth or section height and P is the applied load along negative y-axis. For the zero terms on the left hand side of Eq. (4.2), one can write

$$\begin{bmatrix} A11 & A12 & B12 \\ A12 & A22 & B22 \\ B12 & B22 & D22 \end{bmatrix} \begin{Bmatrix} \varepsilon x \\ \varepsilon y \\ Ky \end{Bmatrix} + \begin{bmatrix} A16 & B11 & B16 \\ A26 & B12 & B26 \\ B26 & D12 & D26 \end{bmatrix} \begin{Bmatrix} \gamma xy \\ Kx \\ Ky \end{Bmatrix} = \begin{Bmatrix} 0 \\ 0 \\ 0 \end{Bmatrix} \qquad \text{Eq. (4.3)}$$

Assuming $\begin{bmatrix} A11 & A12 & B12 \\ A12 & A22 & B22 \\ B12 & B22 & D22 \end{bmatrix} = [Q]$ and $\begin{bmatrix} A16 & B11 & B16 \\ A26 & B12 & B26 \\ B26 & D12 & D26 \end{bmatrix} = [R]$

$$[Q] \begin{Bmatrix} \varepsilon x \\ \varepsilon y \\ Ky \end{Bmatrix} + [R] \begin{Bmatrix} \gamma xy \\ Kx \\ Kxy \end{Bmatrix} = \begin{Bmatrix} 0 \\ 0 \\ 0 \end{Bmatrix} \qquad \text{Eq. (4.4)}$$

$\begin{Bmatrix} \varepsilon x \\ \varepsilon y \\ Ky \end{Bmatrix}$ in terms of $\begin{Bmatrix} \gamma xy \\ Kx \\ Kxy \end{Bmatrix}$ equals

$$\begin{Bmatrix} \varepsilon x \\ \varepsilon y \\ Ky \end{Bmatrix} = - \begin{bmatrix} A11 & A12 & B12 \\ A12 & A22 & B22 \\ B12 & B22 & D22 \end{bmatrix}^{-1} \begin{bmatrix} A16 & B11 & B16 \\ A26 & B12 & B26 \\ B26 & D12 & D26 \end{bmatrix} \begin{Bmatrix} \gamma xy \\ Kx \\ Kxy \end{Bmatrix}$$

or Eq. (4.5)

$$\begin{Bmatrix} \varepsilon x \\ \varepsilon y \\ Ky \end{Bmatrix} = -[Q]^{-1}[R] \begin{Bmatrix} \gamma xy \\ Kx \\ Kxy \end{Bmatrix}$$

For the nonzero terms of Eq. (4.2) and substituting Eq. (4.5)

$$\begin{Bmatrix} P \\ Mx * h \\ Mxy * h \end{Bmatrix} = h \begin{bmatrix} A66 & B26 & B66 \\ B16 & D11 & D16 \\ B66 & D16 & D66 \end{bmatrix} \begin{Bmatrix} \gamma xy \\ Kx \\ Kxy \end{Bmatrix} - h \begin{bmatrix} A16 & A26 & B26 \\ B11 & B12 & D12 \\ B16 & B26 & D26 \end{bmatrix} [Q]^{-1}[R] \begin{Bmatrix} \gamma xy \\ Kx \\ Kxy \end{Bmatrix} \qquad \text{Eq. (4.6)}$$

Assuming $\begin{bmatrix} A66 & B26 & B66 \\ B16 & D11 & D16 \\ B66 & D16 & D66 \end{bmatrix} = [S]$ and $\begin{bmatrix} A16 & A26 & B26 \\ B11 & B12 & D12 \\ B16 & B26 & D26 \end{bmatrix} = [R]^T$ Eq. (4.6) can be written as

$$\begin{Bmatrix} P \\ Mx*h \\ Mxy*h \end{Bmatrix} = h\,[S - R^T Q^{-1} R] \begin{Bmatrix} \gamma xy \\ Kx \\ Kxy \end{Bmatrix} \qquad \text{Eq. (4.7)}$$

[2]Replacing $[S - R^T Q^{-1} R]$ in the above equation by $\begin{bmatrix} Js & JDsy & JDst \\ JDsy & Dy & Dyt \\ JDst & Dyt & Dt \end{bmatrix}$

$$\begin{Bmatrix} P \\ Mx*h \\ Mxy*h \end{Bmatrix} = h \begin{bmatrix} Js & JDsy & JDst \\ JDsy & Dy & Dyt \\ JDst & Dyt & Dt \end{bmatrix} \begin{Bmatrix} \gamma xy \\ Kx \\ Kxy \end{Bmatrix} \qquad \text{Eq. (4.8)}$$

Writing the above equation in structural coordinate system[3]

$$\begin{Bmatrix} -P \\ My' \\ -M_T \end{Bmatrix} = h \begin{bmatrix} Js & JDsy & 2JDst \\ JDsy & Dy & 2Dyt \\ 2JDst & 2Dyt & 4Dt \end{bmatrix} \begin{Bmatrix} \gamma xy \\ -\dfrac{d^2w}{dx^2} \\ -\beta' \end{Bmatrix} \qquad \text{Eq. (4.9)}$$

Note that $My' = M_x * h$ and $M_T = -2M_{xy} * h$.

$$\frac{-P}{h} = \left(J_s \gamma_{xy} - JD_{sy} \frac{d^2w}{dx^2} - 2\beta' JD_{st} \right) \qquad \text{Eq. (4.10)}$$

$$\gamma_{xy} = \frac{{}^{-P}\!/_{h} + JD_{sy} \dfrac{d^2w}{dx^2} + 2\beta' JD_{st}}{J_s} \qquad \text{Eq. (4.11)}$$

---

2 Notation for $\begin{bmatrix} Js & JDsy & JDst \\ JDsy & Dy & Dyt \\ JDst & Dyt & Dt \end{bmatrix}$ is followed from [17] with no changes. Note that Js for example is one term not a multiplication of J and s, same is true for all other elements. The matrix represents stiffnesses associated with: Js (shear), $JDsy$ (shear-bending), $JDst$ (shear-torsion), Dy (bending), Dyt (bending-torsion), Dt (torsion).

3 Everything before Eq. (4.8) is based composite coordinate system and notation

$$\frac{M_{y'}}{h} = JD_{sy}\left(\frac{-P/_{h} + JD_{sy}\frac{d^2w}{dx^2} + 2\beta' JD_{st}}{J_s}\right) - D_y\frac{d^2w}{dx^2} - 2\beta' D_{yt} \qquad \text{Eq. (4.12)}$$

Figure 4.4 shows internal moments about original and deformed axes. The direction of the moment in the figure is based on the right hand rule. However, in the derivation, the decision whether a moment is positive or negative is based on its curvature not the arrow in the figure. For example: at a point $(L-x)$ from the free end, the correct equation for the twisting moment is $M_T = -dw/dx\ P(L-x) + P(w1-w)$. However, it should have been $M_T = \frac{dw}{dx}P(L-x) - P(w1-w)$ if it was to follow the sign in the figure because the arrow for the first term is directed along positive x-axis and negative x-axis for the second term which leads to incorrect twisting moment relation.

$$My' = -P(L-x)\beta \qquad \text{Eq. (4.13)}$$

Substitute My' into Eq. (4.12)

$$\frac{-P(L-x)\beta}{h} + \frac{JD_{sy}}{Js}\frac{P}{h} + 2\left(D_{yt} - \frac{JD_{sy}JD_{st}}{J_s}\right)\beta' = \left(\frac{JD_{sy}^2}{J_s} - D_y\right)\frac{d^2w}{dx^2} \qquad \text{Eq. (4.14)}$$

$$-\frac{M_T}{h} = 2JD_{st}\left(\frac{-P/_{h} + JD_{sy}\frac{d^2w}{dx^2} + 2\beta' JD_{st}}{J_s}\right) - 2D_{yt}\frac{d^2w}{dx^2} - 4D_t\beta' \qquad \text{Eq. (4.15)}$$

The twisting moment from Figure 4.4 is equal to

$$M_T = -\frac{dw}{dx}P(L-x) + P(w1-w) \quad \text{Eq. (4.16)}$$

Substituting M_T into Eq. (4.17) and reorganizing the equation becomes

$$\frac{dw}{dx}\frac{P(L-x)}{h} - \frac{P(w1-w)}{h} + \frac{2JD_{st}}{J_s}\frac{P}{h} + 4\left(D_t - \frac{JD_{st}^2}{J_s}\right)\beta' = 2\left(\frac{JD_{sy}JD_{st}}{J_s} - D_{yt}\right)\frac{d^2w}{dx^2} \quad \text{Eq. (4.18)}$$

Equating Eq. (4.19) and (4.17)

$$\frac{-P(L-x)\beta}{Ah} + \frac{JD_{sy}}{Js}\frac{P}{Ah} - \frac{B}{A}\beta' = \frac{dw}{dx}\frac{P(L-x)}{Bh} - \frac{P(w1-w)}{Bh} + 2\frac{JD_{st}}{Js}\frac{P}{Bh} - \frac{C}{B}\beta' \quad \text{Eq. (4.20)}$$

Where $A = \left(\frac{JD_{sy}^2}{J_s} - D_y\right)$, $B = 2\left(\frac{JD_{sy}JD_{st}}{J_s} - D_{yt}\right)$ and $C = 4\left(\frac{JD_{st}^2}{J_s} - D_t\right)$

Differentiating Eq. (4.18) with respect to x

$$-\frac{P(L-x)\beta'}{Ah} + \frac{P\beta}{Ah} - \frac{B}{A}\beta'' = \frac{d^2w}{dx^2}\frac{P(L-x)}{Bh} - \frac{C}{B}\beta'' \quad \text{Eq. (4.21)}$$

Solving the above equation for $\frac{d^2w}{dx^2}$

$$\frac{d^2w}{dx^2} = -\frac{B\beta'}{A} + \frac{B\beta}{A(L-x)} - \frac{B^2h\beta''}{AP(L-x)} + \frac{Ch\beta''}{P(L-x)}$$

Equating Eq. (4.14) and (4.21) and reorganizing the resulting equation

$$\beta''\left(Ch - \frac{B^2h}{A}\right) + \beta\left(\frac{B}{A}P + \frac{P^2(L-x)^2}{Ah}\right) - \frac{JD_{sy}}{Js}\ \frac{P^2(L-x)}{Ah} = 0 \quad \text{Eq. (4.22)}$$

Multiplying Eq. (4.22) by Ah yields

$$\beta''(AC - B^2)h^2 + \beta[hBP + P^2(L-x)^2] - \frac{JD_{sy}}{J_s}P^2(L-x) = 0$$

Note that the coefficient $\frac{JD_{sy}}{J_s}P^2$of the last term is extremely small for all possible combination of fiber orientations and various range of l/h ratios, therefore it is neglected. Assuming $E = (AC - B^2)$, the final differential equation with non-constant coefficients become

$$\beta'' + \beta\left(\frac{|B|}{Eh}P + \frac{P^2(L-x)^2}{Eh^2}\right) = 0 \qquad \text{Eq. (4.23)}$$

To make the equation work for both clockwise and counterclockwise buckling, absolute value of B shall be considered. This is due to the fact that both configurations lead to exactly the same equation except the sign of the first term in the bracket which is positive for counterclockwise buckling and negative otherwise.

4.5 Solution of the Lateral Torsional Buckling Equation

The final differential equation with non-constant coefficients (Eq. (4.23) is solved using infinite series approach.

Assuming

$$V = \frac{|B|}{Eh}P\,, \qquad W = \frac{P^2}{Eh^2} \quad , \quad (L-x) = X$$

The equation becomes

$$\beta'' + \beta(V + WX^2) = 0 \qquad \text{Eq. (4.24)}$$

The solution is assumed to be of the form

$$\beta = \sum_{n=0}^{\alpha} a_n X^n$$

Hence,

$$\beta' = \sum_{n=1}^{\alpha} n a_n X^{n-1}$$

$$\beta'' = \sum_{n=2}^{\alpha} n(n-1)a_n X^{n-2}$$

$$\sum_{n=2}^{\alpha} n(n-1)a_n X^{n-2} + \sum_{n=0}^{\alpha} a_n X^n \,(V + WX^2) = 0 \qquad \text{Eq. (4.25)}$$

$$\sum_{n=2}^{\alpha} n(n-1)a_n X^{n-2} + V\sum_{n=0}^{\alpha} a_n X^n + W\sum_{n=0}^{\alpha} a_n X^{n+2} = 0$$

Replace $n \to n+2$ and $n \to n-2$ in the first and last terms of the above equation respectively

$$\sum_{n+2=2}^{\alpha} (n+2)(n+2-1)a_{n+2} X^{n+2-2} + V\sum_{n=0}^{\alpha} a_n X^n + W\sum_{n-2=0}^{\alpha} a_{n-2} X^{n-2+2} = 0$$

$$\sum_{n=0}^{\alpha} (n+2)(n+1)a_{n+2} X^{n} + V\sum_{n=0}^{\alpha} a_n X^n + W\sum_{n=2}^{\alpha} a_{n-2} X^{n} = 0$$

For $n = 0$ and $n = 1$ for the first and second term in the latter equation

First term of the series: $a_0 = 2a_2 \qquad a_1 = 6a_3 X$

Second term of the series: $a_0 = Va_0 \qquad a_1 = Va_1 X$

$$2a_2 + 6a_3 X + Va_0 + Va_1 X + \sum_{n=2}^{\alpha} [(n+2)(n+1)a_{n+2} + Wa_{n-2} + Va_n]X^n = 0 \qquad \text{Eq. (4.26)}$$

$2a_2 + Va_0 \equiv 0\,; \quad \rightarrow$ $\boxed{a_2 = -\frac{Va_0}{2}}$

$(6a_3 + Va_1)X \equiv 0\,; \quad \rightarrow$ $\boxed{a_3 = -\frac{Va_1}{6}}$

$$(n+2)(n+1)a_{n+2} + Va_n + Wa_{n-2} \equiv 0 \ ; \ \rightarrow \quad \boxed{a_{n+2} = -\frac{Wa_{n-2} + Va_n}{(n+2)(n+1)}}$$

$$\beta(X) = \sum_{n=0}^{\alpha} a_n X^n$$

$$= a_0 + a_1X + a_2X^2 + a_3X^3 + a_4X^4 \qquad \text{Eq. (4.27)}$$

$$+ a_5X^5 + \ldots a_nX^n$$

$$\beta'(X) = a_1 + 2a_2X + 3a_3X^2 + 4a_4X^3 + 5a_5X^4 + \ldots n\, a_nX^{n-1} \qquad \text{Eq. (4.28)}$$

Applying the boundary condition

$$\beta'(X=0) = 0 \quad \rightarrow \ a_1 = 0$$

Because a_3 is a function of a_1; hence $a_3 = 0$

$n = 2$ $$a_4 = -\frac{Wa_0 + Va_2}{3 * 4}$$

$n = 3$ $$a_5 = -\frac{Wa_1 + Va_3}{5 * 4} = 0$$

$n = 4$ $$a_6 = -\frac{Wa_2 + Va_4}{6 * 5}$$

$n = 5$ $$a_7 = -\frac{Wa_3 + Va_5}{7 * 6} = 0$$

$n = 6$ $$a_8 = -\frac{Wa_4 + Va_6}{8 * 7}$$

. .
. .
. .

$n = 32$ $\quad\quad\quad\quad$ $a_{34} = -\dfrac{Wa_{28} + Va_{30}}{32 * 31}$

$$\beta(X = L) = 0 = a_0 + a_2L^2 + a_4L^4 + a_6L^6 + \ldots a_{32}L^{32} \qquad \text{Eq. (4.29)}$$

The series tend to converge at the 16th term i.e., $a_{32}L^{32}$. To confirm this finding, the series was further extended to $a_{50}L^{50}$ and the contribution of the terms between $a_{32}L^{32}$ and $a_{50}L^{50}$ became practically zero regardless of the layup stacking sequence and properties. The series is thus considered fully converged at the 16th term and the solution is called as closed form solution based on the current finding. However, further verification of the accumulative contribution of higher order terms beyond the 16th term is deferred to future work.

The coefficients of Eq. (4.29) are all functions of a_0; therefore, it can be taken as a common factor. Knowing that W and V are function of P, Eq. (4.29) could be solved using Excel Goal Seek function for the critical load causing lateral torsional buckling in the beam.

4.6 Finite Element Modeling

Finite Element Analysis was performed in ABAQUS. Conventional shell type planar element is used and the buckling load is calculated from linear perturbation. A unit load is applied at the shear center of the free end and the corresponding first Eigen value gives the critical lateral torsional buckling for the beam. S8R element has been used which is recommended for doubly curved thick shell elements. Grid Convergence Index (GCI) analysis according to [36] is performed to investigate mesh refinement effect on the critical load (Table 4.1). An element size of 5 mm was selected for the beams considered. A step-by-step procedure to model rectangular and I-section beam is provided in Appendix A. Analytical and ABAQUS results are reported in the subsequent section for Carbon Fiber Reinforced Polymer (CFRP) and Glass Fiber Reinforced Polymer (GFRP).

Table 4.1: Rectangular CFRP Beam[4] 500x50mm (30/-40/50/-60) Grid Convergence Index (GCI) Analysis

Mesh	Element Size (mm)	Critical Buckling Load, P_{cr}, (N)	f_3-f_2	f_2-f_1	p	f_h=0	GCI_{12}	GCI_{23}	GCI_{23} /$r^p GCI_{12}$
1	2.5	0.13182	1.3E-4	3E-5	2.12	0.13	0.00853	0.036982	1.00
2	5	0.13185							
3	10	0.13198							

Table 4.2: Properties of CFRP laminates prepared in lab

Young Modulus at fiber direction, EL	57488	MPa
Young Modulus at Transverse direction, ET	4198	MPa
Poisson's ratio, v_{LT}	0.119	
Poisson's ratio, v_{TL}	0.00869	
Shear Modulus, G12	2026	MPa
Shear Modulus, G13	2026	MPa
Shear Modulus, G23	2035	MPa

4 Thickness of 0.1mm has been assumed for each layup making the total thickness 0.4mm for each laminate. Beam properties are reported in Table 4.3.

Table 4.3: Properties of CFRP laminates with arbitrary layups

Young Modulus at fiber direction, EL	142730	MPa
Young Modulus at Tranverse direction, ET	13790	MPa
Poisson's ratio, vLT	0.3	
Poisson's ratio, vTL	0.028985	
Shear Modulus, G12	4640	MPa
Shear Modulus, G13	4640	MPa
Shear Modulus, G23	3030	MPa

Table 4.4: Properties of GFRP laminates with arbitrary layups

Young Modulus at fiber direction, EL	45000	MPa
Young Modulus at Tranverse direction, ET	12000	MPa
Poisson's ratio, vLT	0.28	
Poisson's ratio, vTL	0.074667	
Shear Modulus, G12	5500	MPa
Shear Modulus, G13	5500	MPa
Shear Modulus, G23	4950	MPa

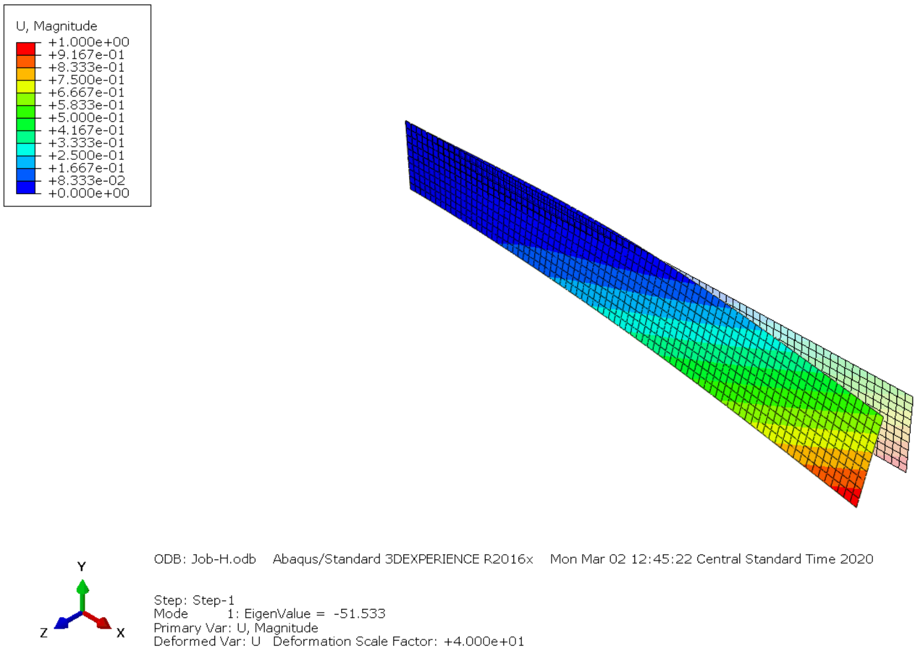

Figure 4.5: Deformed shape of C100-400x50 mm [0]4 with the Eigen Value of 51.533 N

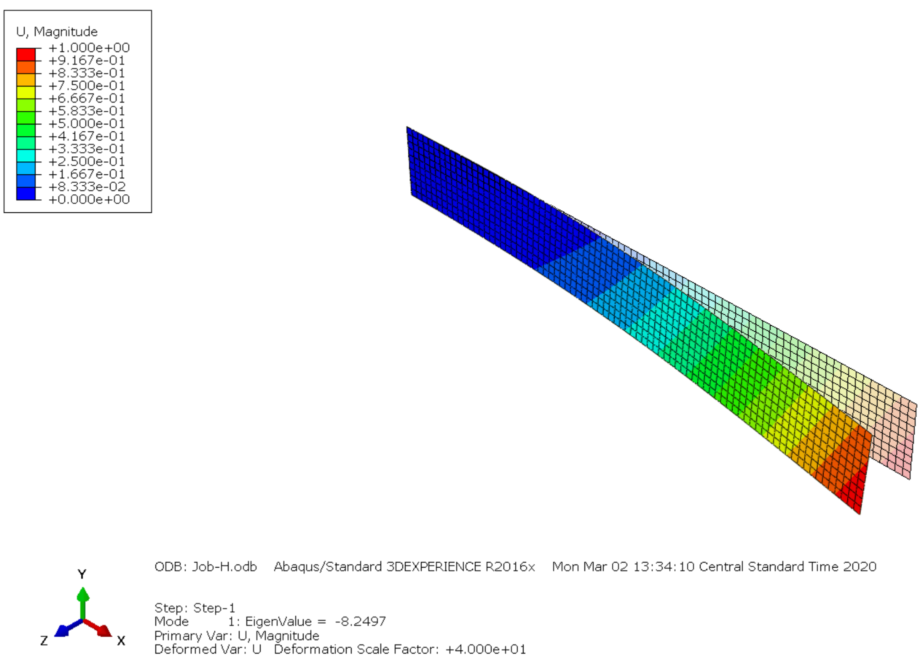

Figure 4.6: Deformed shape of C100-400x50 mm [90]4 with the Eigen Value of 8.249 N

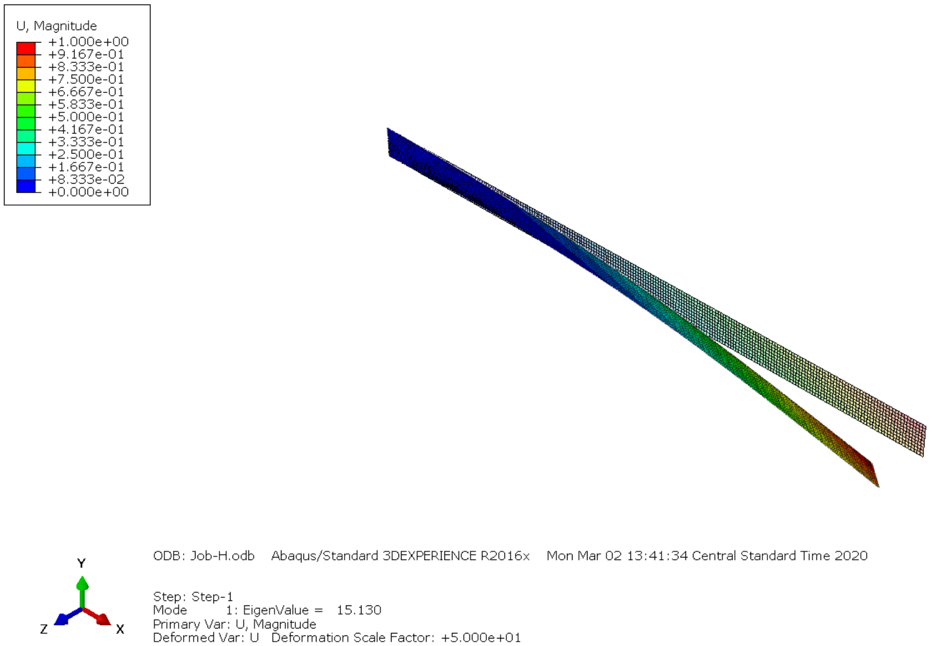

Figure 4.7: Deformed shape of C100-500x25 mm [0]4 with the Eigen Value of 15.130 N

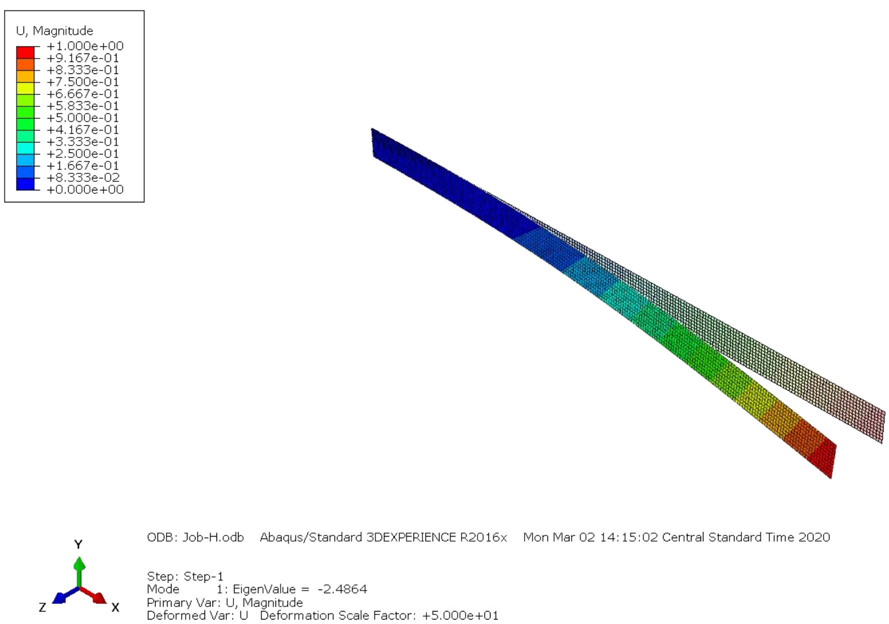

Figure 4.8: Deformed shape of C100-500x25 mm [90]4 with the Eigen Value of 2.486 N

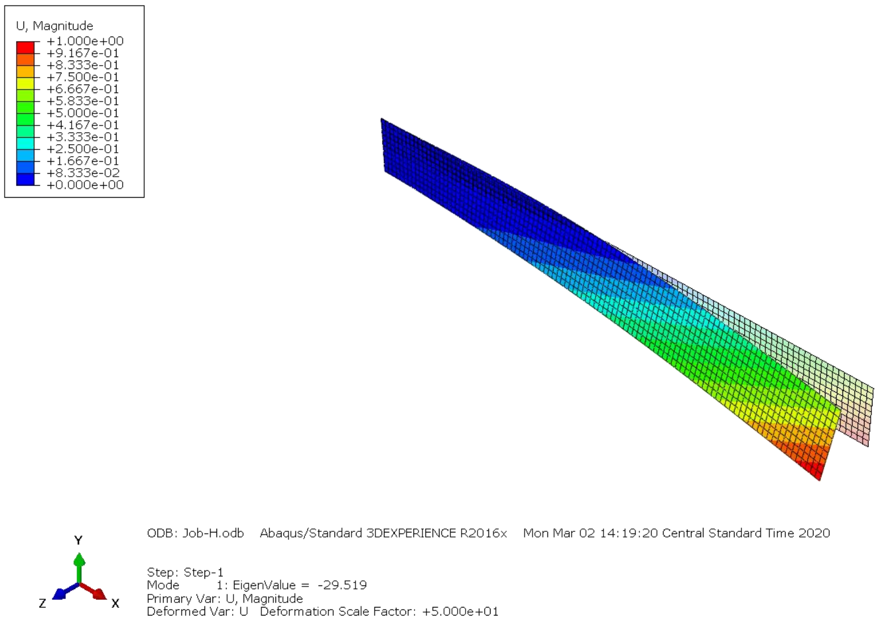

Figure 4.9: Deformed shape of C100-500x50 mm [0]4 with the Eigen Value of 29.519 N

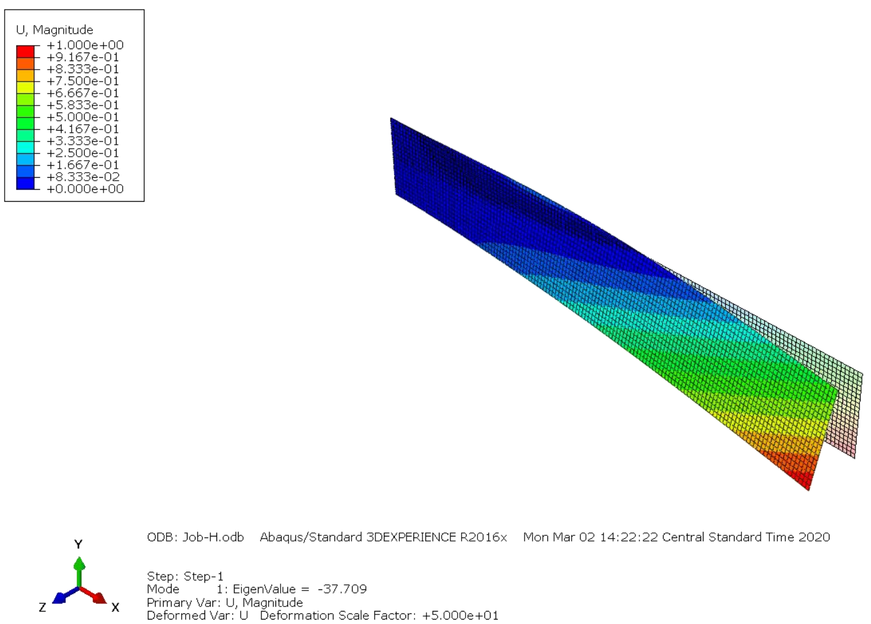

Figure 4.10: Deformed shape of C100-500x75 mm [0]4 with the Eigen Value of 37.709 N

4.7 Results and Discussion

Analytical and finite element results for Carbon Fiber Reinforced Polymer (CFRP) and Glass Fiber Reinforced Polymer (GFRP) laminates with arbitrary layups for a cantilever beam are presented in Figure 4.11. The section was rectangular with a length to depth ration (l/h) of 10, i.e., height=50 mm, length=500 mm. No warping stresses were considered.

In addition to the laminates with arbitrary layups, buckling load using Eq. (4.29) was calculated for the six CFRP beams manufactured in laboratory with 0° and 90° fiber orientations and explained in Chapter 3. Experimental results along with pre-post buckling responses have been presented in Figure 3.6-Figure 3.11. A comparison between finite element results and that of Eq. (4.29) is given in the following table.

Table 4.5: ABAQUS / Numerical and theoretical buckling load using Eq. (4.29)

Beam Designation[5]	**ABAQUS buckling load/ Eigen value, N**	**Buckling load from Eq. (4.29), N**
C100-500x75 $[0]_4$	37.71	29.59
C100-500x50 $[0]_4$	29.51	25.46
C100-500x25 $[0]_4$	15.13	14.59
C100-400x50 $[0]_4$	51.53	42.59
C100-500x25 $[90]_4$	2.48	2.48
C100-400x50 $[90]_4$	8.25	7.92

5 See Table 4.2 for laminate properties

As can be seen, Eq. (4.29) is on the conservative side however the difference for 0° laminates is greater especially when the l/h ratio is higher. One main reason for this difference might be that the twist angle or the angle of section rotation (β) is assumed constant in the formulation as is assumed by Timoshenko. However, it was observed both experimentally and from the nodal displacements of the free end that (β) is not constant along the section height. In fact, the difference for nearly all other layups investigated is considerably small and the change in (β) along the height was negligible. In Table 4.6 buckling load from Eq. (4.29) is compared with ABAQUS and Timoshenko's classical solutions.

Table 4.6: Buckling load comparison for rectangular section cantilever beam

Material	**Height (mm)**	**Length (mm)**	**Buckling load using Eq. (4.29) (N)**	**ABAQUS buckling load/Eigen Value (N)**	**Timoshenko's Solution (N)**
Steel (t=2.62mm)	49.05	500	292.69	302.35	292.78

Table 4.7: ABAQUS / Numerical and theoretical buckling load using Eq. (4.29) for CFRP laminates with arbitrary layups

Layup[6]	**Height (mm)**	**Length (mm)**	**Analytical/Buckling load using Eq. (4.29) (N)**	**ABAQUS buckling load/Eigen Value (N)**	**Error[7] (%)**
0/0/0/0	50	500	0.220	0.262	-19.09
90/90/90/90	50	500	0.069	0.072	-4.35

6 Thickness of 0.1mm has been assumed for each layup making the total thickness 0.4mm for each laminate. Beam properties are reported in Table 4.3.

7 $Error(\%) = (Analytical\ Solution - Eigen\ Valu)/(Analytical\ Solution) * 100$

30/-30/30/-30	50	500	0.290	0.306	-5.52
45/-45/45/-45	50	500	0.198	0.206	-4.04
60/-60/60/-60	50	500	0.151	0.155	-2.65
60/-60/45/-45	50	500	0.138	0.148	-7.25
30/-30/45/-45	50	500	0.191	0.203	-6.28
30/-30/60/-60	50	500	0.136	0.144	-5.88
30/-30/0/0	50	500	0.168	0.186	-10.71
30/-30/0/90	50	500	0.116	0.124	-6.90
30/30/30/30	50	500	0.077	0.084	-9.09
30/-30/-30/30	50	500	0.160	0.171	-6.88
0/90/90/0	50	500	0.208	0.245	-17.79
30/-60/-60/30	50	500	0.091	0.101	-10.99
0/90/0/90	50	500	0.153	0.172	-12.42
-45/30/-30/45	50	500	0.200	0.21	-5.00
0/0/90/90	50	500	0.114	0.125	-9.65
90/0/0/90	50	500	0.101	0.109	-7.92
15/0/-15/30	50	500	0.129	0.142	-10.08
30/-40/50/-60	50	500	0.122	0.132	-8.20
15/30/-45/15	50	500	0.120	0.136	-13.33

Table 4.8: ABAQUS / Numerical and theoretical buckling load using Eq. (4.29) for GFRP laminates with arbitrary layups

Layup[8]	Height (mm)	Length (mm)	Analytical/Buckling load using Eq. (4.29) (N)	ABAQUS buckling load/Eigen Value (N)	Error (%)
0/0/0/0	50	500	0.135	0.147	-8.89
90/90/90/90	50	500	0.070	0.073	-4.29
30/-30/30/-30	50	500	0.139	0.147	-5.76
45/-45/45/-45	50	500	0.119	0.124	-4.20
60/-60/60/-60	50	500	0.098	0.102	-4.08
60/-60/45/-45	50	500	0.099	0.104	-5.05
30/-30/45/-45	50	500	0.121	0.126	-4.13
30/-30/60/-60	50	500	0.100	0.105	-5.00
30/-30/0/0	50	500	0.115	0.123	-6.96
30/-30/0/90	50	500	0.090	0.094	-4.44
30/30/30/30	50	500	0.079	0.084	-6.33
30/-30/-30/30	50	500	0.100	0.105	-5.00
0/90/90/0	50	500	0.129	0.140	-8.53
30/-60/-60/30	50	500	0.086	0.091	-5.81
0/90/0/90	50	500	0.104	0.111	-6.73
-45/30/-30/45	50	500	0.122	0.127	-4.10
0/0/90/90	50	500	0.093	0.099	-6.45

8 Thickness of 0.1mm has been assumed for each layup making the total thickness 0.4mm for each laminate. Beam properties are reported in Table 4.4.

90/0/0/90	50	500	0.081	0.085	-4.94
15/0/-15/30	50	500	0.099	0.106	-7.07
30/-40/50/-60	50	500	0.099	0.104	-5.05
15/30/-45/15	50	500	0.100	0.107	-7.00

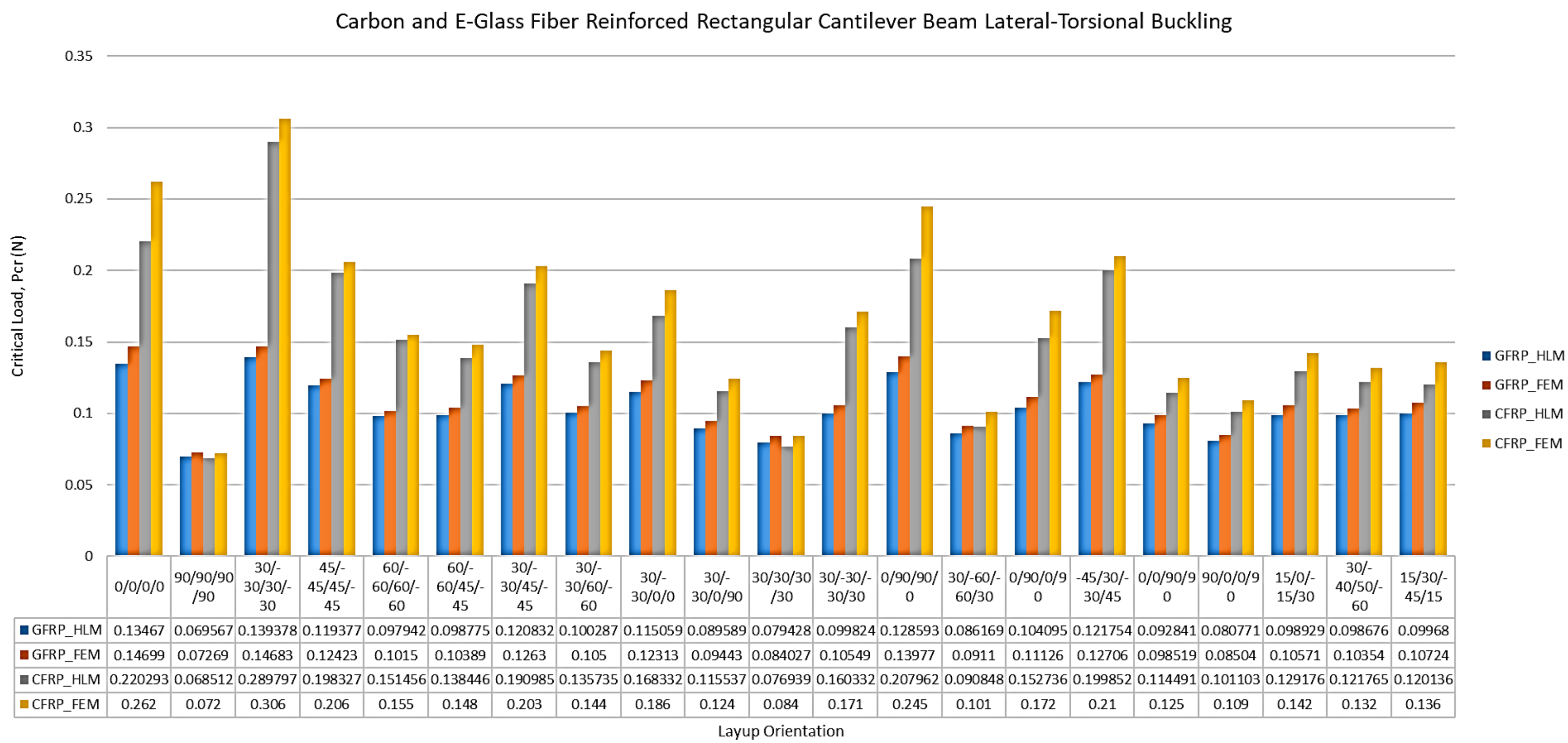

	0/0/0/0	90/90/90/90	30/-30/30/-30	45/-45/45/-45	60/-60/60/-60	60/-60/45/-45	30/-30/45/-45	30/-30/60/-60	30/-30/0/0	30/-30/0/90	30/30/30/30	30/-30/-30/30	0/90/90/0	30/-60/-60/30	0/90/0/90	-45/30/-30/45	0/0/90/90	90/0/0/90	15/0/-15/30	30/-40/50/-60	15/30/-45/15
GFRP_HLM	0.13467	0.069567	0.139378	0.119377	0.097942	0.098775	0.120832	0.100287	0.115059	0.089589	0.079428	0.099824	0.128593	0.086169	0.104095	0.121754	0.092841	0.080771	0.098929	0.098676	0.09968
GFRP_FEM	0.14699	0.07269	0.14683	0.12423	0.1015	0.10389	0.1263	0.105	0.12313	0.09443	0.084027	0.10549	0.13977	0.0911	0.11126	0.12706	0.098519	0.08504	0.10571	0.10354	0.10724
CFRP_HLM	0.220293	0.068512	0.289797	0.198327	0.151456	0.138446	0.190985	0.135735	0.168332	0.115537	0.076939	0.160332	0.207962	0.090848	0.152736	0.199852	0.114491	0.101103	0.129176	0.121765	0.120136
CFRP_FEM	0.262	0.072	0.306	0.206	0.155	0.148	0.203	0.144	0.186	0.124	0.084	0.171	0.245	0.101	0.172	0.21	0.125	0.109	0.142	0.132	0.136

Figure 4.11: Comparison of ABAQUS / Numerical and theoretical buckling load using Eq. (4.29) for GFRP laminates with arbitrary layups. CFRP_HLM and GFRP_HLM on the legend represents Eq. (4.29)

4.8 Conclusion

In this study a generalized analytical solution based on classical laminated plate theory is presented to determine lateral torsional buckling of a rectangular composite beams with arbitrary layups. The solution can be adapted for rectangular section beam beams with various loading and support conditions by using proper boundary conditions. The solution favorably compares with finite element results for beams with arbitrary layup where lateral torsional buckling is the dominant buckling mode. Finite element results tend to be on the higher side especially for laminates with 0-degrees. This might be due to the variation in twisting angle (β) along beam height similar to distortional buckling, which is not accounted for in the formulation. The model is equally applicable to generally anisotropic beams with symmetrical or unsymmetrical layups.

Chapter 5 - Lateral Torsional Buckling Analysis of Thin-Walled Anisotropic Simple I-Beams under Pure Bending

5.1 Abstract

In this chapter, lateral torsional buckling of I-beams with arbitrary layups under pure bending is investigated. Thin-walled I-beams can buckle with various modes depending on the geometry of the cross-section, material properties, loading and support conditions. Common buckling modes are: i.e., lateral, local or a combination of local and lateral which is called distortional buckling. This study assumes that no local or distortional buckling occurs prior to lateral torsional buckling. In other words, beams have high depth to width ratios and are not extremely thin.

Analytical solution is derived using classical laminated plate theory and verified numerically using ABAQUS. The solution is also validated against Timoshenko's classical solution for isotropic I-beam. Differential equation for the lateral torsional buckling with constant coefficients is formulated using the kinematics, constitutive and equilibrium equations. The differential equation is then solved using the infinite series approach yielding closed-form solutions that favorably compares to the finite element results confirming their accuracy. The analytical solution could be adapted for thin-walled composite beams with symmetrical layups under different load and boundary conditions. However, this is beyond the scope of this study.

A parametric study is also performed to investigate length to depth (l/h) and flange and web thickness effects on the critical load.

5.2 Introduction

Thin-walled Carbon Fiber Reinforced Polymer (CFRP) structural shapes are increasingly used in aerospace, automotive, civil and marine structures due to their high stiffness/strength-to-weight ratio, excellent energy absorption, durability, and corrosion resistance characteristics.

One of the commonly used shapes is CFRP I-shape, which is widely known for its efficient load transfer. However, as for many other thin-walled CFRP slender shapes, lateral torsional buckling is the common failure modes for I-sections along with local or distortional buckling which are beyond the scope of this study. In this chapter, CFRP I-beam under pure bending with arbitrary layups known as generally anisotropic are studied considering out-of-plane shear and warping effects.

Davalos and Qiao [10] studied flexural-torsional and lateral-distortional buckling response of wide flange balanced-symmetric pultruded beams. Using the principles of energy, an equation was derived for the total potential energy for flexural torsional buckling using nonlinear elastic theory. Lee and Kim [21] presented a generalized analytical model which is applicable to flexural, torsional or flexural-torsional buckling of composite I-sections with arbitrary layups under axial load. Kabir and Sherbourne [22] have studied the interactive buckling of fibrous composite I-section beams. It was concluded that when local buckling and overall lateral buckling are viewed as separate entities, they result in stable post critical behavior respectively. However, when combined, leads to more degradative effect on the failure load capacity of thin-walled beams.

Cardoso and Vieira [23] presented explicit equations to estimate local buckling critical stress of thin walled composite beam under compression or pure bending. In addition to considering interaction between flange and web and different orthotropy ratios, the procedure allows for a range of flange and web thicknesses and flange to web ratios.

Zeinali, Nazari, and Showkati [24] performed experimental-numerical study on lateral torsional buckling of pultruded FRP I-section beams having different span to height ratios under pure bending. Using Eurocode 3 provisions, reasonable agreement between experimental and numerical results has been reported.

Pandey, Kabir, and Sherbourne [25] have studied the optimal fiber orientation to enhance lateral buckling strength of thin-walled open section composite beams. They concluded that for I-section beams with unidirectional flange layups, the web fiber angle has significant influence on lateral buckling of long span beams. Additionally, for length to depth ratio (l/h) of 12 or higher, optimal fiber orientation for the flanges and web are 0° and $+/-45^{\circ}$ respectively. Barbero and Raftoyiannis [26] studied the elastic buckling modes of pultruded I-beams for different loading conditions. It was concluded that coupling of local and lateral buckling modes always occurs due to lower material stiffness in the transverse direction. Moreover, lateral buckling was found to be the dominant failure mode for I-beams with high depth to width ratios while coupled local and distortional buckling for lower height to width ratios contributed to the reduction in the critical load compare to pure local or pure lateral buckling loads.

5.3 Problem Statement

Obtain a closed form analytical solution for lateral torsional buckling problem of thin-walled I- beam with arbitrary layups under pure bending.

5.4 Formulation for a Section with Arbitrary Shape

For the derivation of the stiffness matrix, three coordinate systems are introduced. The $(\bar{X},\ \bar{Y}, \bar{Z})$ coordinate system with the origin at an arbitrary point, (X, Y, Z) with a fixed origin at the centroid of the section, and (ξ, η, ζ) with origin at the center of the reference plane of k-th wall segment shown in the figure below.

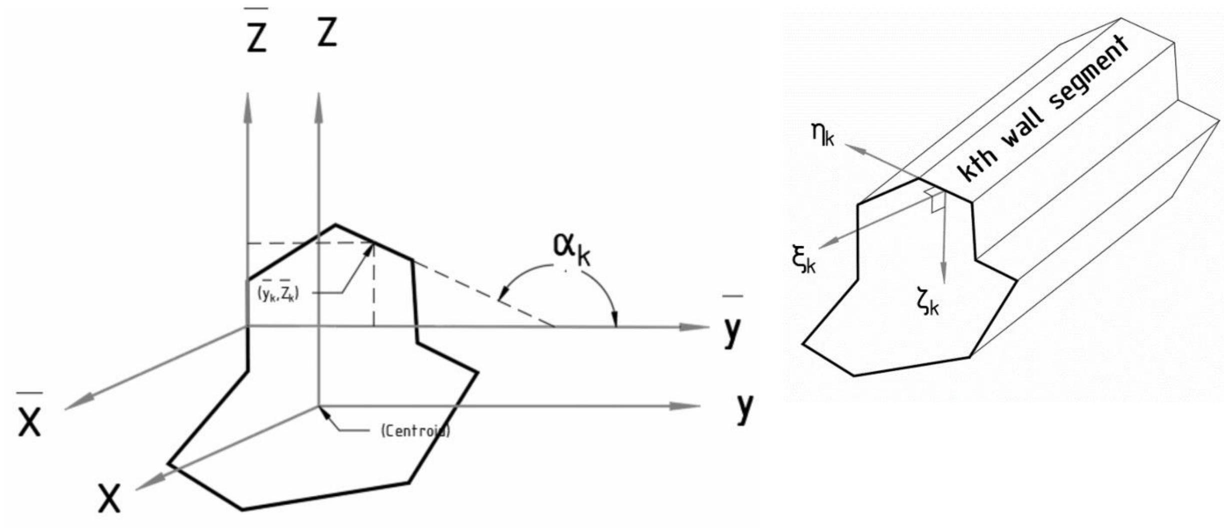

Figure 5.1: Local and global coordinate system

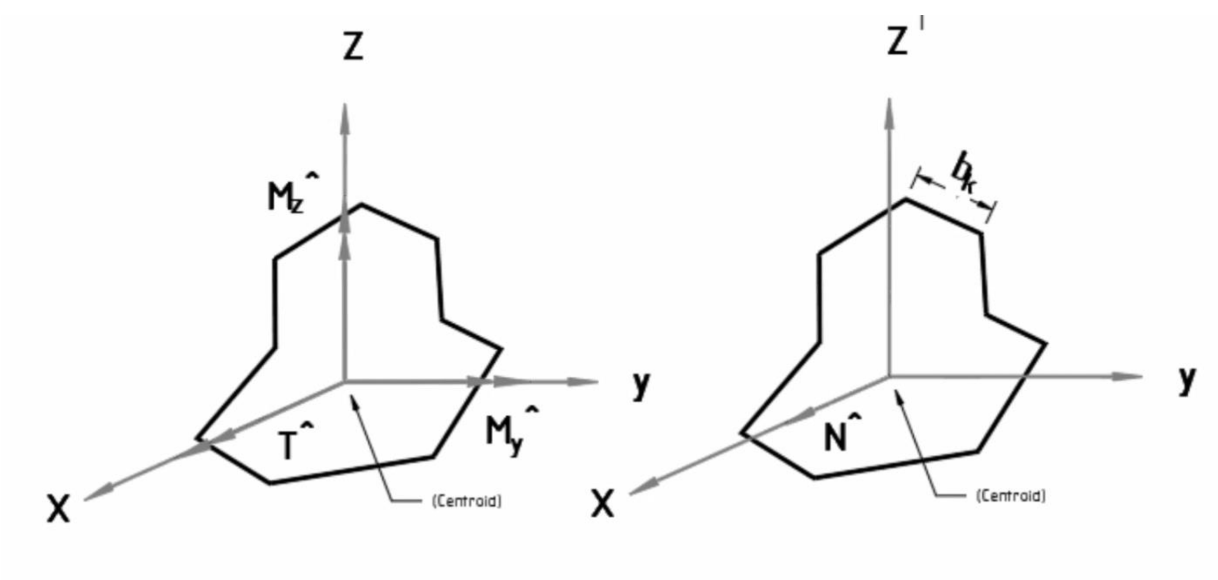

Figure 5.2: Global forces and moments

$$\frac{\partial u}{\partial x} = \varepsilon_x , \qquad \frac{\partial^2 v}{\partial x^2} = -\frac{1}{\rho_z} , \frac{\partial^2 w}{\partial x^2} = -\frac{1}{\rho_y} , \qquad \vartheta = \vartheta_\xi = \frac{\partial \varphi}{\partial x} \qquad \text{Eq. (5.1)}$$

$$\vartheta = \frac{\partial \varphi}{\partial x} = \frac{\partial \left({}^{\partial w}/_{\partial y} \right)}{\partial x} = \frac{\partial^2 w}{\partial x \partial y} \qquad \text{Eq. (5.2)}$$

$$\varepsilon_{\xi k} = \varepsilon_x + z\frac{1}{\rho_y} + y\frac{1}{\rho_z} \qquad \text{Eq. (5.3)}$$

$$\varepsilon_{\xi k} = \varepsilon_k + \eta \mathrm{K}_{sk} \qquad \text{Eq. (5.4)}$$

$$\mathrm{K}_{\xi k} = \frac{1}{\rho_y}\cos(\alpha_k) - \frac{1}{\rho_z}\sin(\alpha_k) \qquad \text{Eq. (5.5)}$$

$$\mathrm{K}_{\xi \eta} = -2\frac{\partial^2 w}{\partial x \partial y} \qquad \text{Eq. (5.6)}$$

The relation for curvature due to twisting using Eq. (5.2) and (5.6) becomes

$$\vartheta = -\frac{1}{2}\mathrm{K}_{\xi \eta} \qquad \text{Eq. (5.7)}$$

Note that the twist of any point in a wall segment is equal to the twist of the whole section.

φ: Angle of twist

$\varepsilon_{\xi k}$: Strain at any arbitrary point on k-th wall segment's reference surface

ε_x: Axial strain at the centroid of the section

ε_k: Axial strain of a wall segment or strain at the center of the wall segment of interest

z: Coordinates of an arbitrary point on k-th wall segment's reference surface along z-axis

y: Coordinates of an arbitrary point on k-th wall segment's reference surface along y-axis

$\mathrm{K}_{\xi k}$: Curvature of the k-th wall segment's axis in $\xi\zeta$ plane (see Figure 5.1)

K_{sk}: Curvature of the k-th wall segment's axis in $\eta\xi$ plane (see Figure 5.1)

b_k: Width of the wall segment

The compliance matrix $[W_k]$ and transformation matrix $[R_k]$ are followed from [28] and modified for I-section beam to account for shear and warping deformations.

$$[W_k] = \frac{1}{b_k}\begin{bmatrix} \alpha_{11} & \alpha_{16} & 0 & \beta_{11} & 0 & -\frac{\beta_{16}}{2} \\ \alpha_{16} & \alpha_{66} & 0 & \beta_{16} & 0 & -\frac{\beta_{66}}{2} \\ 0 & 0 & \varrho & 0 & 0 & 0 \\ \beta_{11} & \beta_{16} & 0 & \delta_{11} & 0 & -\frac{\delta_{16}}{2} \\ 0 & 0 & 0 & 0 & \frac{12}{(\hat{A}_{11})_k b_k^2} & 0 \\ -\frac{\beta_{16}}{2} & -\frac{\beta_{66}}{2} & 0 & -\frac{\delta_{16}}{2} & 0 & -\frac{\delta_{66}}{4} \end{bmatrix} \qquad \text{Eq. (5.8)}$$

$$[R_k] = \begin{bmatrix} 1 & 0 & 0 & Z_k & y_k & 0 \\ 0 & \cos(\alpha_k) & \sin(\alpha_k) & 0 & 0 & 0 \\ 0 & -\sin(\alpha_k) & \cos(\alpha_k) & 0 & 0 & 0 \\ 0 & 0 & 0 & \cos(\alpha_k) & -\sin(\alpha_k) & 0 \\ 0 & 0 & 0 & \sin(\alpha_k) & \cos(\alpha_k) & 0 \\ 0 & 0 & 0 & 0 & 0 & 1 \end{bmatrix}$$

$[\alpha], [\beta]$, and $[\delta]$ matrices are the inverse of $[A], [B]$, and $[D]$ explained in the previous chapter. $\hat{A}_{11}$ is calculated from Eq. 20 of [28] as follows:

$$\begin{bmatrix} \widetilde{A_{11}} & \widetilde{A_{12}} & \widetilde{A_{13}} \\ \widetilde{A_{12}} & \widetilde{A_{22}} & \widetilde{A_{23}} \\ \widetilde{A_{13}} & \widetilde{A_{23}} & \widetilde{A_{33}} \end{bmatrix}_k = \begin{bmatrix} \alpha_{11} & \beta_{11} & \beta_{16} \\ \beta_{11} & \delta_{11} & \delta_{16} \\ \beta_{16} & \delta_{16} & \delta_{66} \end{bmatrix}_k^{-1} \qquad \text{Eq. (5.9)}$$

$$\begin{bmatrix} A11 & A12 & A16 & B11 & B12 & B16 \\ A12 & A22 & A26 & B12 & B22 & B26 \\ A16 & A26 & A66 & B16 & B26 & B66 \\ B11 & B12 & B16 & D11 & D12 & D16 \\ B12 & B22 & B26 & D12 & D22 & D26 \\ B16 & B26 & B66 & D16 & D26 & D66 \end{bmatrix}^{-1} = \begin{bmatrix} \alpha 11 & \alpha 12 & \alpha 16 & \beta 11 & \beta 12 & \beta 16 \\ \alpha 12 & \alpha 22 & \alpha 26 & \beta 12 & \beta 22 & \beta 26 \\ \alpha 16 & \alpha 26 & \alpha 66 & \beta 16 & \beta 26 & \beta 66 \\ \beta 11 & \beta 12 & \beta 16 & \delta 11 & \delta 12 & \delta 16 \\ \beta 12 & \beta 22 & \beta 26 & \delta 12 & \delta 22 & \delta 26 \\ \beta 16 & \beta 26 & \beta 66 & \delta 16 & \delta 26 & \delta 66 \end{bmatrix} \quad \text{Eq. (5.10)}$$

$$\begin{Bmatrix} \widehat{N}_{\xi} \\ \widehat{N}_{\xi\eta} \\ \widehat{N}_{\xi\zeta} \\ \widehat{\mathrm{M}}_{\xi} \\ \widehat{\mathrm{M}}_{s} \\ \widehat{T}_{\xi} \end{Bmatrix}_k = [R_k] \begin{Bmatrix} \widehat{N}_{x} \\ \widehat{N}_{xy} \\ \widehat{N}_{xz} \\ \widehat{\mathrm{M}}_{y} \\ \widehat{\mathrm{M}}_{z} \\ \widehat{T}_{x} \end{Bmatrix}_k$$

$$\begin{Bmatrix} \varepsilon_{\xi} \\ \gamma_{\xi\eta} \\ \gamma_{\xi\zeta} \\ \mathrm{K}_{\xi} \\ \mathrm{K}_{s} \\ \vartheta_{\xi} \end{Bmatrix}_k = [R_k] \begin{Bmatrix} \varepsilon_{x} \\ \gamma_{xy} \\ \gamma_{xz} \\ \dfrac{1}{\rho_y} \\ \dfrac{1}{\rho_z} \\ \vartheta \end{Bmatrix}_k \quad \text{Eq. (5.11)}$$

$$\begin{Bmatrix} \varepsilon_\xi \\ \gamma_{\xi\eta} \\ \gamma_{\xi\zeta} \\ \mathrm{K}_\xi \\ \mathrm{K}_s \\ \vartheta \end{Bmatrix}_k = \frac{1}{b_k}\begin{bmatrix} \alpha_{11} & \alpha_{16} & 0 & \beta_{11} & 0 & -\frac{\beta_{16}}{2} \\ \alpha_{16} & \alpha_{66} & 0 & \beta_{16} & 0 & -\frac{\beta_{66}}{2} \\ 0 & 0 & \varrho & 0 & 0 & 0 \\ \beta_{11} & \beta_{16} & 0 & \delta_{11} & 0 & -\frac{\delta_{16}}{2} \\ 0 & 0 & 0 & 0 & \frac{12}{(\hat{A}_{11})_k b_k^2} & 0 \\ -\frac{\beta_{16}}{2} & -\frac{\beta_{66}}{2} & 0 & -\frac{\delta_{16}}{2} & 0 & -\frac{\delta_{66}}{4} \end{bmatrix}\begin{Bmatrix} \widehat{N}_\xi \\ \widehat{N}_{\xi\eta} \\ \widehat{N}_{\xi\zeta} \\ \widehat{\mathrm{M}}_\xi \\ \widehat{\mathrm{M}}_s \\ \widehat{T}_\xi \end{Bmatrix} \qquad \text{Eq. (5.12)}$$

(^) indicates quantities per unit length of the wall segment.

$$\begin{Bmatrix} \widehat{N}_x \\ \widehat{N}_{xy} \\ \widehat{N}_{xz} \\ \widehat{\mathrm{M}}_y \\ \widehat{\mathrm{M}}_z \\ \widehat{T}_x \end{Bmatrix}_k = \sum_{k=1}^{k}([R_k]^T[W_k]^{-1}[R_k])\begin{Bmatrix} \varepsilon_x \\ \gamma_{xy} \\ \gamma_{xz} \\ \frac{1}{\rho_y} \\ \frac{1}{\rho_z} \\ \vartheta \end{Bmatrix} \qquad \text{Eq. (5.13)}$$

$[P]_{6x6} = [R_k]^T[W_k]^{-1}[R_k]$ shall be calculated for each wall segment separately and then added together to give a new $[P]_{6x6}$ for the whole section.

5.5 Out-of-Plane Shear Effects

Out-of-plane shear effects are calculated based on 2.4.4b, 2.4.8, and 3.4.19a of [37] as follows.

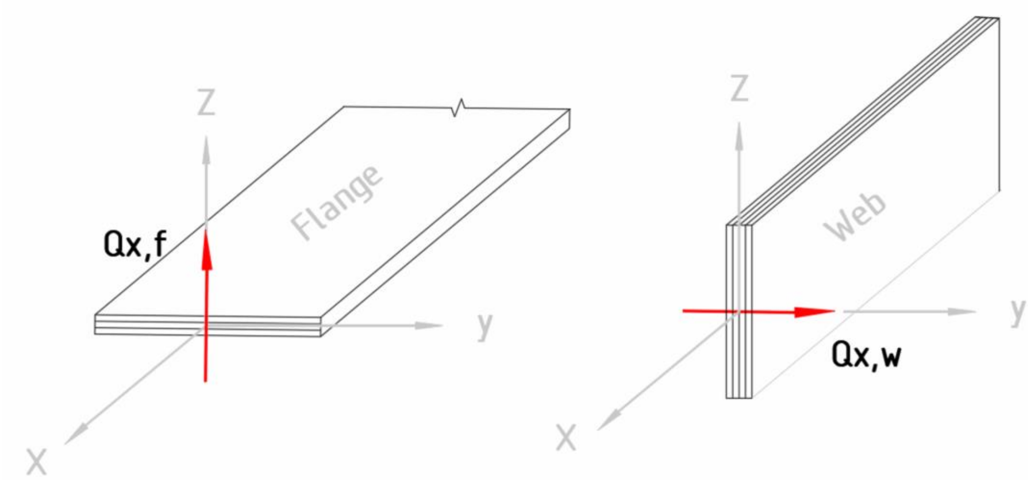

Figure 5.3: Out-of-plane shear stresses for flange and web

$$\begin{Bmatrix} Q_{x,f} \\ Q_{x,w} = 0 \end{Bmatrix} = \mathrm{K} \begin{bmatrix} A_{44} & A_{45} \\ A_{45} & A_{55} \end{bmatrix} \begin{Bmatrix} \gamma_{xz} \\ \gamma_{yz} \end{Bmatrix} \qquad \text{Eq. (5.14)}$$

K is the shear correction factor and its value depends on lamina properties and stacking sequence. In this study an approximate value of ${}^{5}/{}_{6}$ is assumed.

$$(A_{44}, A_{45}, A_{55}) = \sum_{k=1}^{K} (\bar{Q}_{44}^{k},\ \bar{Q}_{45}^{k}, \bar{Q}_{55}^{k})(z_{k+1} - z_k) \qquad \text{Eq. (5.15)}$$

And

$$\begin{aligned} Q_{44} &= G_{23}, Q_{55} = G_{13}, \\ \bar{Q}_{44} &= Q_{44}cos^2\theta + Q_{55}sin^2\theta \\ \bar{Q}_{45} &= (Q_{55} - Q_{44})cos\theta sin\theta \\ \bar{Q}_{55} &= Q_{55}cos^2\theta + Q_{44}sin^2\theta \end{aligned} \qquad \text{Eq. (5.16)}$$

From Eq. (5.14),

$$\gamma_{yz} = -\frac{A_{45}\gamma_{xz}}{A_{55}}$$

$$\gamma_{xz} = \frac{Q_{x,f}}{\mathrm{K}\left(A_{44} - \frac{A_{45}^2}{A_{55}}\right)} \qquad \text{Eq. (5.17)}$$

$$\varrho = \frac{1}{\mathrm{K}\left(A_{44} - \frac{A_{45}^2}{A_{55}}\right)} \qquad \text{Eq. (5.18)}$$

For the web, change γ_{xz} into γ_{xy} and use the corresponding layers to calculate A_{44}, A_{45} and A_{55}.

5.6 Formulation for I-section Beam

In this section, stiffness and compliance matrices are formulated for I-section beam following the same procedure described in the previous section. In the compliance matrix, a new term to account for warping deformation is followed from [29]. Although it is originally derived for orthotropic beams, it is also recommended for balanced anisotropic open section beams. This is further discussed in section 5.9 of this chapter. For the equations that follow, it is assumed that the origin of $(\bar{X},\ \bar{Y}, \bar{Z})$ coordinate system is located at the centroid of the I-section. Hence, both coordinate systems i.e., $(\bar{X},\ \bar{Y}, \bar{Z})$ and (X, Y, Z) share the same origin.

$$\begin{Bmatrix} \varepsilon_x \\ \gamma_{xy} \\ \gamma_{xz} \\ \dfrac{d^2w}{dx^2} \\ \dfrac{d^2v}{dx^2} \\ \beta' \\ -\beta''' \end{Bmatrix}$$

$$= \begin{bmatrix} w_{11} & w_{12} & w_{13} & w_{14} & w_{15} & w_{16} & 0 \\ w_{12} & w_{22} & w_{23} & w_{24} & w_{25} & w_{26} & 0 \\ w_{13} & w_{23} & w_{33} & w_{34} & w_{35} & w_{36} & 0 \\ w_{14} & w_{24} & w_{34} & w_{44} & w_{45} & w_{46} & 0 \\ w_{15} & w_{25} & w_{35} & w_{45} & w_{55} & w_{56} & 0 \\ w_{16} & w_{26} & w_{36} & w_{46} & w_{56} & w_{66} & 0 \\ 0 & 0 & 0 & 0 & 0 & 0 & \dfrac{1}{\widehat{EI}_w} b_{k,flange} \end{bmatrix} \begin{Bmatrix} \widehat{N}_x \\ \widehat{N}_{xy} \\ \widehat{N}_{xz} \\ \widehat{M}_y = M_o \\ \widehat{M}_z = \beta M_o \\ M_{s.v.} \\ \widehat{T}_w \end{Bmatrix} \qquad \text{Eq. (5.19)}$$

β is the twist angle and $\widehat{EI}_w$ is calculated from Eq. 6.238 of [38]. Elements w_{11} to w_{66} are calculated from $[P_{6x6}]^{-1}$ which is equal to the inverse of $([R_k]^T[W_k]^{-1}[R_k])$. The W-matrix above is calculated for flange and web separately.

5.6.1 Section Beam under Pure Bending

For a simply supported I-section beam under pure bending the constitutive relationship becomes:

$$\begin{Bmatrix} \widehat{N}_x = 0 \\ \widehat{N}_{xy} = 0 \\ \widehat{N}_{xz} = 0 \\ \widehat{M}_y = M_o \\ \widehat{M}_z = \beta M_o \\ M_{s.v.} \\ \widehat{T}_w \end{Bmatrix} = \left[\begin{array}{ccc|cccc} S_{11} & S_{12} & S_{13} & S_{14} & S_{15} & S_{16} & S_{17} \\ S_{12} & S_{22} & S_{23} & S_{24} & S_{25} & S_{26} & S_{27} \\ S_{13} & S_{23} & S_{33} & S_{34} & S_{35} & S_{36} & S_{37} \\ \hline S_{14} & S_{24} & S_{34} & S_{44} & S_{45} & S_{46} & S_{47} \\ S_{15} & S_{25} & S_{35} & S_{45} & S_{55} & S_{56} & S_{57} \\ S_{16} & S_{26} & S_{36} & S_{46} & S_{56} & S_{66} & S_{67} \\ S_{17} & S_{27} & S_{37} & S_{47} & S_{57} & S_{66} & S_{77} \end{array}\right] \begin{Bmatrix} \varepsilon_x \\ \gamma_{xy} \\ \gamma_{xz} \\ \dfrac{d^2w}{dx^2} \\ \dfrac{d^2v}{dx^2} \\ \beta' \\ -\beta''' \end{Bmatrix} \qquad \text{Eq. (5.20)}$$

Note that the summation of Saint Venant's torsion and ($M_{s.v.)}$ and warping torsion $\widehat{(T_w})$ is equal to the total twisting moment on the section i.e.,$-M_o \frac{\partial v}{\partial x}$ (Figure 5.5). The 7x7 matrix in Eq. (5.20) shall be calculated for flange and web and added together to give the stiffness matrix for the whole section.

$$S_a = \begin{bmatrix} S_{11} & S_{12} & S_{13} \\ S_{12} & S_{22} & S_{23} \\ S_{13} & S_{23} & S_{33} \end{bmatrix} \qquad S_b = \begin{bmatrix} S_{14} & S_{15} & S_{16} & S_{17} \\ S_{24} & S_{25} & S_{26} & S_{27} \\ S_{34} & S_{35} & S_{36} & S_{37} \end{bmatrix}$$

$$S_c = \begin{bmatrix} S_{14} & S_{24} & S_{34} \\ S_{15} & S_{25} & S_{35} \\ S_{16} & S_{26} & S_{36} \\ S_{17} & S_{27} & S_{37} \end{bmatrix} \qquad S_d = \begin{bmatrix} S_{44} & S_{45} & S_{46} & S_{47} \\ S_{45} & S_{55} & S_{56} & S_{57} \\ S_{46} & S_{56} & S_{66} & S_{67} \\ S_{47} & S_{57} & S_{66} & S_{77} \end{bmatrix} \qquad \text{Eq. (5.21)}$$

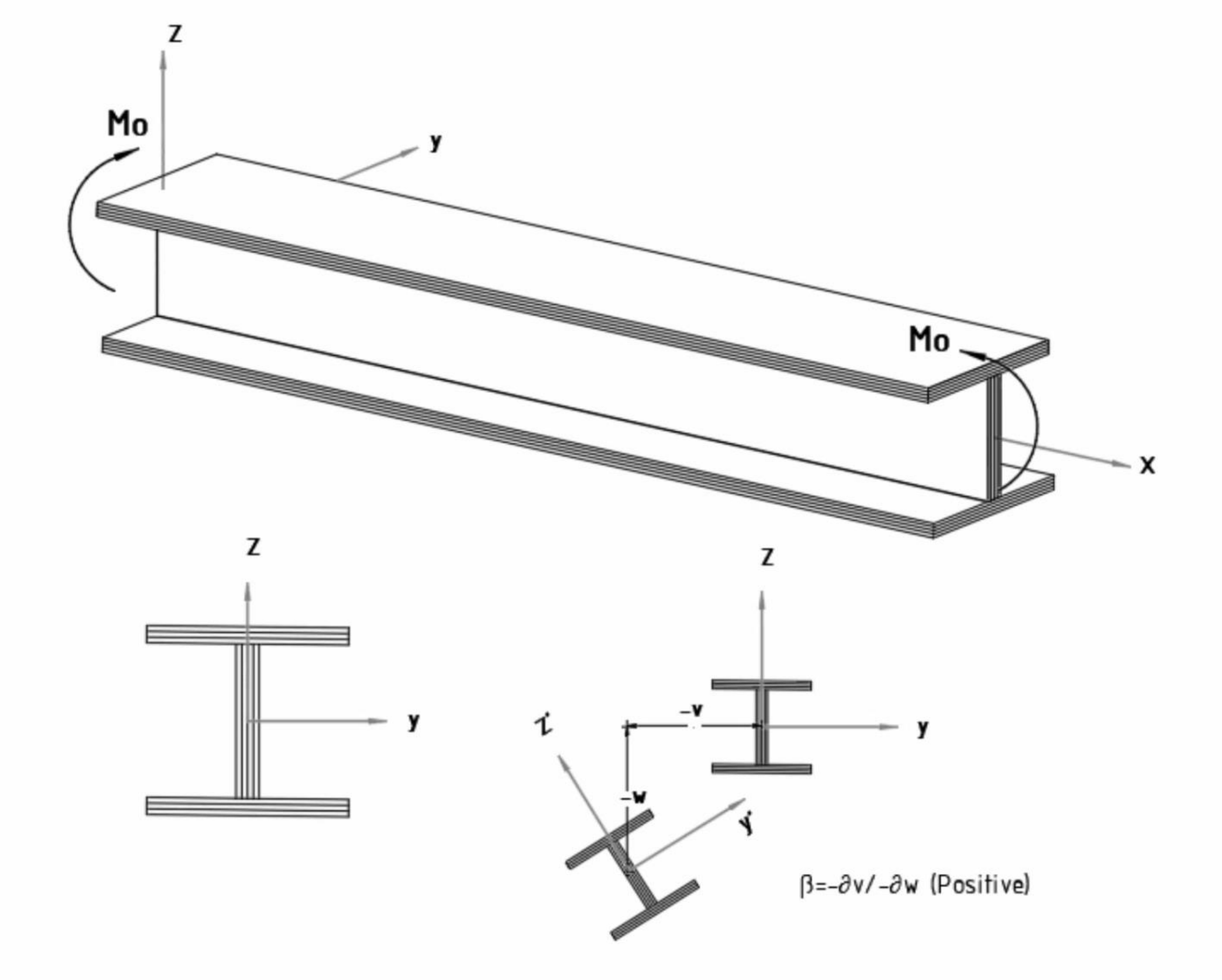

Figure 5.4: I-section beam under pure bending and deformed configuration

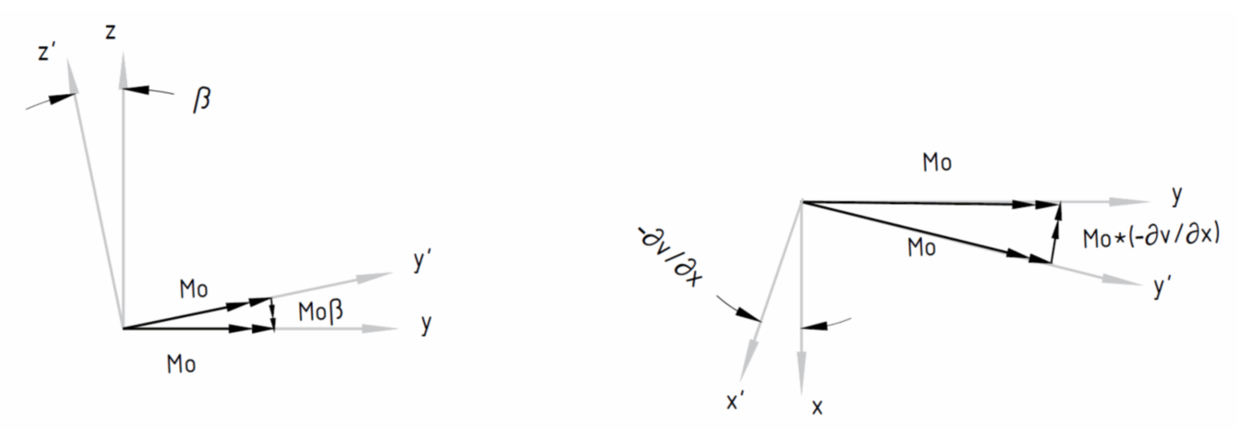

Figure 5.5: Moment along original and deformed coordinate system

From Eq. (5.20) for the zero terms

$$[S_a]\begin{Bmatrix}\varepsilon_x\\ \gamma_{xy}\\ \gamma_{xz}\end{Bmatrix}+[S_b]\begin{Bmatrix}\dfrac{d^2w}{dx^2}\\ \dfrac{d^2v}{dx^2}\\ \beta'\\ -\beta'''\end{Bmatrix}=\begin{Bmatrix}0\\0\\0\\0\end{Bmatrix} \qquad \text{Eq. (5.22)}$$

Using the static condensation approach the relationship between load and displacement becomes

$$\begin{Bmatrix}M_o\\ \beta M_o\\ M_{s.v.}\\ \hat{T}_w\end{Bmatrix}=\{-[S_c][S_a]^{-1}[S_b]+[S_d]\}_{4x4}\begin{Bmatrix}\dfrac{d^2w}{dx^2}\\ \dfrac{d^2v}{dx^2}\\ \beta'\\ -\beta'''\end{Bmatrix} \qquad \text{Eq. (5.23)}$$

For simplicity $[N]=\{-[S_c][S_a]^{-1}[S_b]+[S_d]\}_{4x4}$.

The last row and column of the 4x4 N matrix for any arbitrary layup, in other words, any combination of fiber orientation is zero except N_{44}.This makes the buckling equation easy to solve.

$$\begin{Bmatrix}M_o\\ \beta M_o\\ M_{s.v.}\\ \hat{T}_w\end{Bmatrix}=\begin{bmatrix}N_{11} & N_{12} & N_{13} & 0\\ N_{12} & N_{22} & N_{23} & 0\\ N_{13} & N_{23} & N_{33} & 0\\ 0 & 0 & 0 & N_{44}\end{bmatrix}\begin{Bmatrix}\dfrac{d^2w}{dx^2}\\ \dfrac{d^2v}{dx^2}\\ \beta'\\ -\beta'''\end{Bmatrix} \qquad \text{Eq. (5.24)}$$

$$M_o=N_{11}\left(\frac{d^2w}{dx^2}\right)+N_{12}\left(\frac{d^2v}{dx^2}\right)+N_{13}\beta' \qquad \text{Eq. (5.25)}$$

$$\beta M_o=N_{12}\left(\frac{d^2w}{dx^2}\right)+N_{22}\left(\frac{d^2v}{dx^2}\right)+N_{23}\beta' \qquad \text{Eq. (5.26)}$$

$$M_{s.v.}=N_{13}\left(\frac{d^2w}{dx^2}\right)+N_{23}\left(\frac{d^2v}{dx^2}\right)+N_{33}\beta' \qquad \text{Eq. (5.27)}$$

$$\hat{T}_w = N_{44}(-\beta''') \qquad \text{Eq. (5.28)}$$

From Eq. (5.25)

$$\left(\frac{d^2w}{dx^2}\right) = \frac{M_0 - N_{12}\left(\frac{d^2v}{dx^2}\right) - N_{13}\beta'}{N_{11}} \qquad \text{Eq. (5.29)}$$

Substituting Eq. (5.29) into (5.26)

$$\beta M_0 = N_{12}\left[\frac{M_0 - N_{12}\left(\frac{d^2v}{dx^2}\right) - N_{13}\beta'}{N_{11}}\right] + N_{22}\left(\frac{d^2v}{dx^2}\right) + N_{23}\beta' \qquad \text{Eq. (5.30)}$$

$$\left(\frac{d^2v}{dx^2}\right) = \frac{\frac{N_{12}}{N_{11}}(M_o - N_{13}\beta') - \beta M_0 + N_{23}\beta'}{\left(\frac{N_{12}^2}{N_{11}} - N_{22}\right)} \qquad \text{Eq. (5.31)}$$

Substituting Eq. (5.29) into (5.27)

$$M_{s.v.} = N_{13}\left[\frac{M_0 - N_{12}\left(\frac{d^2v}{dx^2}\right) - N_{13}\beta'}{N_{11}}\right] + N_{23}\left(\frac{d^2v}{dx^2}\right) + N_{33}\beta' \qquad \text{Eq. (5.32)}$$

Substituting Eq. (5.31) into (5.32)

$$\begin{aligned} M_{s.v.} = {} & \frac{N_{13}}{N_{11}}(M_0 - N_{13}\beta') \\ & + \left(-\frac{N_{13}N_{12}}{N_{11}} + N_{23}\right)\left[\frac{\frac{N_{12}}{N_{11}}(M_o - N_{13}\beta') - \beta M_0 + N_{23}\beta'}{\left(\frac{N_{12}^2}{N_{11}} - N_{22}\right)}\right] \\ & + N_{33}\beta' \end{aligned} \qquad \text{Eq. (5.33)}$$

Adding Eq. (5.33 and (5.28) together yields

$$M_{s.v.} + \hat{T}_w = Torque_{total} = -M_0 \frac{\partial v}{\partial x}$$

$$= \frac{N_{13}}{N_{11}}(M_0 - N_{13}\beta')$$

$$+ \left(-\frac{N_{13}N_{12}}{N_{11}}\right. \qquad \text{Eq. (5.34)}$$

$$\left. + N_{23}\right)\left[\frac{\frac{N_{12}}{N_{11}}(M_o - N_{13}\beta') - \beta M_0 + N_{23}\beta'}{\left(\frac{N_{12}^2}{N_{11}} - N_{22}\right)}\right] + N_{33}\beta'$$

$$- N_{44}\beta'''$$

Differentiating Eq. (5.34) with respect to x

$$-M_0\left(\frac{d^2v}{dx^2}\right) = -\frac{N_{13}^2}{N_{11}}\beta''$$

$$+ \left(-\frac{N_{13}N_{12}}{N_{11}} + N_{23}\right)\left[\frac{-\frac{N_{12}N_{13}}{N_{11}}\beta'' - \beta' M_0 + N_{23}\beta''}{\left(\frac{N_{12}^2}{N_{11}} - N_{22}\right)}\right] \qquad \text{Eq. (5.35)}$$

$$+ N_{33}\beta'' - N_{44}\beta''''$$

Substituting Eq. (5.31) into (5.35)

$$M_0\left[\frac{\frac{N_{12}}{N_{11}}(M_o - N_{13}\beta') - \beta M_0 + N_{23}\beta'}{\left(\frac{N_{12}^2}{N_{11}} - N_{22}\right)}\right] - \frac{N_{13}^2}{N_{11}}\beta''$$

$$+ \left(-\frac{N_{13}N_{12}}{N_{11}} + N_{23}\right)\left[\frac{-\frac{N_{12}N_{13}}{N_{11}}\beta'' - \beta' M_0 + N_{23}\beta''}{\left(\frac{N_{12}^2}{N_{11}} - N_{22}\right)}\right] \qquad \text{Eq. (5.36)}$$

$$+ N_{33}\beta'' - N_{44}\beta'''' = 0$$

Rearranging the above equation

$$-N_{44}\beta'''' + \left[N_{33} + \left(-\frac{N_{13}N_{12}}{N_{11}} + N_{23}\right)\left(\frac{-\frac{N_{12}N_{13}}{N_{11}} + N_{23}}{\frac{N_{12}^2}{N_{11}} - N_{22}}\right) - \frac{N_{13}^2}{N_{11}}\right]\beta''$$

$$+\left[\frac{-M_0\left(-\frac{N_{13}N_{12}}{N_{11}} + N_{23}\right) + N_{23}M_0 - \frac{N_{12}N_{13}}{N_{11}}M_0}{\frac{N_{12}^2}{N_{11}} - N_{22}}\right]\beta' - \left(\frac{M_0^2}{\frac{N_{12}^2}{N_{11}} - N_{22}}\right)\beta$$

$$+\left(\frac{\frac{N_{12}}{N_{11}}M_0^2}{\frac{N_{12}^2}{N_{11}} - N_{22}}\right) = 0$$

For simplicity

$$P = N_{44}$$

$$Q = \left[N_{33} + \left(-\frac{N_{13}N_{12}}{N_{11}} + N_{23}\right)\left(\frac{-\frac{N_{12}N_{13}}{N_{11}} + N_{23}}{\frac{N_{12}^2}{N_{11}} - N_{22}}\right) - \frac{N_{13}^2}{N_{11}}\right]$$

$$R = \left[\frac{-M_0\left(-\frac{N_{13}N_{12}}{N_{11}} + N_{23}\right) + N_{23}M_0 - \frac{N_{12}N_{13}}{N_{11}}M_0}{\frac{N_{12}^2}{N_{11}} - N_{22}}\right] = 0$$

$$S = \left(\frac{M_0^2}{\frac{N_{12}^2}{N_{11}} - N_{22}}\right)$$

$$T = \left(\frac{\frac{N_{12}}{N_{11}}M_0^2}{\frac{N_{12}^2}{N_{11}} - N_{22}}\right)$$

With the new terms Eq. (5.36) becomes

$$P\beta'''' - Q\beta'' + S\beta - T = 0$$

$$P\beta'''' - Q\beta'' + S\beta - T = 0 \qquad \text{Eq. (5.37)}$$

Dividing both sides of Eq. (5.37) by P

$$-\frac{Q}{P} = U \quad , \quad \frac{S}{P} = W \quad , \quad -\frac{T}{P} = Z$$

The final differential equation for thin-walled composite I-beam with arbitrary layups under pure bending is:

$$\boldsymbol{\beta'''' + U\beta'' + W\beta + Z = 0} \qquad \textbf{Eq. (5.38)}$$

5.7 Solution of the Buckling Equation for Thin-Walled I-Beam with Arbitrary Layups under Pure Bending

The 4th order differential equation, Eq. (5.35), is solved using infinite series method. The approximate solution for the equation is

$$\beta(x) = \sum_{n=0}^{\propto} a_n x^n \qquad \text{Eq. (5.39)}$$

Differentiating Eq. (5.39)

$$\beta'(x) = \sum_{n=1}^{\propto} n a_n x^{n-1} \qquad \text{Eq. (5.40)}$$

$$\beta''(x) = \sum_{n=2}^{\propto} n(n-1) a_n x^{n-2} \qquad \text{Eq. (5.41)}$$

$$\beta'''(x) = \sum_{n=3}^{\propto} n(n-1)(n-2) a_n x^{n-3} \qquad \text{Eq. (5.42)}$$

$$\beta''''(x) = \sum_{n=4}^{\propto} n(n-1)(n-2)(n-3) a_n x^{n-4} \qquad \text{Eq. (5.43)}$$

Substituting the above into Eq. (5.38)

$$\sum_{n=4}^{\propto} n(n-1)(n-2)(n-3)a_n x^{n-4} + U\sum_{n=2}^{\propto} n(n-1)a_n x^{n-2}$$
$$+W\sum_{n=0}^{\propto} a_n x^n + Z = 0 \qquad \text{Eq. (5.44)}$$

Replacing $n \longrightarrow n+4$ on the first term of the series leads to

$$\sum_{n=0}^{\propto}(n+4)(n+3)(n+2)(n+1)a_{n+4}x^n$$

Replacing $n \longrightarrow n+2$ on the second term of the series leads to

$$U\sum_{n=0}^{\propto}(n+2)(n+1)a_{n+2}x^n$$

With the new terms Eq. (5.44) becomes

$$\sum_{n=0}^{\propto}(n+4)(n+3)(n+2)(n+1)a_{n+4}x^n$$
$$+U\sum_{n=0}^{\propto}(n+2)(n+1)a_{n+2}x^n \qquad \text{Eq. (5.45)}$$
$$+W\sum_{n=0}^{\propto} a_n x^n + Z = 0$$

Taking x^n as the common factor

$$\sum_{n=0}^{\propto}[(n+4)(n+3)(n+2)(n+1)\,a_{n+4} + U\,(n+2)(n+1)a_{n+2} + Wa_n]x^n + Z = 0$$

For $n = 0$;

$$(24a_4 + 2Ua_2 + Wa_0) + Z = 0 \qquad \text{Eq. (5.46)}$$

For $n \geq 1$;

$$(24a_4 + 2Ua_2 + Wa_0) + Z + \sum_{n=1}^{\infty} [(n+4)(n+3)(n+2)(n+1)a_{n+4} + U(n+2)(n+1)a_{n+2} + Wa_n]x^n = 0 \qquad \text{Eq. (5.47)}$$

The value of Z is found to be extremely small[9] regardless of the laminate staking sequence and beam dimensions, therefore it is neglected in the calculations that follow.

$$24a_4 + 2Ua_2 + Wa_0 \equiv 0 \qquad \text{Eq. (5.48)}$$

for $n \geq 1$

$$[(n+4)(n+3)(n+2)(n+1)a_{n+4} + U(n+2)(n+1)a_{n+2} + Wa_n] \equiv 0 \qquad \text{Eq. (5.49)}$$

For $n = 1$;

$$120\, a_5 + 6Ua_3 + Wa_1 = 0 \qquad \text{Eq. (5.50)}$$

For $n = 2$;

$$360\, a_6 + 12Ua_4 + Wa_2 = 0 \qquad \text{Eq. (5.51)}$$

For $n = 3$;

$$840\, a_7 + 20Ua_5 + Wa_3 = 0 \qquad \text{Eq. (5.52)}$$

For $n = 4$;

---

9 For different laminate sequence and beam height ratios, Z was found to be in the range of (10^{-30}-10^{-35})

$$1680\, a_8 + 30Ua_6 + Wa_4 = 0 \qquad \text{Eq. (5.53)}$$

For $n = 5$;

$$3024\, a_9 + 42Ua_7 + Wa_5 = 0 \qquad \text{Eq. (5.54)}$$

For $n = 6$;

$$5040\, a_{10} + 56Ua_8 + Wa_6 = 0 \qquad \text{Eq. (5.55)}$$

For $n = 7$;

$$7920a_{11} + 72Ua_9 + Wa_7 = 0 \qquad \text{Eq. (5.56)}$$

Expanding Eq. (5.39) and using the boundary conditions lead to

$$\beta(x) = \sum_{n=0}^{\propto} a_n x^n = a_0 + a_1 x + a_2 x^2 + a_3 x^3 + . . . + a_n x^n$$

$$\beta(0) = \beta(L) = 0 \quad \Longrightarrow \boldsymbol{a_0 = 0}$$

$$\beta''(0) = \beta''(L) = 0 \quad \Longrightarrow \boldsymbol{a_2 = 0}$$

Hence $a_4 = a_6 = a_8 = a_{10} = 0$;

From Eq. (5.50)

$$a_5 = -\frac{Wa_1 + 6Ua_3}{120}$$

From Eq. (5.52)

$$a_7 = \frac{20U\left(\frac{Wa_1 + 6Ua_3}{120}\right) - Wa_3}{840}$$

From Eq. (5.54)

$$a_9 = \left(\frac{-840U^2W + 840W^2}{120 * 840 * 3024}\right)a_1 + \left(\frac{-5040\,U^3 + 10080\,UW}{120 * 840 * 3024}\right)a_3$$

From Eq. (5.56)

$$a_{11} = -\frac{72U}{7920}\left[\left(\frac{-840U^2W + 840W^2}{120 * 840 * 3024}\right)a_1 + \left(\frac{-5040\,U^3 + 10080\,UW}{120 * 840 * 3024}\right)a_3\right]$$

$$-\frac{W}{7920}\left[\left(\frac{20\,UW}{120 * 840}\right)a_1 + \left(\frac{U^2 - W}{840}\right)a_3\right]$$

Knowing that $\beta(L) = 0$:

$$\beta(L) = 0 = a_1L + a_3L^3 + a_5L^5 + a_7L^7 + a_9L^9 + a_{11}L^{11}\ldots \qquad \text{Eq. (5.57)}$$

Substitute a_5, a_7, a_9, a_{11} into the above equation to find relationship between a_1 and a_3 which yields

$$a_3 = -\left(\frac{E}{F}\right)a_1 \qquad \text{Eq. (5.58)}$$

Where

$$E = \left[L - \frac{WL^5}{120} + \left(\frac{20\,UW}{120 * 840}\right)L^7 + \left(\frac{840\,W^2 - 840\,U^2W}{120 * 840 * 3024}\right)L^9 - \frac{72\,U}{7920}\left(\frac{-840\,U^2W + 840\,W^2}{120 * 840 * 3024}\right)L^{11} - \frac{W}{7920}\left(\frac{20\,UW}{120 * 840}\right)L^{11}\right] \qquad \text{Eq. (5.59)}$$

$$F = \left[L^3 - \left(\frac{6\,U}{120}\right)L^5 + \left(\frac{U^2}{840}\right)L^7 - \left(\frac{W}{840}\right)L^7 + \left(\frac{10080\,UW - 5040U^3}{120 * 840 * 3024}\right)L^9 - \frac{72\,U}{7920}\left(\frac{-5040\,U^3 + 10080\,\,UW}{120 * 840 * 3024}\right)L^{11} - \frac{W}{7920}\left(\frac{U^2 - W}{840}\right)L^{11}\right]$$

Knowing that $\beta''(L) = 0$:

$$\beta''(L) = 0 = 6\,a_3 L + 20\,a_5 L^3 + 42\,a_7 L^5 + 72\,a_9 L^7 + 110\,a_{11} L^9 \ldots \qquad \text{Eq. (5.60)}$$

Substituting a_5, a_7, a_9, a_{11} which are functions of a_1 and a_3 into the above equation and knowing that $a_3 = -\left(\frac{E}{F}\right)a_1$, Eq. (5.60) can be solved for the critical bending moment M_0 using Excel "Goal Seek" function.

5.8 Finite Element Modeling

Finite Element Analysis is performed in ABAQUS. Conventional shell type planar element is used and the buckling load is calculated from linear perturbation. A shell edge load of unit magnitude (1N) is applied on the flanges on both ends, with the top flange in compression and bottom in tension. The load is linearly reduced to zero at the center of the beam with the top half in compression and bottom half in tension to represent positive bending moment. The corresponding first Eigen value times the resulting bending moment gives the critical lateral torsional buckling of the beam. S8R element has been used which is recommended for doubly curved thick shell elements. Grid Convergence Index (GCI) analysis is performed according to [36] to investigate mesh refinement effects on the critical load (Table 5.1). Element size of 12.5 mm is considered for the beam. Procedure for modeling I-beam is provided in the Appendix. Analytical and ABAQUS results are reported in the subsequent section for Carbon Fiber Reinforced Polymer (CFRP) I-beam with arbitrary layups for flanges and web.

Table 5.1: Large CFRP I-Beam F 0/0/0/0 W 45/-45/-45/45 Grid Convergence Index Analysis

Mesh	Element Size (mm)	Eigen Value	Critical Moment, M_0, (N.mm)	f_3-f_2	f_2-f_1	p	f_h=0	GCI_{12}	GCI_{23}	GCI_{23}/r^pGCI_{12}
1	12.5	638.19	4.9099E+7	1.53E+5	4.07E+4	1.92	4.91E+7	0.03743	0.14123	1.00
2	25	638.72	4.9140E+7							
3	50	640.72	4.9293E+7							

Table 5.2: Properties of CFRP laminates used for analysis

Young Modulus at fiber direction, EL	57488	MPa
Young Modulus at Transverse direction, ET	4198	MPa
Poisson's ratio, v_{LT}	0.119	
Poisson's ratio, v_{TL}	0.00869	
Shear Modulus, G12	2026	MPa
Shear Modulus, G13	2026	MPa
Shear Modulus, G23	2035	MPa

Table 5.3: Properties of Isotropic beam

Young Modulus at fiber direction, EL	200000	MPa
Young Modulus at Transverse direction, ET	200000	MPa
Poisson's ratio, v_{LT}	0.3	
Poisson's ratio, v_{TL}	0.3	
Shear Modulus, G12	76923	MPa
Shear Modulus, G13	76923	MPa
Shear Modulus, G23	76923	MPa

5.9 Results and Discussion

In the following, critical moment, M_o, for thin walled I-beam with arbitrary layups under pure bending is presented by solving Eq. (5.38). To investigate the effects of l/h and depth to width ratios, two I-sections (small and large) are modeled with their dimensions given in Table 5.4 -5.6. For comparison, the critical moment, M_o, from analytical and numerical solutions (ABAQUS) are provided in Table 5.9 and 5.9 for small and large I-section beams.

For the large I-beam, critical moment (M_o) from Eq. (5.38) is overall conservative and more consistent with finite element results as shown in Figure 5.13. However, it becomes conservative for arbitrary layups as the warping effects become significant. This might be due to the warping stiffness ($\widehat{EI}_w$) which is originally derived for orthotropic beams and used here for all other layups including generally anisotropic without modification. Although according to [29], the warping stiffness may be used for balanced, anisotropic open section beam, there is a need to further modify the term to be used for generally anisotropic open section beams such as 0/30/60/90 or 15/-30/45/-60 in Table 5.10 where the difference between analytical and finite element solution becomes significantly high. Nonetheless, assumptions such as constant twisting rotation of the section and plane section remains plane after bending all contribute to the small difference in the critical bending moment.

For small I-beam, the analytical solution in general leads to non-conservative M_o values when a distortional buckling mode is likely to happen. Distortional buckling is a combination of local and lateral buckling modes. I-beams are prone to distortional buckling when they have low depth to width ratios or when flange and web thicknesses are very small (Figure 5.12).

The critical moment for equivalent steel section using Eq. (5.38) is close to the Timoshenko's classical solution but not exactly the same (Table 5.8). Again, this is due to the warping stiffness terms which is used for isotropic beam without modification. The warping stiffness ($\widehat{EI}_w$) was replaced by the warping rigidity in Timoshenko's solution and the critical moment was found to be exactly matching with that of Timoshenko for both beam sections.

Table 5.4: Small isotropic I-section dimensions

Material	Flange width (mm)	Web height (mm)	Flange thickness (mm)	Web thickness (mm)	Length (mm)
Steel / isotropic	38.1	53.08	4	4	609.6

Table 5.5: Large isotropic I-section dimensions

Material	Flange width (mm)	Web height (mm)	Flange thickness (mm)	Web thickness (mm)	Length (mm)
Steel / isotropic	178	380	12	8	5000

Table 5.6: Large CFRP I-section dimensions

Material	Flange width (mm)	Web height (mm)	Flange thickness (mm)	Web thickness (mm)	Length (mm)
CFRP	178	380	12	8	5000

Table 5.7: Small CFRP I-section dimensions

Material	Flange width (mm)	Web height (mm)	Flange thickness (mm)	Web thickness (mm)	Length (mm)
CFRP	38.1	53.08	4	4	609.6

Table 5.8: Critical bending moment for isotropic beam under pure bending

Beam Designation	Material	Beam length (mm)	**Buckling load using Eq. (5.38) (N.mm)**	**ABAQUS buckling load/Eigen Value (N.mm)**	**Timoshenko (N.mm)**
Small	Steel	609.6	8.32 E+06	8.06 E+06	8.65 E+06
Large	Steel	5000	2.17 E+08	2.38 E+08	2.20 E+08

As shown, the analytical results are slightly on the conservative side for the large beam. Overall they are in good agreement with Timoshenko's and finite element results.

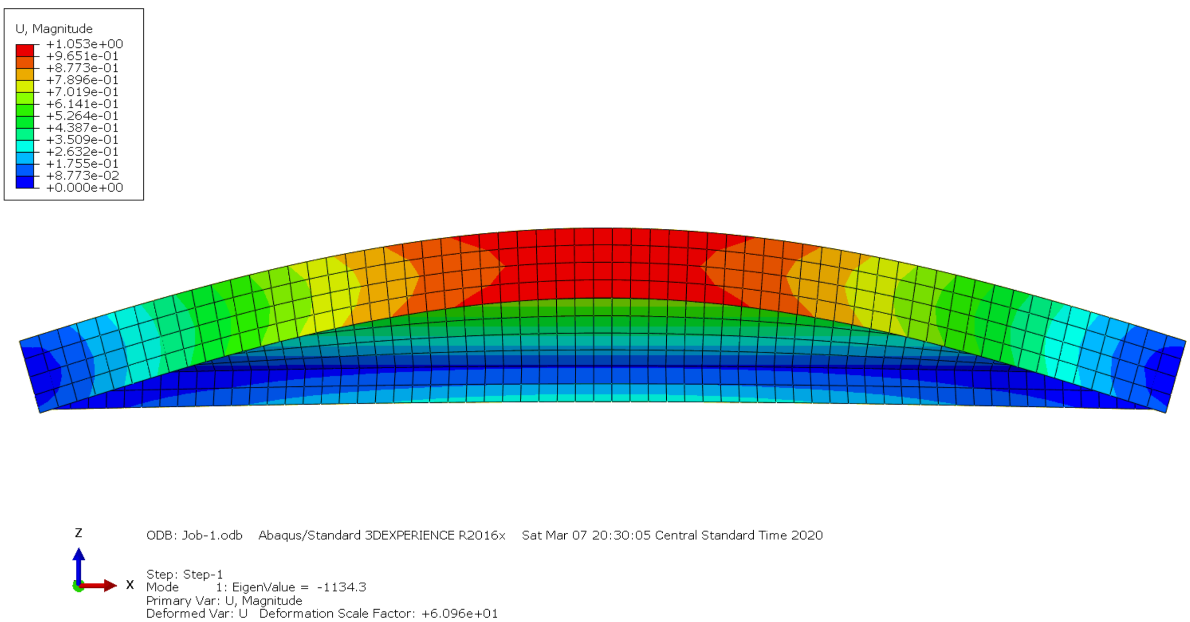

Figure 5.6: Small steel I-beam deformed shape top view

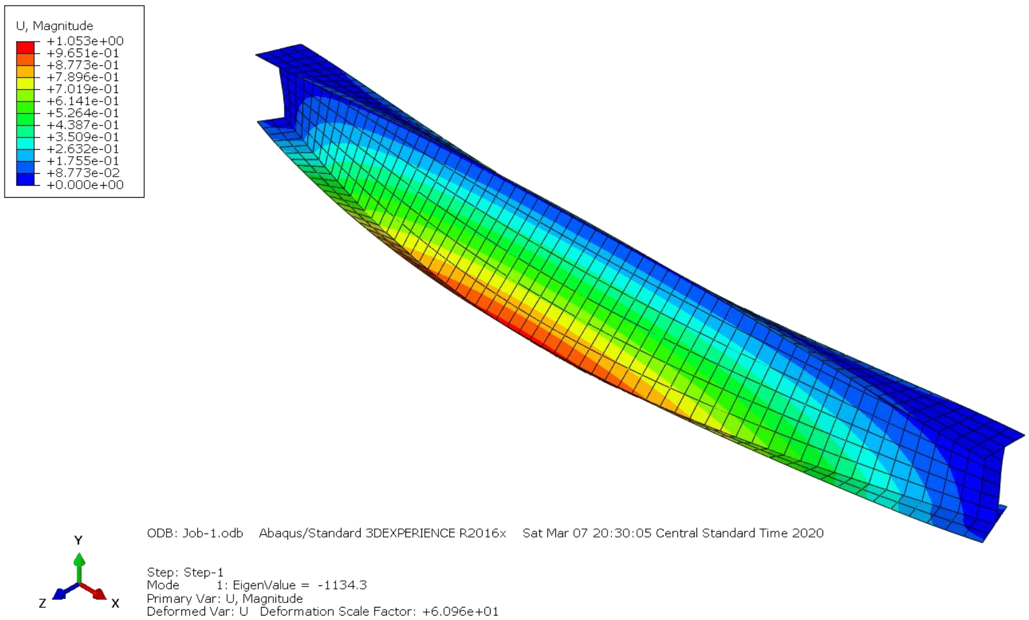

Figure 5.7: Small steel I-beam deformed shape isometric view

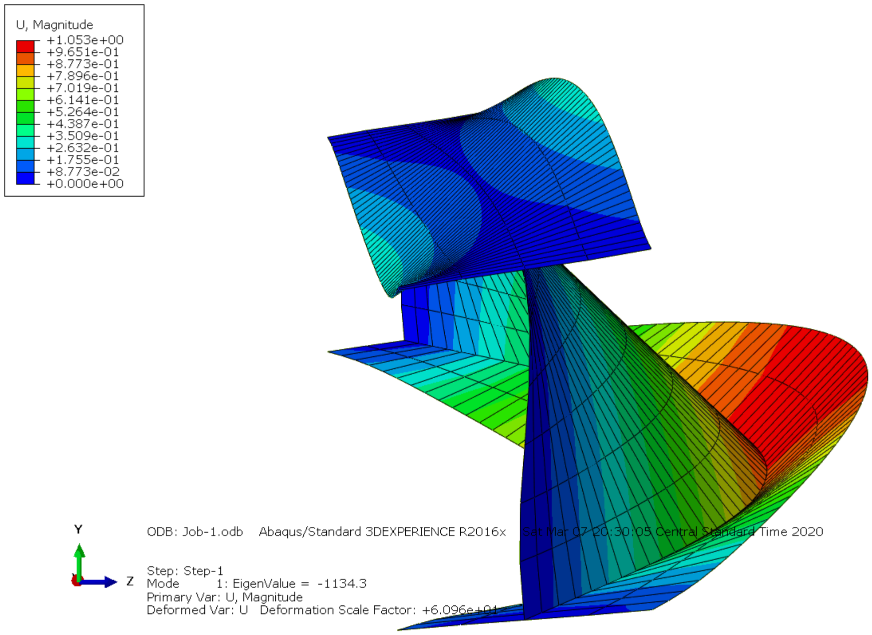

Figure 5.8: Small steel I-beam deformed shape front view

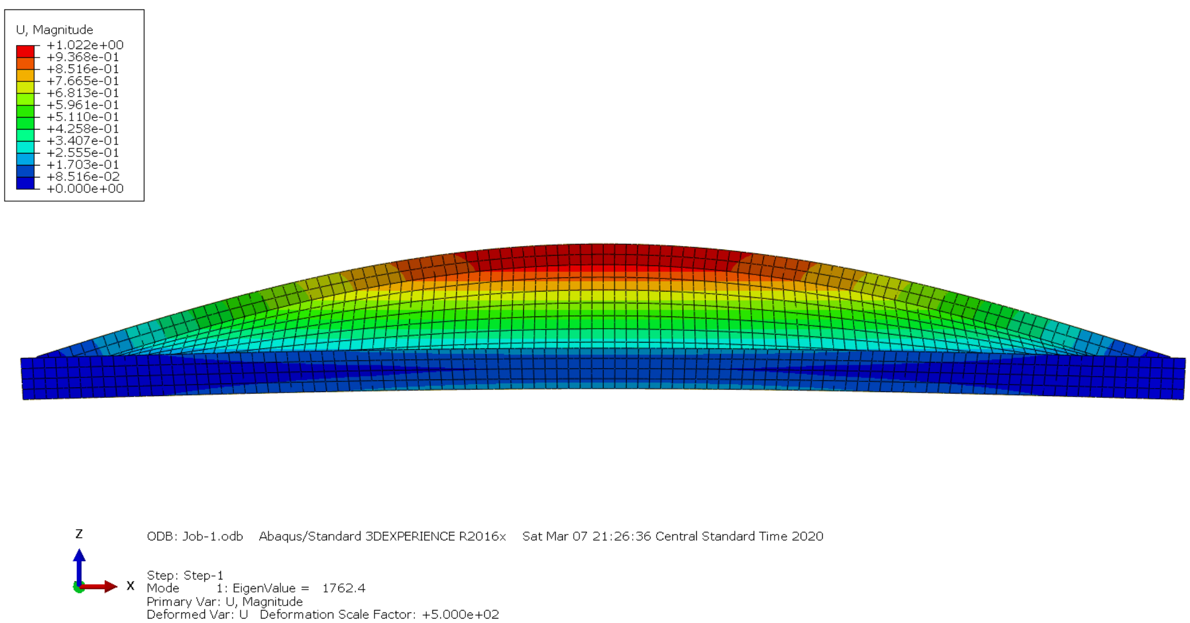

Figure 5.9: Large steel I-beam deformed shape top view

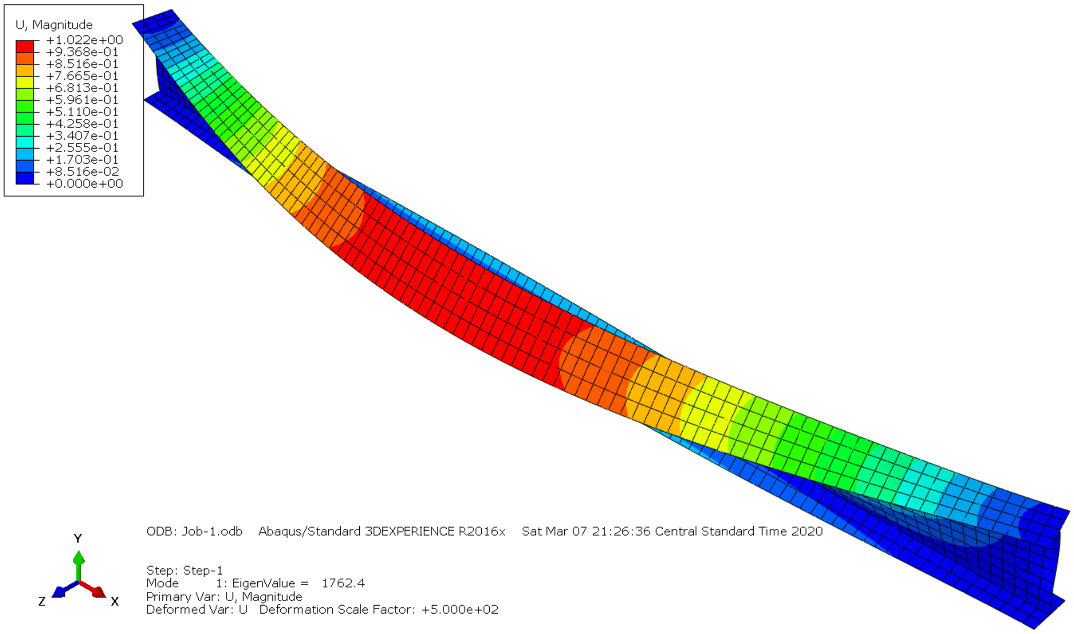

Figure 5.10: Large steel I-beam deformed shape isometric view

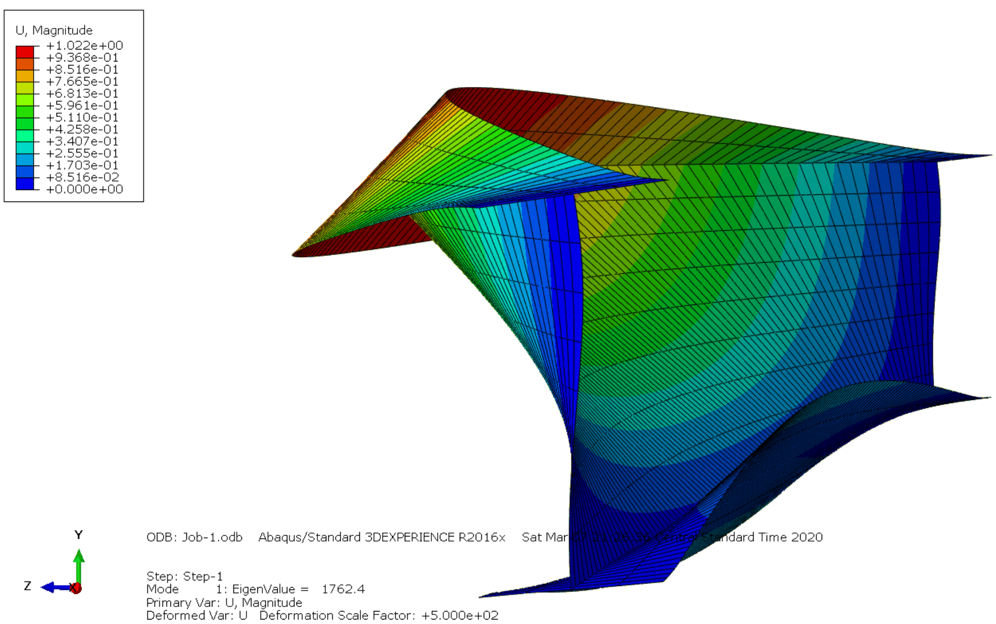

Figure 5.11: Large steel I-beam deformed shape front view

Table 5.9: Critical bending moment for small CFRP beam with arbitrary layups under pure bending

Layup		Beam length (mm)	Analytical/Buckling load using Eq. (5.38) (N.mm)	ABAQUS buckling load/Eigen Value (N.mm)	Error[10] (%)
Flange	Web				
0/0/0/0	45/-45/45/-45	609.6	1.81 E+6	1.45 E+6	19.89
0/0/0/0	45/-45/-45/45	609.6	1.74 E+06	1.45 E+6	16.67
0/0/0/0	0/0/0/0	609.6	1.60 E+06	1.45 E+6	9.38
90/90/90/90	90/90/90/90	609.6	1.88 E+05	1.87 E+05	0.53
30/30/30/30	30/30/30/30	609.6	4.75 E+05	4.26 E+05	10.32
45/-45/45/-45	45/-45/45/-45	609.6	5.39 E+05	4.70 E+05	12.80
45/-45/-45/45	45/-45/-45/45	609.6	4.71 E+05	4.26 E+05	9.55
-60/-60/-60/-60	60/60/60/60	609.6	2.28 E+05	2.22 E+05	2.63
0/90/0/90	0/90/0/90	609.6	8.54 E+05	8.41 E+05	1.52
0/90/90/0	0/90/90/0	609.6	9.09 E+05	8.63 E+05	5.06
60/-30/30/-60	60/-30/30/-60	609.6	6.19 E+05	5.71 E+05	7.75
60/-30/-30/60	60/-30/-30/60	609.6	4.25 E+05	4.07 E+05	4.24
0/30/60/90	0/30/60/90	609.6	5.46 E+05	6.27 E+05	-14.84
15/-30/45/-60	15/-30/45/-60	609.6	7.24 E+05	7.21 E+05	0.41

10 $Error(\%) = (Analytical\ Solution - Eigen\ Valu)/(Analytical\ Solution) * 100$

Table 5.10: Critical bending moment for large CFRP beam with arbitrary layups under pure bending

Layup		Beam length (mm)	Buckling load using Eq. (5.38) (N.mm)	ABAQUS buckling load/Eigen Value (N.mm)	Error (%)
Flange	Web				
0/0/0/0	45/-45/45/-45	5000	5.19 E+07	4.96 E+07	4.43
0/0/0/0	45/-45/-45/45	5000	5.13 E+07	4.96 E+07	3.31
0/0/0/0	0/0/0/0	5000	5.01 E+07	4.96 E+07	1.00
90/90/90/90	90/90/90/90	5000	4.78 E+06	5.42 E+06	-13.39
30/30/30/30	30/30/30/30	5000	1.14 E+07	1.25 E+07	-9.65
45/-45/45/-45	45/-45/45/-45	5000	1.22 E+07	1.37 E+07	-12.30
45/-45/-45/45	45/-45/-45/45	5000	1.09 E+07	1.24 E+07	-13.76
-60/-60/-60/-60	60/60/60/60	5000	5.57 E+06	6.35 E+06	-14.00
0/90/0/90	0/90/0/90	5000	2.57 E+07	2.80 E+07	-8.95
0/90/90/0	0/90/90/0	5000	2.75 E+07	2.83 E+07	-2.91
60/-30/30/-60	60/-30/30/-60	5000	1.59 E+07	1.77 E+07	-11.32
60/-30/-30/60	60/-30/-30/60	5000	1.06 E+07	1.19 E+07	-12.26
0/30/60/90	0/30/60/90	5000	1.43 E+07	2.04 E+07	-42.66
15/-30/45/-60	15/-30/45/-60	5000	1.8 E+07	2.26 E+07	-25.56

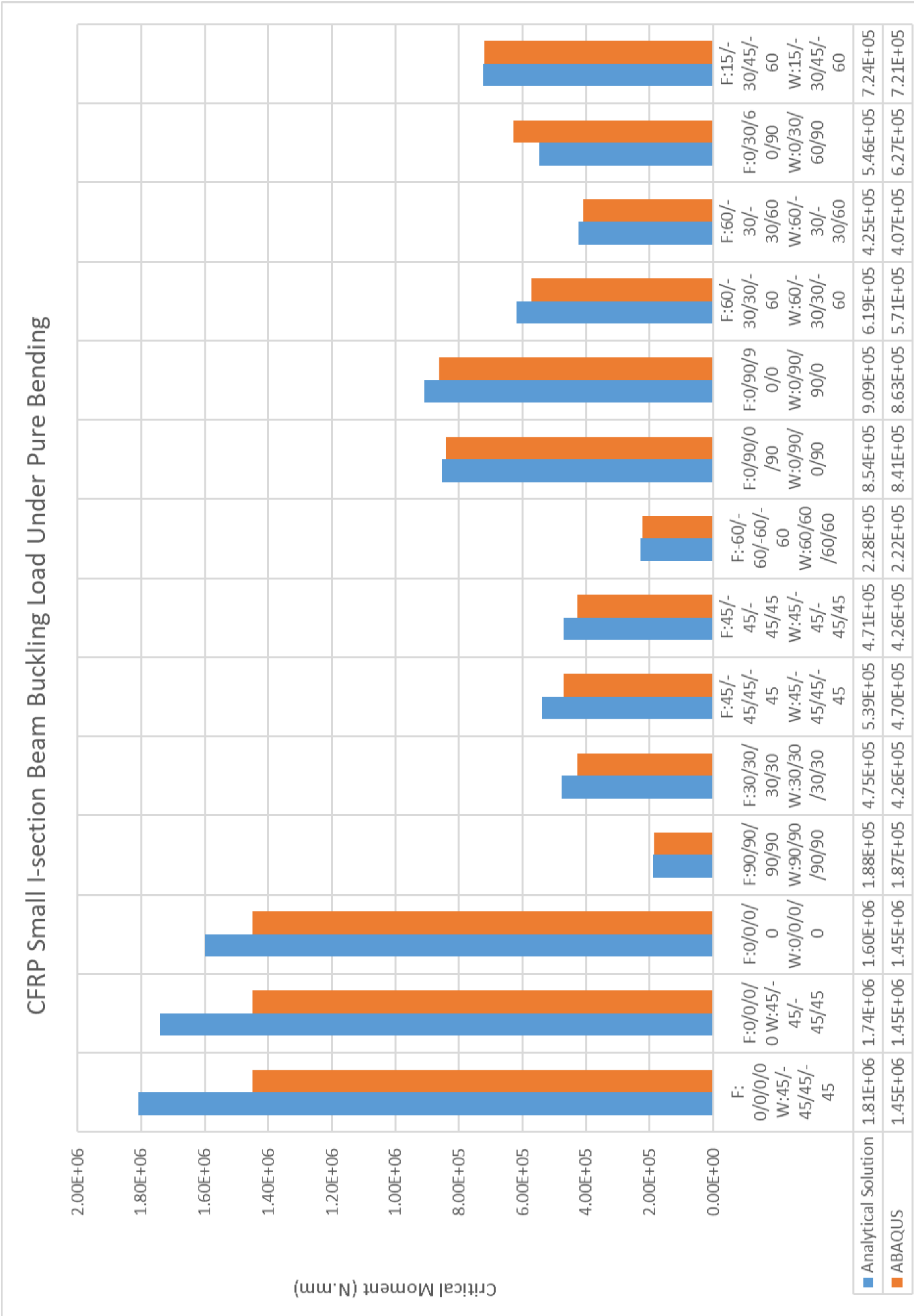

Figure 5.12: CFRP Small I-section buckling load under pure bending

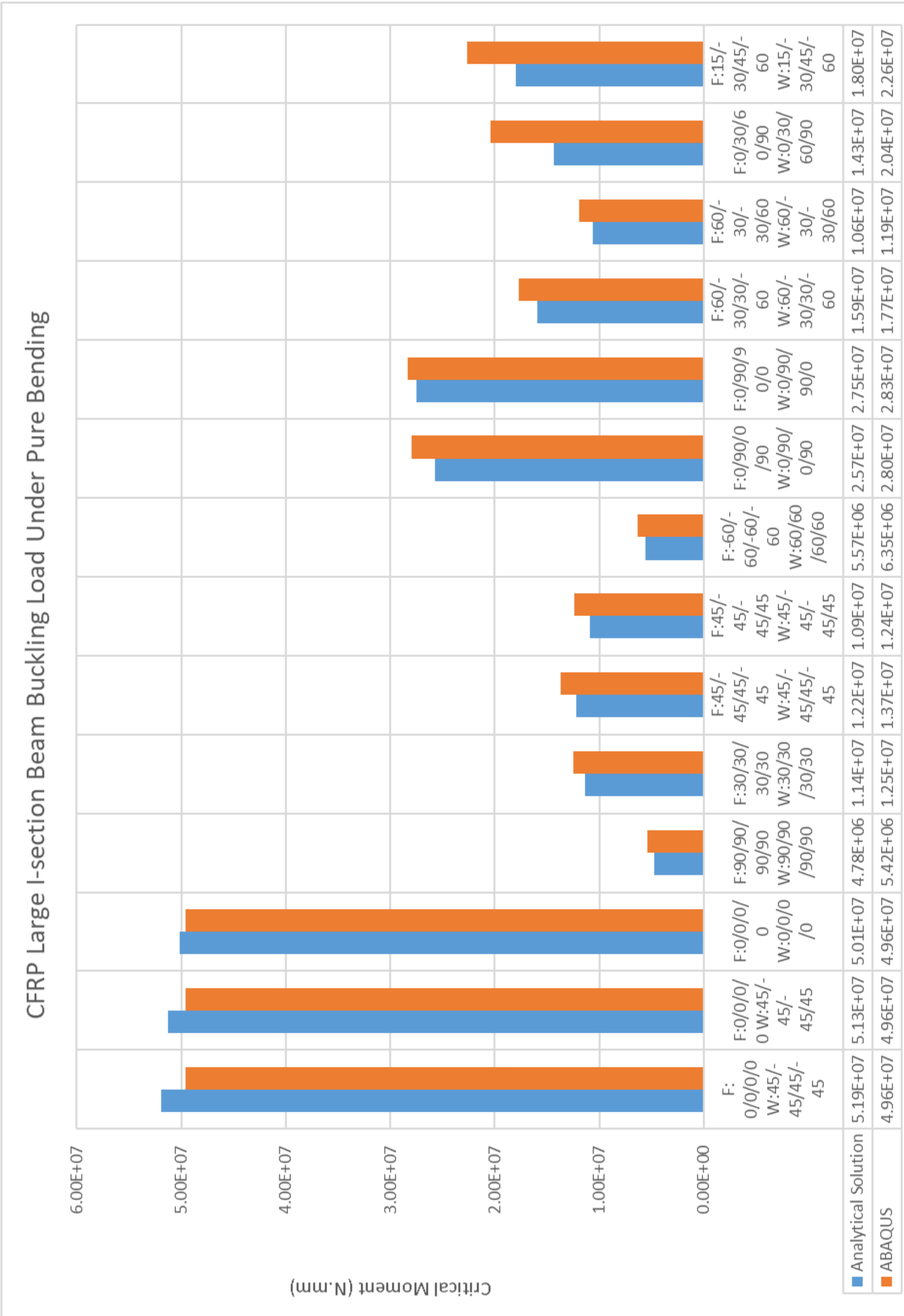

Figure 5.13: CFRP Large I-section buckling load under pure bending

5.10 Conclusion

The closed form analytical solution is conservative and more consistent with finite element results for I-beams with lateral torsional buckling as the dominate failure mode. This includes majority of the I-beams used in civil engineering structures that often have higher depth to width ratios and larger thicknesses for both flanges and web. I-beams with smaller depth to width ratios and small thickness often fail due to local buckling or a combination of local and lateral buckling which is called distortional buckling. For example, a small I-beam having flange width =38mm, and web width =50mm and thickness=1mm will most likely fail in distortional buckling. Such beams are used in aerospace applications for giving extra stiffness to plates or panels to which they are attached.

The warping stiffness term that is originally derived for orthotropic beams, shall be modified for generally anisotropic beams. Using the present warping stiffness term without further modifications can lead to large errors. Therefore, a modified warping stiffness is essential to improve the accuracy and consistency of the analytical solution.

To understand which buckling mode (local, lateral or distortional) is most likely to take place requires a more in depth understanding of the relationship between section geometry, lamina properties, stacking sequence and load and boundary conditions which is beyond the scope of this work.

Chapter 6 - Conclusion and Recommendations

6.1 Conclusion

In this study, lateral torsional buckling of thin-walled rectangular and I-section CFRP beams with arbitrary layups is studied. A closed form analytical solution using classical laminate plate theory is obtained for rectangular cantilever beam. The solution could be adapted for beams with different load and support conditions, however it is beyond the scope of this study. The proposed solution is validated against finite element results which compares favorably confirming its accuracy.

A closed form analytical solution for CFRP I-beam with arbitrary layup under pure bending is also presented which takes into account restrained warping and out-of-plane shear effects. The solution assumes lateral torsional buckling as the dominant buckling mode for the beam; meaning that no local or distortional buckling occurs. The proposed solution matches well with finite element results especially for beams with lateral torsional buckling as the dominant failure mode. Furthermore, it offers good agreement between Timoshenko's classical buckling solution for isotropic beams of different length-to-depth (l/h) and web-to-flange thickness ratios.

The warping stiffness term that is originally derived for orthotropic beams shall be modified for generally anisotropic beams. Using the present warping stiffness term in the solution without any modifications, can lead to significant errors. Hence, introducing a modified warping stiffness is essential to improve the accuracy and consistency of the proposed analytical solution.

Despite the small uncertainties in measurement, the proposed experimental technique was reasonably accurate to measure twisting rotation of the section as well as lateral and vertical deflection for a load-controlled case. The generated load vs. twisting rotation plots well compares with the Riks analysis confirming the method's accuracy.

6.2 Recommendations

1. The warping stiffness term which is originally derived for orthotropic beams shall be modified for anisotropic beams. Introducing a modified warping stiffness would further improve the accuracy and consistency of the present solution for I-beams .
2. To know which buckling mode (local, lateral or distortional) is most likely to happen requires a more in depth understanding of the relationship between section geometry, lamina properties, stacking sequence and load and boundary conditions.
3. For more accurate results especially for the case of unidirectional (0°) layups, the buckling solution shall allow variation of the twisting rotation (β) along height or depth of the section.
4. Extend the procedure to solve for critical load of I-beam with arbitrary layups having different load and boundary conditions including hybrid beams of various cross sections (rectangular, hollow square, channel, I shape, etc.)

Chapter 7: References

[1] K. H. Hnaihen, "The Appearance of Bricks in Ancient Mesopotamia," *Athens Journal of History,* pp. 73-96, 2020.

[2] R. F. Gibson, Principles of Composite Material Mechanics, McGraw Hill, Inc., 1994.

[3] A. A. Griffith, "The phenomena of rupture and flow in solids," Philosophical Transactions of the Royal Society, 1920.

[4] Z. P. Bazant, "Size effect on structural strength: a review," *Archive of Applied Mechanicss,* vol. 69, pp. 703-725, 1999.

[5] L. C. Bank and P. J. Bednarczyk, "A beam theory for thin walled composite beams," *Composite Science and Technology,* vol. 32, no. 4, pp. 265-277, 1988.

[6] E. J. Barbero, Introduction to Composite Materials Design, CRC, 1999.

[7] H. Ahmadi, "Lateral torsional buckling of anisotropic laminated composite beams subjected to various loading and boundary conditions," 2017.

[8] H. A. Rasheed, Strengthening Design of Reinforced Concrete with FRP, Taylor & Francis Group, 2015.

[9] O. Kalny, R. J. Peterman and G. Ramirez, "Performance Evaluation of Repair Technique for Damaged Fiber-Reinforced Polymer Honecomb Bridge Deck Panels," *Journal of Bridge Engineering, ASCE*, pp. 75-86, 2004.

[10] J. F. Davalos and P. Qiao, "Analytical and Experimental Study of Lateral and Distortional Buckling of FRP Wide-Flange Beams," *Journal of Composites for Construction,* vol. 1, no. 4, pp. 150-159, 1997.

[11] V. Z. Vlasov, "Thin-Walled Elastic Beams," Office of Technical Services, U.S. Department of Commerce, TT-61-11400, Washington DC, 1961.

[12] E. J. Barbero, R. Lopez_Anido and J. F. Davalos, "On the Mechanics of Thin-Walled Laminated Composite Beams," *Journal of Composite Materials,* pp. 806-829, 1993.

[13] G. J. Turvey, "Effects of load position on the lateral buckling response of pultruded GRP cantilevers-comparisons between theory and experiment," *Composite Structures,* vol. 35, pp. 33-47, 1996.

[14] H.-w. He and F. Gao, "Effect of Fiber Volume Fraction on the Flexural Properties of Unidirectional Carbon Fiber/Epoxy Composites," *International Journal of Polymer Analysis and Characterization,* pp. 180-189, 2015.

[15] J. Reddy, "A General Non-Linear Third Order Theory of Plates with Moderate Thickness," *International Journal of Non-Linear Mechanics,* pp. 677-686, 1990.

[16] M. V. V. Murthy, "An Improved Transverse Shear Deformation Theory for Laminated Anisotropic Plates," NASA, Technical Report 1903, 1981.

[17] J. N. Reddy, "A Simple Higher-Order Theory for Laminated Composite Plates," *Journal of Applied Mechanics,* pp. 745-752, 1984.

[18] L. P. Kollar and A. Pluzsik, "Bending and Torsion of Composite Beams (Torsional-Warping Shear Deformation Theory)," *Journal of Reinforced Plastics and Composites,* pp. 441-480, 2012.

[19] H. Ahmadi and H. A. Rasheed, "Lateral torsional buckling of anisotropic laminated thin-walled simply supported beams subjected to mid-span concentrated load," *Composite Structures,* vol. 185, pp. 348-361, 2018.

[20] T. P. Vo and J. Lee, "Flexural-torsional buckling of thin-walled composite box beams," *Thin-Walled Structures,* vol. 45, no. 9, pp. 790-798, 2007.

[21] J. Lee and S.-E. Kim, "Flexural-torsional buckling of thin-walled I section composites," *Computers & Structures,* vol. 79, pp. 987-995, 2001.

[22] M. Z. Kabir and A. N. Sherbourne, "Lateral-Torsional Buckling of Post-Local Buckled Fibrous Composite Beams," *Journal of Engineering Mechanics,* vol. 124, no. 7, pp. 754-764, 1998.

[23] D. C. Cardoso and J. D. Vieira, "Comprehensive Local Buckling Equations for FRP I-Sections in Pure Bending or Compression," *Composite Structures,* pp. 301-310, 2017.

[24] E. Zeinali, A. Nazari and H. Showkati, "Experimental-Numerical Study on Lateral-Torsional Buckling of PFRP Beams under Pure Bending," *Composite Structures,* pp. 1-9, 2020.

[25] M. D. Pandey, M. Z. Kabir and A. B. Sherbourne, "Flexural-Torsional Stability of Thin-Walled Composite I-Section Beams," *Composites Engineering,* pp. 321-342, 1995.

[26] E. J. Barbero and I. G. Raftoyiannis, "Lateral and Distortional Buckling of Pultruded I-Beams," *Compsoite Structures,* pp. 261-268, 1994.

[27] J. Mottram, "Lateral-torsional buckling of a pultruded I-beam," *Composites,* vol. 23(2), pp. 81-92, 1992.

[28] L. P. Kollar and A. Pluzsik, "Analysis of Thin-Walled Composite Beams with Arbitrary Layup," *Journal of Reinforced plastics and composites,* vol. 21, no. 16, pp. 1423-1465, 2002.

[29] A. Pluzsik and L. P. Kollar, "Effects os Shear Deforamtion and Restrained Warping on the Displacement of Composite Beams," *Journal of Reinforced Plastics and Composites,* vol. 21, no. 17, pp. 1517-1525, 2002.

[30] A. Pluzsik and L. P. Kollar, "Torsion of Closed Section, Orthotropic, Thin-Walled Beams," *Internationial Journal of Solids and Structures,* vol. 43, pp. 5307-5336, 2006.

[31] L. Shan and P. Qiao, "Flexural-torsional buckling of fiber-reinforced plastic composite open channel beams," *Composite Structures,* vol. 68, pp. 211-224, 2005.

[32] J. C. Massa and E. J. Barbero, "A Strength of Materials Formulation for Thin Walled Composite Beams with Torsion," *Journal of Composite Materials,* pp. 1560-1594, 1998.

[33] L. P. Kollar, "Flexural-torsional buckling of open section composite columns with shear deformation," *International Journal of Solids and Structures,* vol. 38, pp. 7525-7541, 2001.

[34] S. P. Timoshenko and J. M. Gere, Theory of Elastic Stability, Second ed., Mineola, New York: Dover Publications Inc., 1961.

[35] "Structural Strengthening Products & Services," Structural Technologies, [Online]. Available: www.structuraltechnologies.com. [Accessed 2019].

[36] L. Kwasniewski, "Application of grid convergence index in FE computation," *Bulletin of the Polish Academy of Sciences,* vol. 61, no. 1, pp. 123-128, 2013.

[37] J. N. Reddy, Mechanics of Laminated Composite Plates and Shells, CRC Press LLC, 2004.

[38] L. P. Kollar and G. S. Springer, Mechanics of Composite Structures, Cambridge University Press, 2003.

[39] L. P. Kollar, Mechanics of Composite Structures, New York: Cambridge University Press, 2003.

Appendix A - Modeling Procedure for Composite Beams in ABAQUS

Modeling Composite Beams

In the following, a step-by-step procedure for modeling CFRP beam in ABAQUS is presented.

Steps	Description
Step 1:	Open ABAQUS/CAE and click on “With Standard/Explicit Model”. Double click on “parts” in the Model Tree. Give a name to the part (i.e., top flange) →select 3D from the modeling space →deformable →shell →planar.
Step 2:	Using the Toolbox Area, draw the member. In the Prompt Area, click on the red X  and Done. The generated part will appear on the Model Tree. To see the part, click on the + sign in front of the Parts to expand.
Step 3:	In the Model Tree, click on materials →give name→click on mechanical in the material behaviors window→ Elasticity→Elastic. From the drop down menu select lamina as type→enter material properties i.e., E_1, E_2, Nu_{12}, etc. Make sure to use consistent units. For example: if the force is in N and distance in mm then stress has to be in MPa or N/mm2.

Steps	Description
Step 4:	In the Model Tree, click on sections → select category i.e., shell → composite → continue. Click in the blank space under material and pick appropriate material from the list→add thickness → orientation angle → and integration points. Right click in the blank space to insert or delete rows. Always delete rows that are not needed.
Step 5:	To change fiber orientation or thickness, go to section in the Model Tree → right click → edit.
Step 6:	Double click on the part of interest in the Model Tree and assign section  from the Toolbox Area. Follow the instructions on the prompt area. Repeat the same process for all parts you have created until each part is assigned a section.
Step 7:	From the Model Tree, click on assembly, select parts in the parts section to create instances. Check the box saying dependent (mesh on part) and check the box Auto-offset from other instances as shown in the figure below.

<table>
<tr><th>Steps</th><th>Description</th></tr>
<tr><td></td><td>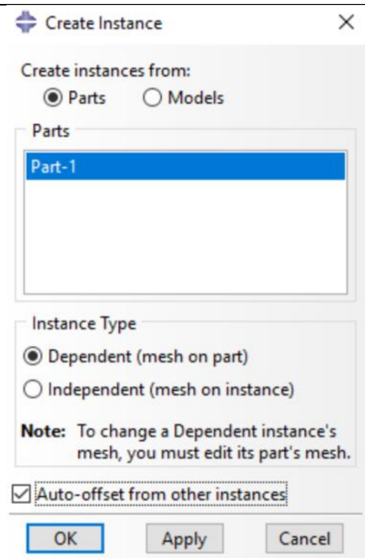
</td></tr>
<tr><td>Step 8:</td><td>If certain instances need to be rotated, click on rotate instance in the Toolbox Area  and follow instructions on Prompt Area. Check the orientation using different view options on the Toolbar.</td></tr>
<tr><td>Step 9:</td><td>For a non-prismatic member (tapered), go to XY plane and use create constraint option to create face to face, parallel edge, edge to edge etc. constraints. For example: to place top and bottom flanges on a tapered web of an I-beam, flanges shall be rotated 90 degrees so they are in the XZ plane. Go to XY plane → click on  in the Toolbox Area → select parallel edge  → click on the lower edge of I-beam then edge of the lower flange. Follow instructions in the Prompt Area. Repeat the same process for placing top flange. Then click on 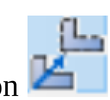 and select the instances to translate. In the case of I-beam, translate lower and top flange</td></tr>
</table>

Steps	Description
	one by one. Select the lower flange, say Done, click on 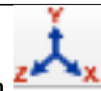 in the Toolbar for isometric view → select a start point for the translation vector (in this case the middle point along the width of the flange) → select an end point for the translation vector where the point on the flange needs to be when assembled. Repeat the same process for the top flange. Follow instructions in the Prompt Area until the I-beam is assembled. For a prismatic I-beam, there is no need to select parallel edge unless the flanges are not exactly in the XZ plane.
Step 10:	Merge / cut instances by clicking 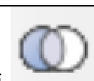 in the Toolbox Area. Fill out the dialog box → name the new part → select Geometry from the operation box →suppress and remove in the original instances and geometry sections respectively. Click continue and follow instructions. A new part will be created that can be accessed from the Model Tree by clicking the + sign in front of Assembly to expand the list and then + in front of Instances to see the new part 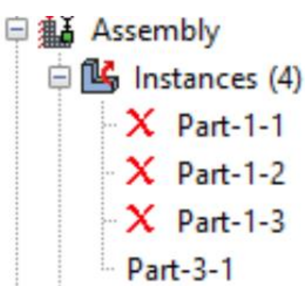
Step 11:	In the Model Tree, click on + in front of Steps to expand → initial → right click on the BCs to create boundary conditions. Select Displacement/Rotation and continue,

Steps	Description
	select regions for boundary condition. You may need to rotate the part  to properly add boundary conditions. For the pure bending case and simply supported I-beam, Z-axis displacement is restrained on both ends and both edges of the top and bottom flange. XYZ displacements restrained in the mid height of web on one end and Y-axis displacement restrained on the other end in the same location. 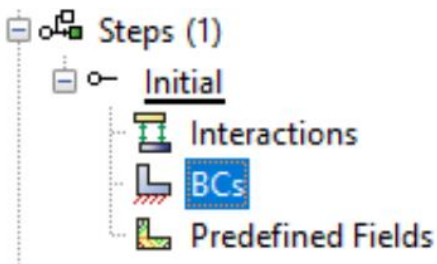
Step 12:	In the Model Tree, right click on the Step to create a new step. From the procedure type drop down menu → select Linear Perturbation → Buckle → continue. In the Edit Step window →select Subspace or Lanczos for the Eigensolver →fill the spaces i.e., number of Eigenvalue requested, maximum Eigenvalue of interest and maximum number of iterations, etc. The new step could be accesses through the Model Tree by expanding Steps on the list.
Step 13:	From the Module in the Context Bar → select load → click on 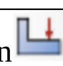 to create load. Select the Step you created from the dropdown menu → from the load category select Mechanical and the corresponding load type → continue. You may edit the load by clicking on  next to  in the Toolbox Area. Follow instructions in the Prompt Area to properly apply load(s). For pure bending case, shell edge load

Steps	Description
	was selected for the top and bottom flanges of the same magnitude but opposite sign (in the magnitude box). Linearly distributed load was applied on the web resulting a couple. It can be applied on the web by clicking on 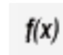 as shown in the figure below. 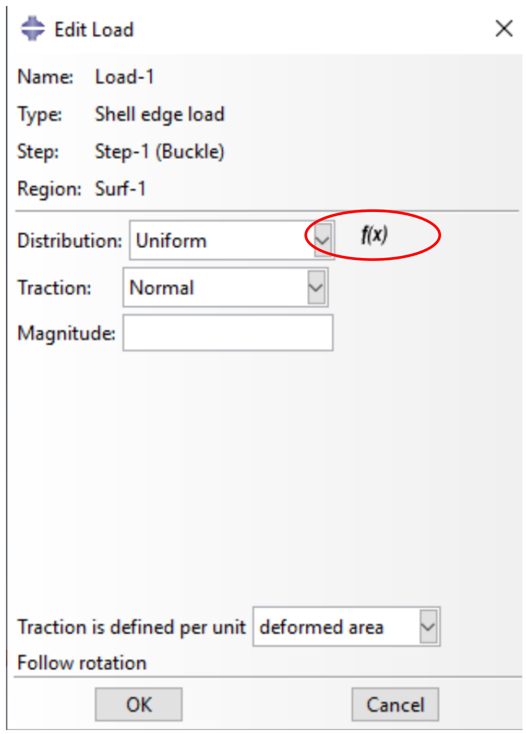

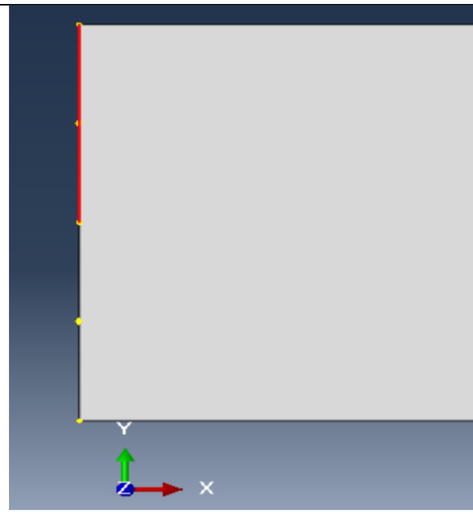

Give name to the new loading function →select Expression Field from the type section → click continue. The Create Expression Field window will open as shown below

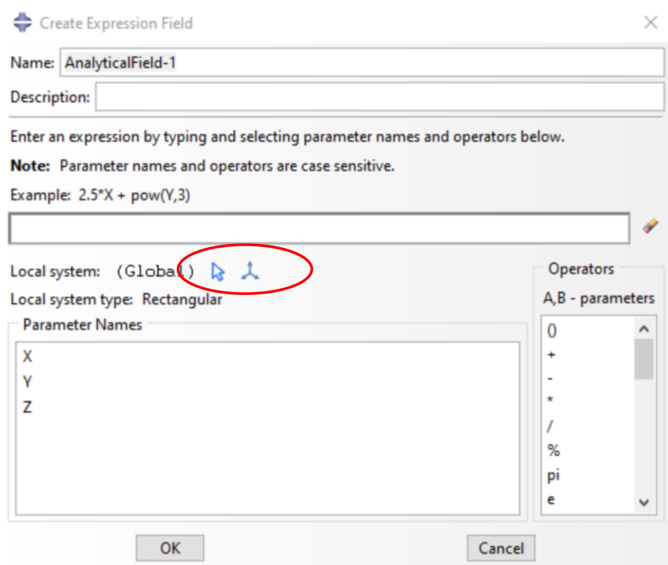

Create datum coordinate system by clicking  and selecting appropriate coordinate system type i.e., rectangular, cylindrical or spherical. Select a point to be the origin and follow the instructions until the datum is set.

Steps	Description
	You may need to partition an edge and select a point to serve as origin for the datum coordinate system. To do so → click on + sign in front of the Assembly and Instances to expand → right click on the part of concern → click on Make Independent. From the Module → select Part → click on 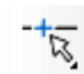 to select appropriate partitioning method. In this case, the web was partitioned at the mid height / mid depth. Now, with the datum coordinate system established and the web partitioned at mid height on both ends → click on 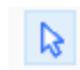 → click on Datum CSYS List on the bottom right corner in the Prompt Area → select the Datum Coordinate System introduced previously. In the space provided write function for your load using the listed parameters and operators → click OK and proceed. For instance, for the datum coordinate system with the origin at the mid depth of the web and a linearly distributed load with magnitude of 1 N at the top and zero at the mid height, the function would be Y*1/25; where Y is along web height, 1 is load magnitude and 25 mm is half of the web height at which linearly distributed load is applied. From the Edit Load window, select the function (which is named AnalyticalField-1 by default), traction type and load magnitude with correct sign depending whether the load is in tension or compression. Notice that the magnitude of the load is already taken into account in the loading function or AnalyticalField so there is no need to enter the actual magnitude. Considering the load direction, enter 1 or -1 for the load magnitude. The loading function can be accessed via Fields in the Model Tree.

Steps	Description
Step 14:	From the Module → select Mesh → click on 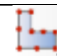 to seed part instance. Enter approximate global size for meshing. Enter maximum deviation factor and other parameters, if applicable. Click on  in the Toolbox area for mesh part instance and follow instructions in the Prompt Area. If the mesh was not regular which might be the case when the member is tapered or there exists an opening, go to Mesh menu → Controls→ select regions to be assigned mesh controls. On the Mesh Control window → select Quad-dominated for element shape → Structured → continue. Then check the box saying: “Automatically delete meshes invalidated by mesh control changes”. To select appropriate element type, go to Mesh menu → click on element type → → select the regions to be assigned element types. From the Element Type window → select Shell from the family section → Quadratic from the geometric order. Then select degree of freedom per node, etc. Mesh again as described above.
Step 15:	From the Module, select Job and follow instructions.

RIKS Analysis Tips in ABAQUS

Linear analysis shall be performed prior to nonlinear RIKS analysis. Hence, two models are needed: one for linear analysis and the next one for RIKS analysis. The second model will be built to perform nonlinear analysis. The following steps describe RIKS analysis and how to extract data for plotting.

Steps	Description
Step 1:	To build model, follow the same steps as described in the previous section. In the Model Tree, right click on Model-1 → click on Copy Model. Name the second model (i.e., Model-2) which will be used for nonlinear RIKS analysis.
Step 2:	Go to Model-1→ right click on Job → create a new job (i.e., Job-1). On Create Job window → select Model-1 →continue. Before submitting the job, right click on Model-1 in the Model Tree → select Edit Keywords → scroll down and at the end of the file () type: *Output, field, variable=PRESELECT *NODE FILE U

Steps	Description
	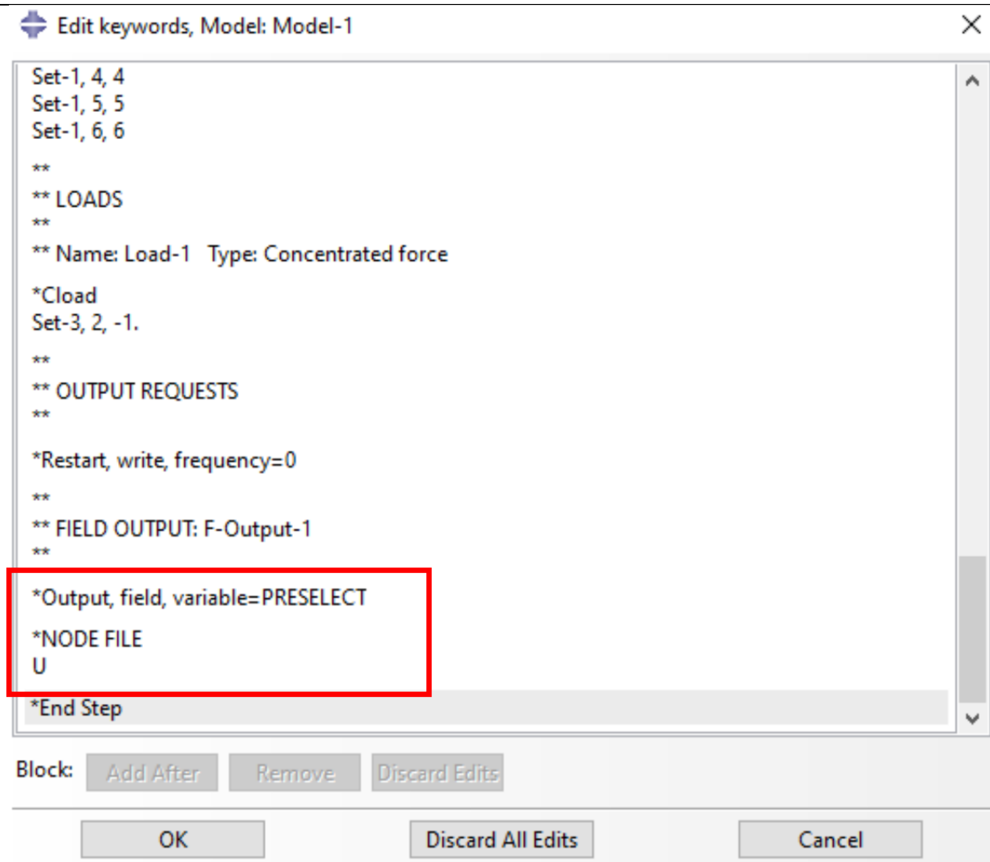
Step 3:	Right click on Job-1 → select Data Check → click on Submit to run linear buckling analysis. Once the analysis is successfully completed, right click on Job-1 → select Results to see the first Eigen mode and Eigen value on the viewport (bottom left corner). Record the first Eigen value as it will be needed in the next step.
Step 4:	From the Context bar, select Model-2. If the model is for isotropic material, material properties (stress-strain curve) shall be modified accordingly. Materials are introduced similar to step 3 of the previous section with the distinction that stress-strain characteristics beyond the elastic region shall also be defined.

Steps	Description
	New materials shall be assigned to the section in the Model Tree. Right click on the Sections → select the new materials from the list in the materials section. 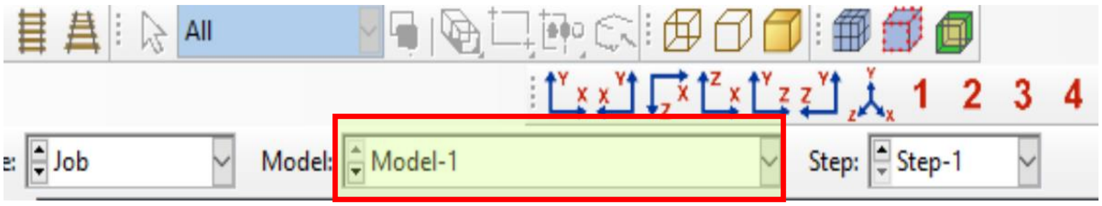
Step 5:	In the Model Tree, expand Steps → right click on Step-1→ Replace → General → Static → select Riks in the Replace Step window. Select Nlgeom:On which represent nonlinear geometry. On the incrementation tab, change Initial to 0.1, Minimum to 1E-015, and Maximum to 1.0.
Step 6:	Select Model-2 as explained before from the Context bar →select load from the Module. It can also be accessed via Model Tree by clicking the + sign in front of it. Click on the load and replace the previous load with the Eigenvalue from running Model-1, in other words, linear buckling analysis.
Step 7:	Create a new job (Job-2) for Model-2, make sure Model-02 is highlighted on the Create Job window.
Step 8:	Right click on Model-2 → Edit Keywords and type the following after material properties as shown in figure below. *IMPERFECTION, FILE=Job-1, STEP=1 1,1 ** --

<table>
<tr><th>Steps</th><th>Description</th></tr>
<tr><td></td><td>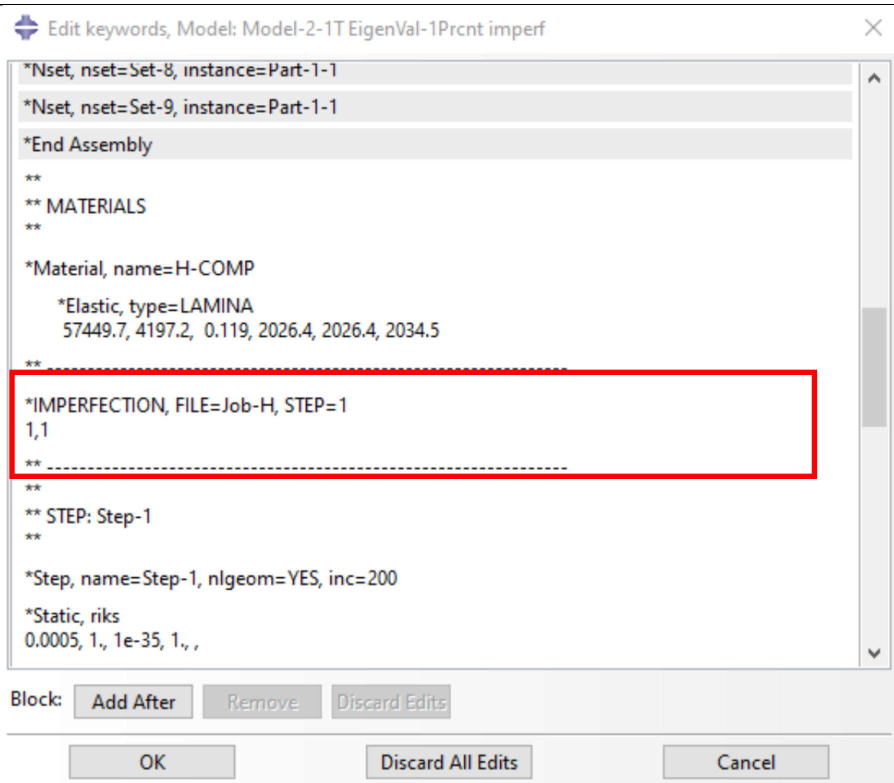

Right click on Job-2 and submit to run nonlinear analysis. Click on Monitor to see any errors or messages while the analysis is running. Once the analysis is completed, go to results. On the Results Tree to the left → expand Output Databases → expand Job-2 → expand History Outputs → double click on the Load Proportionality Factor: LPF to view the LPF vs Arc length graph. If the graph has reached the maximum and started to decline then select Job from the Module → go back to Job-2 in the Model Tree and right click → select Kill the results.</td></tr>
<tr><td>Step 9:</td><td>To extract the results, select visualization for the Module → click on 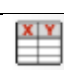 → ODB History Output → select load proportionality factor from the list → click on the plot.</td></tr>
</table>

Steps	Description
	On the Results Tree to the left → expand XY Data → right click on the _temp file → Edit. In the Edit XY Data, X and Y coordinates of the LPF vs Arc length curve are given. Copy the Y-coordinates (LPF) into Excel and multiply it by the Eigenvalue from linear analysis. Click again on  → select ODB field output → click ok. On the XY data from ODB Field Output window → click on the Variables tab → select Unique Nodal from the dropdown list. Check relevant boxes i.e., U: spatial displacement or UR: Rotational displacements. Then click on the Element/Nodes tab → Pick from View Port → Edit Selection → and click on node(s) of interest in the viewport → then click on Save. The data for the selected node(s) can be accesses via the Results Tree and by expanding XY Data. Right click on the node name and select Edit to view the data.

Steps	Description